University of Strathclyde

Control Strategy for Variable-speed Wind Turbine in Below Rated Wind Speed

Investigate a control strategy to improve the power capture

Hanif Aryanmanesh
Supervisor: Prof. William E. Leithead

MPhil Thesis

May 2018

"I hereby declare that this work has not been submitted for any other degree/course at this University or any other institution and that, except where reference is made to the work of other authors, the material presented is original and entirely the result of my own work at the University of Strathclyde under the supervision of Prof. William E. Leithead."

ACKNOWLEDGMENTS

The author wishes to express his sincere gratitude to his supervisor Prof. Leithead, for his constant guidance and kind encouragement throughout the course of the research project. The generous supervision given by him was invaluable and reflected his comprehensive knowledge.

Also, the author would like to thank Dr. Hong Yu as his second supervisor, which he received tremendous support and help from her in many ways.

Last but no means least the author would like to express his sincere appreciation to the member of his family for their considerate attitude, financially and unfailing support throughout his research period.

TABLE OF CONTENTS

LIST OF FIGURES

LIST OF TABLESS

ABSTRACT

Generating electrical power from renewable sources has increased substantially over the past decades and one of the most capable is wind power. From this energy source, the electrical power is directly generated using wind turbines. The type of the wind turbine used for this project is a variable-speed horizontal-axis wind turbine. Comparing variable speed wind turbines with constant speed wind turbines, variable speed machines have several advantages over constant speed machines, which outweigh the substantial cost of the power electronics necessary to obtain variable speed operations. The major advantage in below rated wind speed is additional energy capture and in above rated wind speed the frequent mentioned advantage is additional power-train compliance and associated load alleviation.

In variable speed wind turbines, the operational strategy is regularly selected to maximise the energy capture. For this purpose, the operating state of the wind turbine is caused to track the C_{pmax} curve, which is the maximum aerodynamic efficiency curve. The accuracy of this tracking depends on the controller designed for the wind turbine and the control strategy used. The purpose of this project is to investigate a control strategy for a variable-speed wind turbine in below rated wind speed to improve the power capture. To achieve the objective of this thesis, a controller to track the C_{pmax} curve is designed in this project.

The controller is validated using a Simulink model developed to the wind turbine. The Simulink model tested for different wind speeds from 4 m/s to 12 m/s with different turbulences from 5% to 20%.

NOTATION AND ACRONYMS

Notation

α	Rectifier firing angle (°)	
β	Pitch angle (°)	
β_0	Optimum pitch angle (°)	
β_d	Pitch angle demand (°)	
λ	Tip-speed ratio	
λ_0	Optimum tip-speed ratio	
Ω	Rotor speed	(rad/s)
Ω_0	Rotational angular velocity	(rad/s)
$\Omega_r r$	Tangential blade element speed	(rad/s)
Ω_z	Zero-torque speed	(rad/s)
ρ	Density of air (1.2256 kg/m^3)	
γ	Turbulent wind speed decay factor	
γ_1	Low-speed shaft external damping coefficient	
γ_1^*	Low-speed shaft internal damping coefficient	
γ_2	High-speed shaft external damping coefficient	
γ_2^*	High-speed shaft internal damping coefficient	
θ_G	Rotational displacement of the gearbox	(rad)
θ_H	Hub angular/rotational displacement	(rad)
θ_R	In-plane rotor rotational displacement	(rad)
ϕ_H	Fore-and-aft angular displacement of the hub	(rad)
ϕ_R	Out-of-plane rotor rotational displacement	(rad)
σ_v	Wind turbulence intensity	
ω	White Gaussian noise	
ω_g	Generator speed (rad/s)	
A	Area (m^2)	
$A_{-\infty}$	Downstream cross-sectional area (m^2)	

A_∞ Upstream cross-sectional area (m^2)

A_D Disc area (m^2)

C_P Power coefficient

C_{pmax} Maximum power coefficient

C_Q Torque coefficient

C_T Thrust coefficient

D_{GB} Gearbox mounting

D_T Fore-and-aft damping force (N)

F Force (N)

F_1 In-plane rotor aerodynamic torque (N.m)

F_2 Out-of-plane rotor aerodynamic torque (N.m)

f_D Drag force (N)

f_L Lift force (N)

h Height of the rotor (m)

I_1 Rotor inertia ($kg.m^2$)

I_2 Generator inertia ($kg.m^2$)

J_c Tower/Rotor cross-coupling inertia ($kg.m^2$)

J_H^* Hub inertia ($kg.m^2$)

J Rotor inertia ($kg.m^2$)

J_T Total moment of wind turbine inertia ($kg.m^2$)

J_X Tower/Gearbox cross-coupling inertia ($kg.m^2$)

K_1 Low-speed shaft stiffness (kg/s^2)

K_2 High-speed shaft stiffness (kg/s^2)

K_E Edge-wise stiffness (kg/s^2)

K_F Flap-wise stiffness (kg/s^2)

K_T Tower stiffness (kg/s^2)

L Length scale of the turbulence

m Mass (kg)

N Gearbox ratio

P Power (kW)

P_{av}	Available power	(kW)
P_g	Generated power	(kW)
R	Radius of rotor	(m)
R_c	Distance from the hub to the centre of blade mass	(m)
T	Torque	(kN.m)
T_D	Drive-train torque	(kN.m)
T_{dem}	Demanded torque	(kN.m)
T_e	Generator torque	(kN.m)
T_f	Aerodynamic torque	(kN.m)
$\hat{T}_f$	Estimated aerodynamic torque	(kN.m)
V	Wind speed	(m/s)
$\hat{V}$	Mean wind speed	(m/s)
$V_{-\infty}$	Downstream wind speed	(m/s)
V_{rel}	Relative speed	(m/s)

Acronyms

ANN	Artificial neural network
DSP	Digital signal processor
ESC	Extremum seeking control
GUI	Graphic user interface
HAWT	Horizontal axis wind turbine
KE	Kinetic Energy
MIMO	Multi-input multi output
MISO	Multi-input single output
OTR	Optimally tracking rotor
PMSG	Permanent-magnet synchronous generator
PV	Photovoltaic
PWM	Pulse width-modulation
RO	Renewable obligation
SISO	Single input single output
TSK	Takagi-Sugeno-Kang
VAWT	Vertical axis wind turbine
WECS	Wind energy conversion system

1. INTRODUCTION

"Stream is not stronger than it was hundred
Years ago, but it is put to better use."
…… ***Emerson***

The main objective of this project is to investigate a control strategy for a variable-speed wind turbine in below rated wind speed to improve the energy capture design and improve the tuning of a controller.

Much research has been conducted into wind turbine control systems with consideration of energy capture for variable-speed wind turbines. Many different approaches and strategies exist for the purpose of maximise the energy capture by the wind turbine. In this thesis, the objective is to develop an auto-tuning controller to maximise energy capture in below rated wind speed.

This Thesis is organized as follows. Chapter 2 is an overview of renewable energy and the global and the UK targets for using renewable sources. Different types of renewable resources are discussed in this section and the wind energy source, which this project is mainly concerned with, is reviewed. Also, a description of wind turbine technology and an introduction to variable-speed wind turbine is included in this chapter.

In chapter 3 previous works of assessing the energy capture capability of variable-speed wind turbines during below rated operations is reviewed.

Chapter 4 provides the mathematical modelling of the wind speed, and the dynamics of a variable-speed wind turbine is investigated to determine suitable models to support the control design task. The model of power generation is also described in this chapter.

In chapter 5 the Simulink simulations of the models determined in chapter 4 are validated.

Chapter 6 discussed the possible choices for control strategy and their objectives for the control design task.

In chapter 7 optimisation of the control system to track the C_{pmax} curve and maximise energy capture is investigated and finally in chapter 8 the conclusions are summarized.

Chapter 8 presents the conclusion of the research.

2. OVERVIEW

"Every great advance in science has issued from a new audacity of imagination."
*……. **John Dewey***

2.1 Renewable Energy

2.1.1 Introduction to Renewable Energy

Energy plays a very important role in human life with people consuming it in different ways such as home, transport, business, etc. but most people are not aware of the source of energy. There are many types of energy technology which have been exploited round the world and compared to conventional technology, Renewable Energy is rather new and, therefore, inevitably immature.

Generally, energy sources are used to generate electricity and heat production, and also, in some cases, to generate energy for transport. Renewable energy can provide all these three needs for energy from natural energy sources that are essentially inexhaustible.

Compared to renewable energy, fossil fuels form very slowly relative to the rate of energy use, so fossil fuels are constantly depleting. Also, burning fossil fuel harms the earth's environment and makes changes to the earth's climate by producing greenhouse gases. Greenhouse gases are responsible for locking in the heat that normally radiates back into space, but renewable energy does not produce any greenhouse gases or only produces a little when compared to fossil fuels. Using renewable energy has many other advantages, other than reducing greenhouse gases and carbon dioxide, which can be mentioned:

- Resources of renewable energy are safe, local and replenishable so the lack of energy source would not be a concern in the future.

- Using renewable energy reduces dependence on other non-renewable energy which is hard to produce.
- Renewable energy keeps the earth's environment clean.

Renewable energy exists in different types of natural resources such as wind, water, solar radiations, tides and geothermal heat. The main source that renewable energy develops from is the sun's radiation which is the earliest form of energy to be used. Solar power produces two forms of direct radiation and other indirect forms such as bio energy, geothermal, water or wind power. As societies became more sophisticated, they have started to think of taking advantage of natural energy and started to propose ways to develop and use more renewable energy.

Over the past few years growth of renewable energy shows impressive progress which has been well documented ([1], [4], [10], [11], [13]) and the emphasis on renewable energy has been highlighted continuously as to its importance for the immediate and long-term future. Nevertheless, a large amount of the world's primary sources are already renewable sources.

2.1.2 Present Consumption of Energy

At present the fossil fuels, mainly coal, oil and natural gas, provide three quarter's of the world's energy. The average consumption of primary energy in North America (almost 350 GJ) is almost five times the rest of the world average. European countries and the former Soviet Union are consuming roughly half of this amount and the rest of the world only about one fifth. By knowing the average rate of energy consumption at present it can be estimated that the world coal reserves should last for approximately 200 years, natural gas for about 60 years and oil for around 40 years [4].

Energy use in the UK is classified into four main sectors: domestic, commercial and institutional, industrial and transport. The energy provided for final consumers in these sectors is generally the result of a series of energy conversions. The types of energy are normally known as: primary energy, delivered energy and useful energy. In the process of converting energy from primary to delivered energy, roughly one third of energy is lost [4].

The UK government predicts a great role for renewable energy in the next few years and aims to increase the amount of electricity from renewable sources to 20 percent by 2020.

Renewable energy in the UK is described in more details in section 2.1.4.

In the UK, delivered energy exists in five different types:

- **Liquid fuels** which are mainly oil and its derivatives such as petroleum, gasoline, diesel, etc.
- **Gaseous fuels,** mostly natural gas such as methane.
- **Solid fuels** include products from fuel wood but coal is the most important one.
- **Electricity** is generally produced from fossil fuels or nuclear power stations and renewable sources still make a small contribution to produce electricity in the UK.
- **Heat** is sometimes directly delivered to buildings using community heating in the form of hot water and steam. The heat may be provided from geothermal sources.

Of the above sectors, heat is used most in different forms for cooking, space heating, washing, etc. and provided by burning fuels or electricity.

The other type of energy that is considered significant is motive power to transport cars and drive machinery. Currently the energy used to deliver this type of power is generally provided by oil but electricity is used to provide some energy for this sector. Electricity also has an important role in transport from electric railways to lifts and heavy industrial machines.

2.1.3 Global Overview of Renewable Energy

Figure 2.1, [13] shows the share of renewable energy in global energy consumption. Renewable energy supplies around 19 percent of the world's energy including traditional biomass, large hydropower and "new" renewables. 13 percent of this 19 percent is traditional biomass, the consumption of which is increasing only slightly in some regions and even decreasing in others as it is being used more efficiently and is also being substituted with more modern energy forms. Hydropower represents 3.2 percent and other renewable energies constitute the rest of the 19 percent including solar/geothermal at 1.4 percent, bio fuels at 0.6 percent and wind/power generation at 0.7 percent.

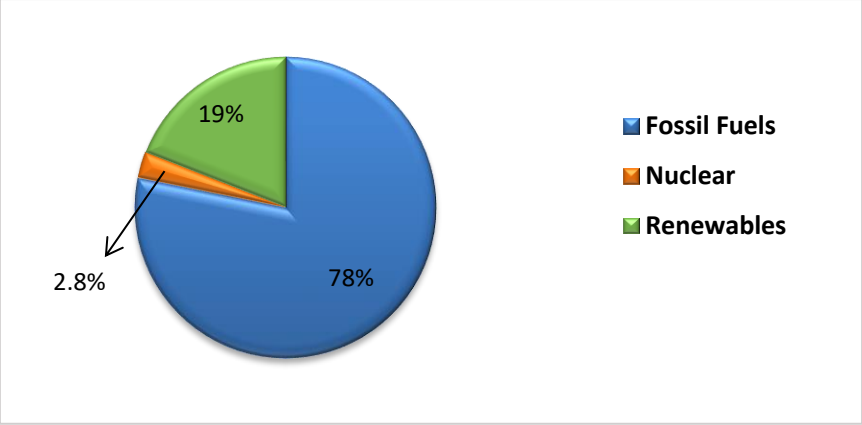

Figure 2.1 – Share of renewable in global energy consumption

From the end of 2004 to 2009 the global renewable energy capacity grew by 10-60 percent per annum. The chart of the growth of renewable energy during these five years is shown in Figure 2.2, [13]. In period 2004-2009, grid-connected solar photovoltaic (PV) increased quicker than other renewable technologies by a rate of 60 percent for the five year period. Other renewable technologies also grew rapidly with an annual average rate of 20 percent for ethanol and 51 percent for biodiesel.

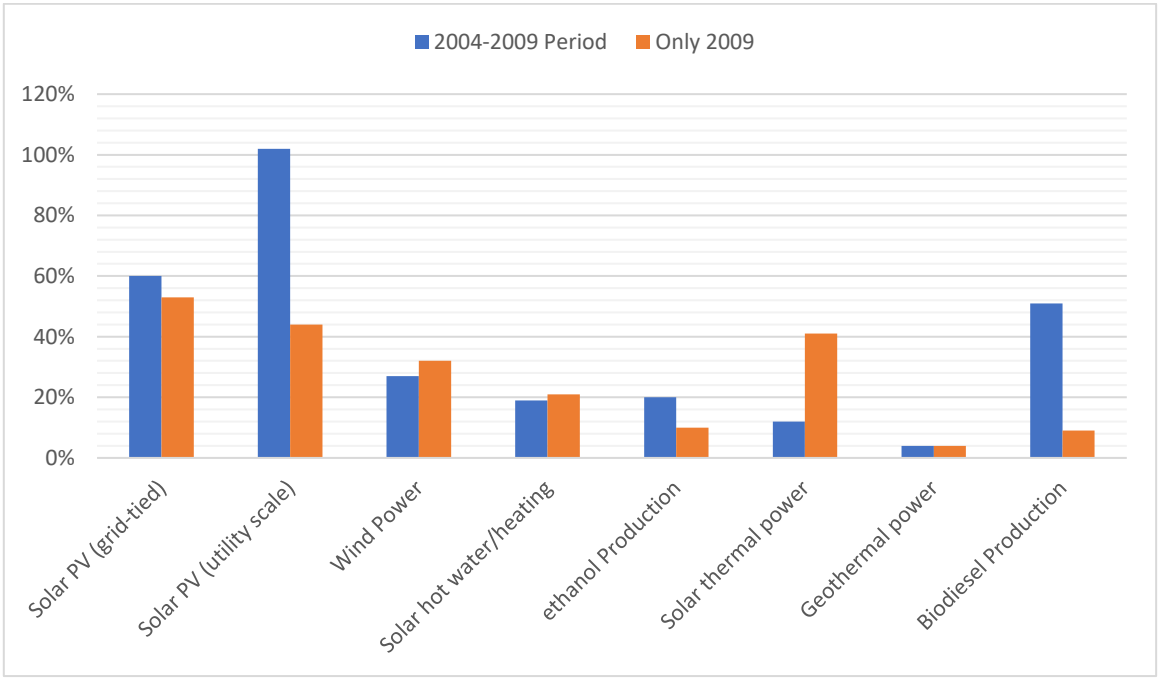

Figure 2.2 - Average rates of growth of renewable energy capacity in 2004-2009

Availability of global renewable power capacity increased by 7 percent from 2008 to 2009 and reached 1,230 gigawatts (GW). The renewable energy includes a quarter of entire world

electrical power generation installed capacity and now provides 18 percent of the world's electricity. Figure 2.3, [13] shows the share of global electricity from renewable energy.

Great progress in renewable energy has been made in the past few years. In 2009 renewables got to a total of 305 GW which indicates a 22 percent improvement during 2008 (not including hydropower). In recent years hydropower has been rising annually by about 30 GW, but between all renewables, wind power capacity increased the most by 38 GW in 2009 and other renewables such as solar PV capacity improved by more than 7 GW.

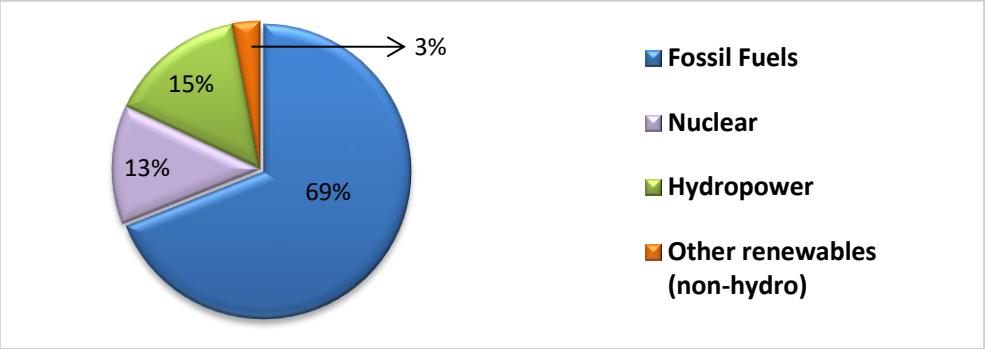

Figure 2.3 – Share of global electricity from renewable energy

2.1.4 Renewable Energy in the UK

The UK has a great opportunity to produce renewable energy because of its geographical position. It is surrounded by the world's largest resources of wind, wave and tidal energy.

In 2002 the renewable obligation (RO) was introduced to UK renewable industry to incentivise renewable generation as part of the wider electricity market and since then electricity generation has increased significantly. This obligation made all the licensed electricity suppliers in England and Wales provide a certain amount of their electricity from renewable energy. The same action has applied to Scotland and Northern Ireland which have their own RO. This has given a boost to generating electricity from renewable sources with about 5 percent of the UK's total electricity produced from renewable at the end of 2007 in comparison to 1.8 percent in 2002.

Under the EU Renewable Energy Directive, the UK government is committed to reach an average of 15 percent of energy from renewable energy resources and to lower CO_2 emissions (by 50 percent) by 2020. In comparison to 2008, this amounts to a seven-fold increase. To meet this 15 percent target, the aim is to produce 30 percent of the UK's

electricity from renewable energy, up from around 5.5 percent today. It also, plans to get 12 percent of heat from renewable sources mainly generated from biomass, biogas and solar. Finally, the generation of transport power from renewables is planned to reach 10 percent from the current 2.6 percent, mainly by electrification of the rail network.

2.1.4.1 Wind Energy Industry in the UK

To produce electricity from the wind in the UK, wind turbines are placed in the windy parts of the countryside. In 1991, the first wind farm in the UK was built at Delabole in Cornwall. The amount of electricity produced from the wind turbines sited off-shore is bigger than the amount produced from the wind turbines on-shore. A turbine with 2.5 megawatts (MW) at a reasonable site can generate 6.5 million units of electricity each year which is the annual need for over 1,400 households. The wind energy industry has grown impressively over the past few years. The industry growth is reflected in Table 1, [14] which illustrates all the growth, including projects being planned, those not built but consented, operational and under construction, for both on-shore and off-shore development in 2009. The off-shore wind industry coming on line later than the on-shore sector. The off-shore installation began with installing two turbines off the coast of Blyth, Northumberland in 2000. The capacity of the off-shore schemes is greater than on-shore schemes and the number of off-shore schemes lower.

Table 1 – UK wind energy status in June 2009

Status	Off-shore Schemes	On-shore Schemes
Operational	9	207
Under Construction	10	37
Consented, not built	8	125
Projects in planning	3	272

2.1.4.2 UK's Target

The energy production and consumption historically in the UK has been based on natural fossil fuels resources. This means the UK has not been as active in exploiting renewable energy. The UK has a target to achieve (15 percent) energy consumption from renewable energy by 2020 compared to 2005 when it was only 1.5 percent. Figure 2.4, [11] shows the

small improvement in renewable energy consumption in the past few years and the 2020 UK target. It also can be seen that in order to reach the target, a greater level of deployment will be needed.

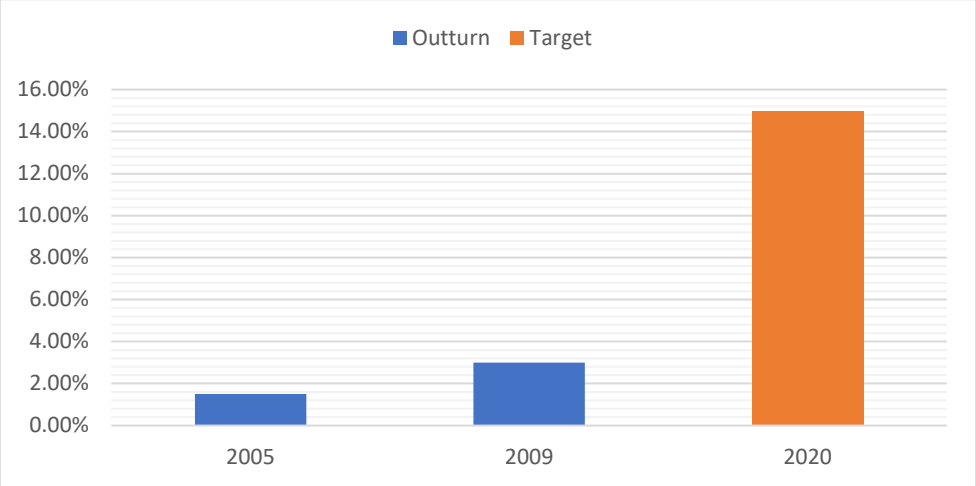

Figure 2.4 – Average of energy consumption in the UK from renewable energy

The UK has initiated a plan to reduce greenhouse gas emission by 12.5 percent between 2008 and 2012 and in 2010 to reduce it to 20 percent below the 1990 level and is considering reaching to 60 percent below the 1990 level by 2050.

The UK has a target to reach 20 percent of energy from renewables by 2020. This includes a binding 10 percent for the transport sector.

Looking further ahead to 2050, in Britain's energy supply system, by setting four energy `Scenarios`, produced by the UK Royal Commission on Environment Pollution, it is expected that renewables will play an even bigger role.

2.1.5 Renewable Energy Resources

Renewable Energy can be defined as `energy provided from continuous energy which does not have a limited supply and can be use repeatedly and recurring in the natural environment`.

Renewable energy is very useful because of the benefits it provides. One of the main benefits is the environmental benefit. Compared to conventional technology, Renewable energy technology is a clean source and has a much lower environmental impact. Climate

change and depletion of fossil fuel reserves are other reasons making renewable energy more attractive.

The main source of renewable energy coming from the sun's radiation is solar energy which can produce useful energy directly and indirectly. Other sources of renewable energy are hydropower, wind power, wave power and bioenergy. Two other sources of renewables are Tidal energy and geothermal energy which are known as non-solar renewable sources.

Solar

A range of technologies can be used directly to convert the sun's radiation to useful energy. It can be used to provide hot water and space heating. Solar radiation also has the ability to be converted directly to electricity by installing photovoltaic (PV) modules on the roof or facades of buildings.

Apart from direct uses of solar energy, solar radiation also can be converted to useful energy indirectly. One of the simplest examples of indirect use of solar radiation is when a large fraction of solar radiation reaching the earth's surface is absorbed by the oceans. This makes the oceans warm and adding water vapour to the air. The water vapour condenses and makes rain to feed the rivers, into which dams and turbines can be placed to extract energy.

Solar thermal energy is very suitable and economical for large demands such as household, farming, industrial and commercial sectors for providing heat and hot water. This type of energy source is effective for water heating, refrigeration, cooking and drying.

Wind

To produce electricity today, wind energy is one of the important sources and a pollution-free technology used all over the world. Wind energy is an important type of renewable energy and it is the fastest growing energy technology in the world. Wind energy is described in more details in section 2.2.

Bioenergy

Bioenergy is generally generated from materials available in the environment such as wood, straw or animal wastes. These materials can be directly converted into biofuels by burning

them to provide charcoal and biodiesel, for example. Biomass is another type of bioenergy that includes all the living matter on the earth which exists in the thin surface layer called the biosphere.

Only a small and tiny fraction of the total mass of the earth contains biomass but this tiny fraction has a large energy store.

In many developing countries, traditional biomass such as firewood, rice husks and animal residues can simply be burned to produce heat, and this continues to account for a huge part of energy usage. Bioenergy has no global companies to provide detailed reports on bioenergy production and consumption, unlike the fossil fuels. In countries where large forestry industries are located and have well-developed technologies, the energy contribution from biomass is important for processing residues and wastes.

Geothermal

Of the different types of renewable energy, geothermal is the only form that is independent of the sun. The source of geothermal energy is the heat from the earth which is tapped to drive a turbine to create electricity. This energy source is an established and economic energy source used in the world.

Around 10,715 megawatts (MW) of geothermal power is online in 24 countries in the world. Also, an extra 28 gigawatts (GW) of direct geothermal heating capacity is installed to provide heat for area and space, industrial processes, desalination and agriculture applications.

Because of the reliability and profitability of geothermal power, it is one of the environmental friendly energy sources but has historically been limited to areas near tectonic plate boundaries. Geothermal energy discharges greenhouse gases trapped deep within the earth but these emissions are much lower than the emissions released from fossil fuels. Therefore, geothermal power has the ability to help moderate global warming if widely deployed to replace fossil fuels.

The available resource for geothermal energy is more than enough to supply energy needs of the planet but only a very small fraction may be profitably exploited and exploration of

deep resources is expensive. Consideration of geothermal energy in the future depends on improvements in technology, energy price, interest rates etc.

Hydropower

Hydropower is indirect solar power like most other renewable sources. Electricity production from hydropower is one of the best-known technologies for producing power reliably at low cost.

Hydroelectricity provides around one-sixth of the global annual electric power output and about 90 percent of electricity from renewable.

Hydropower uses the water flow from the water that runs into rivers and streams to run turbines to produce electricity. The quantity of power generated depends on the rate of flow and volume of water available. Normally hydroelectric systems are divided into two broad types which are large-scale (more than 5MW) and small-scale (less than 5MW). Another type with a scale of few tens of kilowatts is available. It is often known as “micro hydro”; this type of hydroelectric system is usually not connected to the electricity grid.

The UK development of both small-scale and large-scale hydroelectric power is mainly determined by the size of catchment areas and the rainfall in these areas.

Wave energy

Waves are created by winds blowing across the surface of the ocean. Wave energy is extracted by using a variety of devices. The UK has one of the world’s largest wave energy resources because of the position of the UK on the north-eastern rim of the Atlantic.

The UK wave energy resource is divided into two categories, shoreline and offshore. The Oscillating Water Column is the main technology established for shoreline wave power. This contains of a partially submerged, hollow structure that is open to the sea below the water line. This encloses a column of air on top of a column of water. Waves make the water column rise and fall, alternatively applying pressure and depressurizing the air line. Air flows through a turbine to and from the atmosphere and the rotation of the turbine generates electricity.

Offshore wave devices exploit the more powerful wave regimes existing in deep water. Many different kinds of offshore devices have been developed but commercially none has been deployed yet.

Tidal

Tidal energy is often confused with wave energy but its sources are totally different. Tidal energy is used to convert energy in tides to electricity. The power of tides can be harnessed by building a low dam or 'barrage' in which the rising waters are captured and allow flowing back through electricity generation turbines.

The method used by a tidal barrage to generate energy is to allow tidal waters to fill an estuary through sluice gates and then empty it through turbines. Electricity is produced from the tidal barrage by using large axial flow turbines which have diameters of up to 9m. Tidal barrages have very long lifetimes and could last for about 120 years, with repair and turbine generator replacement at 40 years intervals. After the tidal barrage, the tidal stream is another way to exploit the rise and fall of tidal water. The technology of tidal streams and wind turbines is very similar. The required turbine diameter for this technology is at least 10m because even if the speed of water is slower than wind, the density of water is higher and consequently the energy density is higher. The maximum diameter of turbines depends on bending moments caused by the water flow.

2.2 Wind Energy

2.2.1 Wind Energy Overview

The Earth's rotation and the irregular heating of the planet's surface by the sun cause the movement of air across the earth's surface. This is wind.

The air over the earth's crust acts as an absorber and reflector throughout the day and the land absorbs energy that comes from the sun. Nevertheless, a larger portion of energy is reflected back, heating the atmosphere. A great deal of this energy absorption appears over the lakes and oceans when energy is absorbed by water or involved in evaporation, thus the air remains cool. The warm air, which is over the land, expands, becomes lighter then rises, causing heavier, cooler air over the water to move in and replace it. Since the water cools at slower rate than land at night, the breezes are reversed.

Wind energy was one of the first energy sources that was not dependent on animals and was first used to push boats. Wind energy also been used for milling grain, pumping water and other mechanical power purposes. Nowadays, there are many windmills all over the world used for water pumping but the main purpose of wind energy is using it as a pollution-free energy to generate electricity. To obtain electricity from wind energy, modern windmills, called wind turbines, are used. Their operation will be discussed later on in this chapter.

The amount of energy produced from the wind is very large. Huge amounts of energy are also transferred directly to the wind from the sun. The entire capacity of power that could produced from the wind surrounding the earth has been estimated to the order of 10^{11} gigawatts (GW), [4].

Energy generation from the wind is dependent on variations in the wind direction, wind speed and temperature. The physical properties of air are the main issues associated with extracting energy from the wind. Because the density of air is low, to get a noticeable amount of energy from moving air, devices need to be capable of intercepting large areas.

Generally, air is a relatively unstable commodity. Unlike water, air streams cannot be collected to store energy.

Wind power is one of the fastest growing types of renewable energy in the world. The capacity of wind energy since 1990 has been doubled every three years.

2.2.2 Energy and Power in Wind

The type of energy in the wind is kinetic energy. Kinetic energy is the energy of motion. The kinetic energy in the wind depends on the mass (m) of moving air and the velocity (V). Kinetic energy (KE) is

$$KE\ (J) = \frac{1}{2} * m\ (kg) *\ V^2\ (ms^{-1}) \qquad (2.1)$$

The kinetic energy in the wind can be calculated by considering the wind passing through a circular area A with a velocity V. Figure 2.5, [4] explains this graphically.

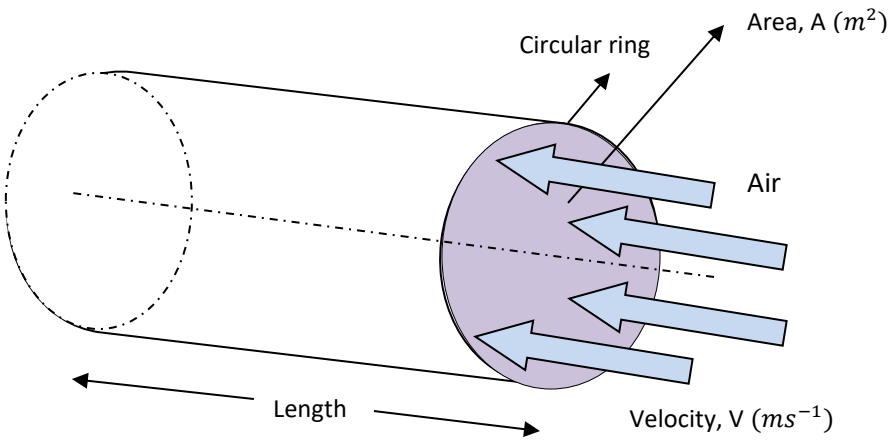

Figure 2.5 - Circular area, A of air passing through with a velocity, V

Considering Figure 2.5, if the air travels through the circular ring or hoop enclosing a circular area, A, with a velocity, V, a cylinder of air with a length, l, will flow through the circular ring each second as the air is passing. Therefore, a volume of air will pass through the ring each second. The mass of air flowing through the ring per second can now be obtained from multiplying the volume of air flowing per second by the density of air, ρ. In other words this relationship can be defined as:

$$m =\ \rho\ * air\ volume\ flowing\ per\ second$$

where m represents the mass of air flowing per second and density of air, ρ, is 1.2256 kgm^{-3}. As the volume of air per second can be obtained from multiplying the length of the cylinder of air flowing each second by area, the above equation can be rearranged as:

$$m = \rho * A * l$$

where l represents the cylinder length of flowing air per second

Now substituting for m in (2.1) resulting:

$$KE\ (J) = \frac{1}{2} * \rho\ (\mathrm{kgm^{-3}}) * \mathrm{A}\ (\mathrm{m^2}) * l\ (m) * \mathrm{V^2}\ (m^2\mathrm{s^{-2}}) \qquad (2.2)$$

The energy per unit time is equal to power i.e. $P = \frac{KE}{t}$; therefore, the kinetic energy (KE) in the wind per second is equal to the power (P) in the wind. So, by considering this, (2.2) can be rearranged as:

$$P\ \left(\frac{J}{s}\right) = \frac{1}{2} * \rho\ (\mathrm{kgm^{-3}}) * \mathrm{A}\ (\mathrm{m^2}) * \frac{l}{t}\ (\frac{m}{s}) *\ \mathrm{V^2}\ (m^2\mathrm{s^{-2}}) \qquad (2.3)$$

$\frac{l}{t}$ is equal to the velocity of air in length, l, therefore, $\frac{l}{t} = v$. Substituting this in (2.3) resulting:

$$P = \frac{1}{2} * \rho * \mathrm{A} * V^3 \qquad (2.4)$$

Based upon (2.4) the unit of power in the wind is $\frac{kgm^2}{s^3}$.

Considering (2.4), the power in the wind is proportional to

- The density of air: At higher height in mountain regions the density of air is lower but in cold climates the average density is possibly up to 10 percent higher than in tropical regions.
- The area through which the wind is passing.
- The velocity of the wind. The output power in the wind strongly depends on the velocity of the wind. i.e. if the wind velocity rises (For example from 2 $\mathrm{ms^{-1}}$ to 3 ms^{-1}), then the power of the wind increases by a factor of more than three.

The power in the wind is not the power extracted by a wind turbine. Some energy is lost in the conversion process.

2.3 Basic Wind Turbine Technology

2.3.1 General Description

A wind turbine is a mechanical device that takes the energy from the wind, which is kinetic energy, and converts it into electricity. The device used to convert mechanical energy to generated electricity is called a wind generator. When mechanical energy is used to drive machinery for example pumping water or grinding grain, the device is called a windmill.

Nowadays, wind turbines are constructed in a wide range of horizontal axis and vertical axis types with different sizes. Small turbines are used for applications such as charging batteries or auxiliary power on sailing boats but large grid-connected arrays of turbines are appropriate for providing an increasingly large source of commercial electric power.

The components of the conventional horizontal axis wind turbines can be separated into three parts; rotor, generator and the structural support components. The rotor is about 20 percent of the wind turbine cost. This includes the blades converting wind energy to low speed rotational power. Approximately 34 percent of the wind turbine cost is for generator components including the electrical generator, the control electronics and most likely a gearbox component, which converts the incoming rotation of low speed shaft to high speed shaft rotation appropriate for generating electricity. A gearbox converts the rotor speed of approximately 22 rpm to 1,500 rpm. The structural support component is about 15 percent of the turbine cost. This includes the tower and rotor yaw mechanism.

2.3.2 Type of Rotors

Over time several designs have been developed for wind turbines. Most of the designs include a rotor driven by the wind induced lift or drag forces.

Generally wind turbines can be classified as either vertical-axis or horizontal-axis wind turbines depending on the type of rotor. The construction of horizontal-axis and vertical-axis wind turbines is shown in Figure 2.6.

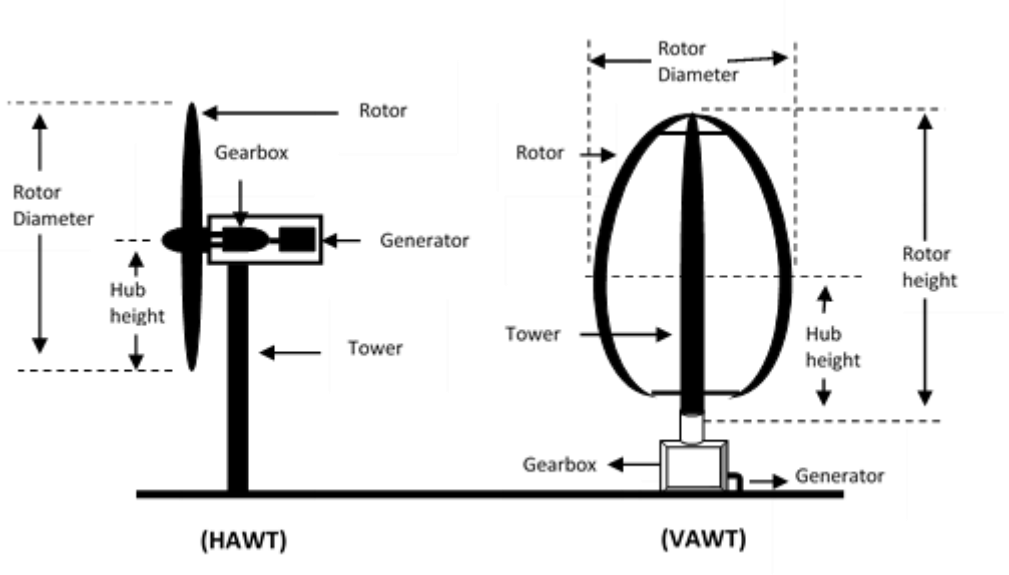

Figure 2.6 - Horizontal-axis and Vertical-axis wind turbines

The type of vertical-axis illustrated in Figure 2.6 has a Darrieus rotor and they are able to capture the wind from any direction without yawing. Location of the generator and transmission devices at ground level is one of the other interesting features of this type of wind turbine.

Vertical-axis wind turbines have some attractive advantages but because of lower energy capture, construction of vertical-axis wind turbines has been declining during the last few decades. Today, almost all the grid-connected wind turbines being constructed are horizontal-axis with either two bladed or three bladed rotors.

The rotor is connected to the main shaft and placed at the top of the tower where the wind has more energy and is less turbulent. The tower also holds up a nacelle. The nacelle is placed behind the turbine's hub, inside which the entire turbine's components including the gearbox and the generator are assembled. Figure 2.7 shows the positions of the turbine's components in the nacelle.

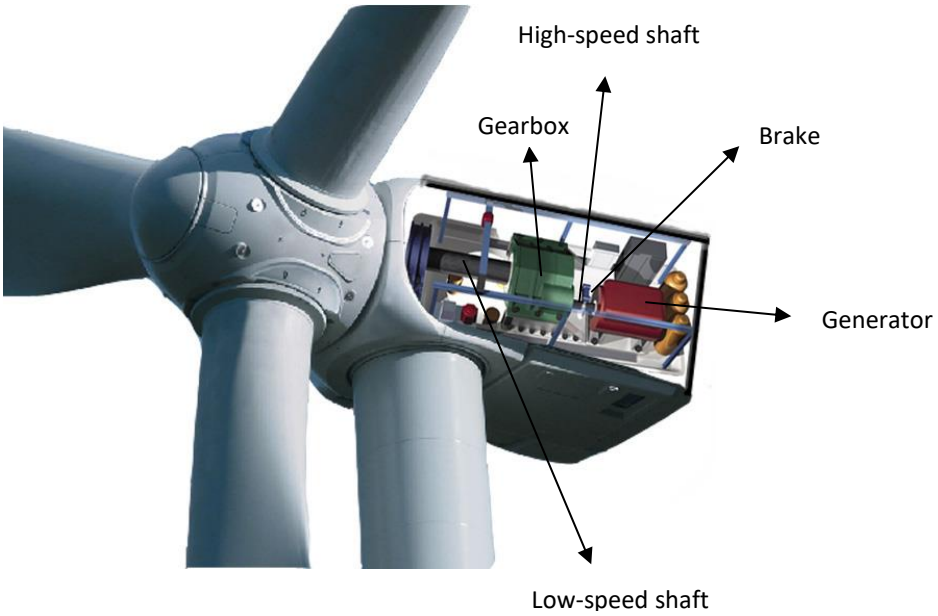

Figure 2.7 – Nacelle

The rotor and nacelle can be turned by the yaw mechanism. In this operation, the rotor turns to face the wind to capture energy as much as possible. And finally, the power electronics are placed at ground level.

2.3.3 Aerodynamics of Wind Turbines

The physics of the forces developed from the behaviour of an object in airflow is called aerodynamics.

The purpose of using wind turbines is to generate electric power and the efficient use of them has been developed by application of aerodynamics to the rotor blade. The basic theory of wind turbine aerodynamics is based on the theory of airplane and helicopter rotors. However, the aerodynamics of wind turbines are different from helicopter rotors.

The actuator disc theory and blade element theory are the two main approaches to obtain aerodynamic models for wind turbines.

Actuator Disc

In this theory, the wind turbine is regarded as an actuator disc. The actuator disc is a generic device that extracts energy from the wind. Regarding Figure 2.8, [3], the actuator disc is immersed in an airflow that is incompressible. Because the actuator disc extracts kinetic energy from the wind, the upstream wind speed, V, should be greater than the downstream wind speed, $V_{-\infty}$. Thus, the disc area, A_D, has to be greater than the upstream cross-

sectional area, A_{∞}, for the stream tube enclosing the disc. The upstream cross-sectional area also is smaller than the downstream cross-sectional area, $A_{-\infty}$.

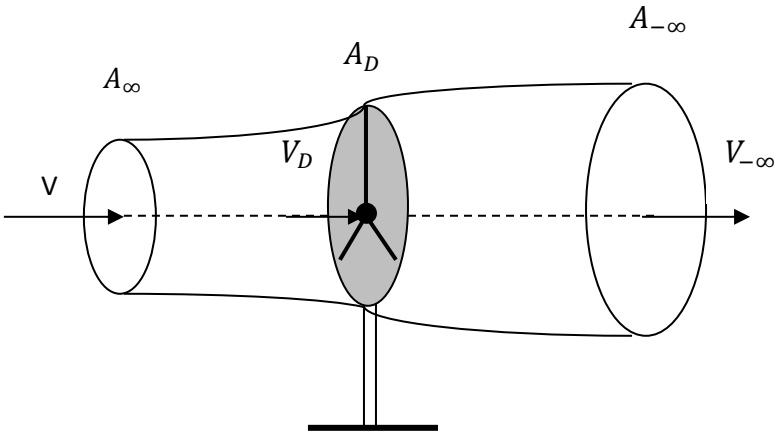

Figure 2.8 - Actuator disc immersed in airflow

Blade element

Blade element theory for wind turbines is used to determine the torque, power and axial thrust force. In this, the aerodynamic force which acts on radial blade elements of small length is analysed. To carry out the analysis, the stream tube, which contains the turbine swept area, is divided into concentric annular stream tubes of small radial length, each of them acts separately.

A transversal section of a blade element is shown in Figure 2.9, [3], viewed from the tip of the blade. This diagram shows the aerodynamic forces on the blade element. At a relative wind speed, V_{rel}, the blade element travels in the airflow, which as a first approach can be imagined as the composition of the upstream wind speed, V, and the tangential blade element speed, $\Omega_r r$. Afterwards an action, the so-called lift force, f_L, is clarified. This happens when around the blade element, the airflow sets up a differential pressure which results in a force perpendicular to the local air movement direction. A drag force, f_D, also occurs in the flow direction.

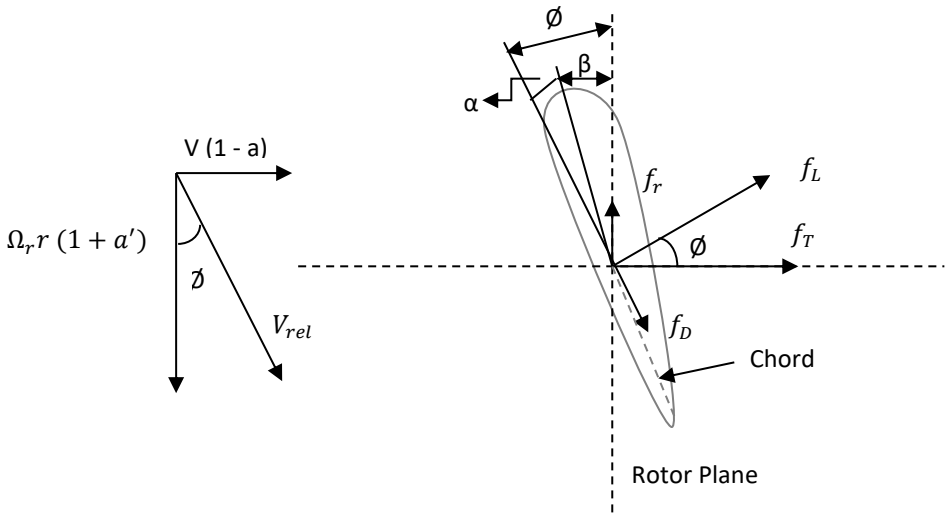

Figure 2.9 - Performance of aerodynamic forces applied on blade element

2.3.4 Force, Torque and Power

The expressions for force, torque and power are presented below.

$$F = \frac{1}{2}\rho\pi R^2 V^2 C_T(\lambda, \beta) \quad (2.5)$$

$$T = \frac{1}{2}\rho\pi R^3 V^2 C_Q(\lambda, \beta) \quad (2.6)$$

$$P = \frac{1}{2}\rho\pi R^2 V^3 C_P(\lambda, \beta) \quad (2.7)$$

C_P is the power coefficient which is the conventional way of representing the ability of a wind turbine to capture energy from the wind and is defined as a ratio of power delivered by the wind turbine to power in the wind.

C_Q is the torque coefficient of the wind turbine and its relation to power coefficient is

$$C_Q = {}^{C_P}/_{\lambda}$$

The tip-speed-ratio, λ, is:

$$\lambda = \frac{\Omega R}{V} \qquad \Omega = \text{Rotor Speed}$$

In the case of variable-pitch rotors, this parameter is very important and, together with β, determines the operating condition of a wind turbine.

The maximum value that the power coefficient can reach, corresponding to the maximum possible energy capture for a wind turbine, is known as the Betz Limit. According to this law

the maximum energy that can be extracting from the wind is 59.3 percent of the energy in the wind. The maximum value of the power coefficient, C_{Pmax}, is $^{16}/_{27} = 0.5926$.

The torque and power coefficients have an important role in control. The Figure 2.10, [3], portrays a typical torque coefficient, C_Q, and power coefficient, C_P, for a fixed-pitch wind turbine.

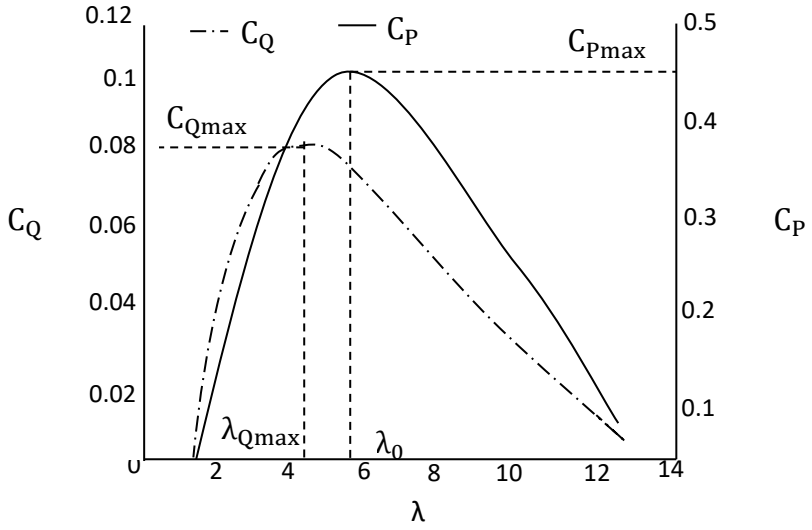

Figure 2.10 - C_Q and C_P of fixed-pitch wind turbine

When β_0, which is the optimum pitch angle, is very small, almost zero, the power coefficient is maximum at (λ_0, β_0). This has two important consequences. The first one is when C_P is maximum at β= 0, then any changes of pitch angle cause lower power capture and the second one is the maximum conversion efficiency is achieved at λ_0. Maximum efficiency can be achieved for variable-speed wind turbine operation over an extensive range of wind speed at least up to rated power. By adjusting the rotational speed proportional to the wind speed, it operates at the optimum tip speed ratio.

2.4 Variable-speed Wind Turbine

2.4.1 Introducing Variable-speed Wind Turbines

Most utility-scale wind turbines are operated at constant speed but most turbines being installed today are variable-speed turbines. The key objective of using these machines is to increase the performance of wind generation and reduce drive-train loads. Comparing variable-speed wind turbines to other types of turbines they have the ability to capture more power. In this type of wind turbine, a power converter is required to interface to the transmission system.

The best situation for a wind turbine to extract energy is when the angle of the airflow over the wind turbine blade aerofoil is in the very small range. This means since the angle of the wind speed changes continuously, the rotational speed of the wind turbine should be proportional to the wind speed.

Two types of generator are used for wind turbines, induction and synchronous generators. The type of the generator used for variable-speed wind turbines is mostly a synchronous generator and it is connected indirectly to the grid.

Comparing variable-speed to constant-speed wind turbines, they have lower power and drive-train load transients and capture more energy from the wind. These types of machines have improved grid-connection properties but have little damping in the drive-train dynamics. Another benefit of variable-speed wind turbines compared to constant-speed wind turbines is that they make less noise. Variable-speed machines have some disadvantages compared to constant-speed turbines such as the cost of the converter and power electronics.

Variable-speed operation enables wind turbines to work at high efficiency. However constant speed wind turbines only reach peak efficiency at one wind speed.

The operation of variable-speed wind turbines in four different modes in below rated and above rated wind speed is explained in the next section.

2.4.2 Operation

The power curve of a wind turbine is depicted in Figure 2.11, [23].

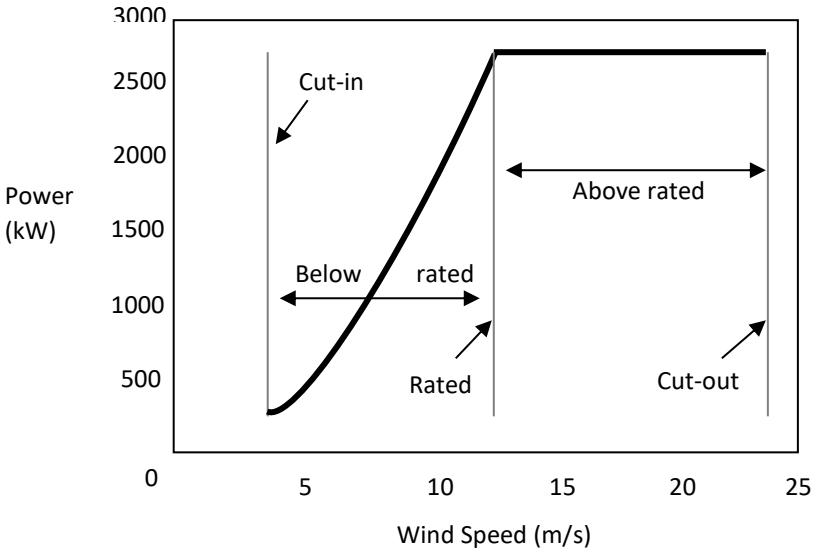

Figure 2.11 - Wind Turbine's ideal Power Curve

In a variable-speed wind turbine there are four modes of operation between the cut-in and cut-out wind speed. The first three modes happen when the wind speed is below rated but the fourth mode occurs when the wind speed is above rated. In below rated wind speed conditions, power generated changes with wind speed but the last mode, when the wind speed is above rated, the power generated and the rotor speed are held constant at the wind turbine rated power and rated speed. The first mode occurs at just above cut-in at low wind speed. In this mode, the wind turbine operates at constant rotor speed. In the second mode, which is in moderate wind speed, the rotor speed is changed to maximise aerodynamic efficiency. In the third mode, the operation again is at constant rotor speed. This mode is in higher wind speed just below rated. In the first three modes, when the wind speed is in below rated, the wind turbine is adjusted by changing the generator reaction torque. The wind turbine operation in the fourth mode is regulated by adjusting the reaction torque from the generator and also changing the pitch of the blades about their longitudinal axes, normally the blades pitch together. In large-MW wind turbines the blades have individual actuators which allows each blade to pitch separately.

3. PREVIOUS WORK

"Of all the forces of nature, I should think the Wind contains the greatest amount of power."
…… ***Abraham Lincoln***

The aim of the work presented in this thesis is to improve the effectiveness of a 330 kW scale variable-speed wind turbine in extracting energy from the wind in below rated wind speed by using an appropriate control strategy. Much research has been done into maximizing the energy capture by the wind turbine and investigating new methods of control.

Different approaches include M.G. Simões, B.K. Bose, R.J. Spiegel, [8], who presented a fuzzy logic based control of a variable speed wind generation system. Fuzzy logic is used to optimize the efficiency and controller performance. The power flow to a double-sided pulse width modulated converter system by a squirrel cage induction generator is described in [8]. This converter system delivers the power to a utility grid or supplies an autonomous system. The wind turbine system has fuzzy logic control with vector control in the inner loops. The method of extracting maximum power in fuzzy logic control systems as proposed in [8] is done by applying three fuzzy logic controllers in the system. The first controller tracks the desired generator speed for optimal aerodynamic efficiency. The machine flux is set by a second fuzzy controller to optimize the machine-converter system efficiency. A third fuzzy controller performs robust speed control against wind gust and turbine torque variation.

A 3.5 kW wind generation system is simulated in [8] to validate all the control strategies and performance of the system. The turbine is modelled with varying torque and some wind turbulence to verify the robustness of the third fuzzy controller. As the first fuzzy controller

increases the generator speed, the output power slowly increases; the machine accelerates to the desired speed with the generated power less than the aerodynamic power. The results indicate a temporary sag in the output power before achieving steady state power. If the speed excessively increases then the power production could be negative. To avoid such conditions, the maximum speed increment should be limited to a reasonable value, which in this case is 75 RPM. The performance of the system with variable wind speed, when the three fuzzy controllers are in operation, is shown in Figure E.1 (in Appendix E.) [8]. If the generator speed remains fixed and the first and the second fuzzy controllers are not working, output power increases with increasing wind velocity. The operation of the first fuzzy controller gives higher power. The incremental power gain caused by the second fuzzy controller gradually diminishes to zero as the wind velocity increases.

Another approach to improve the power capture in below rated wind has been proposed in [7]. Methods for increasing power capture on a variable speed horizontal-axis wind turbine (HAWT) are investigated.

As described in the previous chapter, three main operating regions are defined for a variable-speed wind turbine. The investigation in [7] focused on region 2 operation.

Since there is no accurate way to determine the gain value of the control scheme for a variable speed wind turbine and the aerodynamics of wind turbines change over time, it is not certain if the maximum power would be captured for the gain value used in standard control. In [7] new control ideas are introduced to address these issue by using smaller gain values than is standard to determine, first, the changes in power capture, second, an optimally tracking rotor control scheme and finally, an adaptive control scheme.

It is claimed that using a gain value of 5% - 20% smaller than the gain used for standard region 2 control schemes for a variable speed wind turbine results in improved capture of the energy available in the wind, depending on its turbulence. The reason for this claim is not clearly given in [7]. Figure E.2, obtained by [7], illustrates the average energy capture for a turbine with a very low rotor inertia ($J = 1000\ Kgm^2$) and the Control Advanced Research Turbine (CART). The turbine is a 600 kW, two-bladed, upwind turbine, with rotor inertia of 388,500 $kg.m^2$. In Figure E.2, nominal power capture is the maximum energy capture by the turbine with very low rotor inertia at 1.0. The simulations used three different 100 Hz

sampled wind data sets as inputs. The curves are a result of simulating the CART's behaviour 24 times and lasting one hour for each simulation with a different value of the torque control gain. This figure shows optimum power capture is achieved at anywhere from 89% to 93% of nominal optimal control torque gain. From the star marked curves in Figure E.2, it is seen that reducing the controller gain by an average of 10% below the nominal value causes an increase of 0.5% in energy capture. This is a simple method with no cost and could be implemented on any existing wind turbine, which employs standard torque controller in region 2.

The next approach considered in [7] is an optimally tracking rotor (OTR) control scheme. This method is tested in simulation. This came from the observation that significant power loss occurred in region 2, in which the generator torque is used by the controller of the OTR, as a result of assisting in accelerating and decelerating the rotor in response to the wind speed changes. Depending on various parameters, verified by running 24 one hour simulations [7], the improvement of power capture obtained by this method is about 1.2%.

A small wind generation system (15 kW) is applied in [5] with Neural-Network controller to estimate the wind speed and capture the maximum power available in the wind. The new control system delivers maximum possible electric power, high efficiency and high reliability without mechanical sensors. The wind generation system proposed in [5] has been developed and analysed using a turbine direct drive permanent-magnet synchronous generator (PMSG) and in addition, the proposed method is applied to a 15 kW variable speed cage induction machine wind generation system. A diode six-pulse rectifier, a pulse width-modulation (PWM) inverter and a digital signal processor (DSP) controller are also considered in [5]. An artificial neural network (ANN)-based control algorithm is implemented by a DSP controller. This is performed by estimating the actual wind speed and generating the optimum rotor speed, based on the derived wind speed. The actual rotor speed in [5] is controlled by a PI controller by changing the switching ratio of the PWM inverter. Thus, the load line of the PMSG almost matches the maximum power line of the wind turbine. The reason for using the inverter in [5] is to control the output power delivered to the load. The output power is achieved by changing the switching ratio of the insulated bipolar transistor (IGBT) inverter. The results achieved in [5] show, that the turbine power at 3.5 kW, is fairly close to the rated maximum power of 3.7 kW as wind

speed reaches 11 m/s. The accuracy of the measurement of turbine power is less at smaller values, which affects the control performance at wind speed of 6 m/s or lower.

The method proposed in [5] has the following features compared to the traditional control strategies. These are

i. Better tracking of the wind turbine maximum mechanical power at both dynamic and steady states.
ii. Developing a neural-network-based wind speed estimator to provide fast and accurate wind velocity information.
iii. Presenting a sensorless neural-network-based scheme to compensate the potential drift of wind turbine power coefficient.

Nonlinear robust control to maximize energy capture in a variable speed wind turbine is discussed in [2]. A desired blade pitch angle and rotor speed trajectory generator is considered in [2]. It delivers the optimal set-point to be tracked while ensuring the trajectory remains bounded. A robust control strategy is presented in [2] to track the desired trajectory and increase the power capture in variable speed wind turbines at low to medium wind speed.

The filtered observation error is also defined in [2] to facilitate the later design and analysis. It is stated that aerodynamic rotor power is hard to measure, therefore, an estimated power capture is used instead. An optimum seeking algorithm, used in [2], is Powell's method. The simulation results achieved in [2], Figure E.3, Figure E.4 and Figure E.5, show that the maximum power coefficient, which is obtained using blade-element momentum theory, is 0.4405 and the result of the optimum seeking algorithm was within 5% of the nominal optimum blade pitch angle and rotor speed.

Other approaches to improve power capture such as exploitation of maximum energy from variable speed wind power generation system are presented in [15] and Maximizing Wind Turbine Energy Capture using Multivariable Extremum Seeking Control is described in [6].

For improvement of efficiency of variable speed wind turbines, adaptive control systems able to cope with time variances of the system under control are claimed to be essential [15]. On this basis, an adaptive Takagi-Sugeno-Kang (TSK) model is presented in [15] to

extract maximum energy from the wind with a variable speed wind power generation system. The methodology is based on given input-output numerical data and generates the Takagi-Sugeno-Kang (TSK) fuzzy model, which enables estimation of the maximum extractable power from a variable speed wind turbine with the highest possible accuracy [15]. The design in [15] is based on fuzzy clustering methods for partitioning and continuously optimizes the internal parameters and adapts them to the system.

A self-optimizing controller scheme called “Extremum seeking control (ESC)” is applied to a 600 kW variable speed wind turbine and presented in [6] to maximize the energy capture. The ESC proposed in [6] aims to tune both blade pitch and rotor torque. The input parameters of the ESC loop in [6] are the pitch and the rotor torque references and the output variable is the rotor power. In this process, ESC searches for the optimal control torque and pitch angle based on the measurement of the rotor power. An anti-wind up ESC was applied in [6] to prevent disabling the ESC process due to actuator saturation. To improve the transient performance under sudden changes of wind, the integrator and high-pass filter resetting schemes were applied. Simulation results in [6] show both methods can improve the transient performance, while the integrator resetting works better.

The presented ESC improves energy capture for Region 2 operation. For Region 3, other adaptive control methods using models with faster transient performance are better solutions because the primary objectives in region 3 are speed regulation and disturbance rejection.

The benefit of using the method discussed in [6] is independent from accurate turbine modelling and wind measurement.

All the control methods described in this chapter are seeking to increase the energy extracted from the wind. It is investigated in [22] whether the control method plays a role in this matter and the claim that better controller design would increase the energy capture is examined. A Simulink model of the wind turbine and its controller is used in [22] in order to investigate the aerodynamic efficiency of the rotor of the wind turbine.

To validate the model in [22] the controller is extensively tested by using different controller gain values when tracking the below rated C_{Pmax} curve. The simulations are conducted for

uniform wind speed, and also for the turbulent wind with turbulences of 5%, 10% and 15%. To verify the model in [22], the simulations being used are compared with GH Bladed, which is widely accepted in wind energy community. It is confirmed that, the Simulink model gives similar results and operational behaviour. In [22] full runs for wind speeds from cut-in to cut-out are conducted using the optimum gain for the controller.

A full set of runs was conducted in [22] and the bin method was used to collate results. The efficiencies for wind turbulence intensities of 5%, 10% and 15% are estimated.

The results for the efficiency at different turbulences of wind speed in [22] show that the efficiency is almost one, i.e. at maximum theoretical efficiency. It is harder for the rotor to cope with the fluctuations in the wind when turbulence increases, resulting in a slight loss of energy capture. This energy loss occurs in below rated region in the range of 4 m/s and 12 m/s wind speed, at which the rotor speed is controlled to extract the maximum possible energy from the wind.

All the results for turbulence intensities of 5%, 10% and 15% are compared in [22] for mean wind speeds of 7.5 m/s and 8.5 m/s (Table 4 and Table 5 in Appendix E.). The results reveal almost no energy loss when the right operating strategy is chosen. Changing operating strategy, e.g. changing the below rated maximum power coefficient tracking curve, results in loss of energy capture. The results for different wind turbulences with different controller gains for both mean wind speeds of 7.5 m/s and 8.5 m/s is 99.93% of rotor efficiency in this case. Tracking a curve above or below the ideal curve, results in loss of energy capture. The rotor efficiency could drop to 99.22% in certain circumstances.

Table 4 and Table 5 demonstrate the aerodynamic efficiency difference between different controller gains in different wind turbulences and when the wind speed is less than 0.2%. Even with a weak controller gain such as 0.12, a great amount of energy is captured, so designing a controller to improve the controller gain is not very important and it is not justified economically.

4. MODELLING

"Below wind and crack your cheeks, Rage! Blow!"
*……. **Shakespeare – King Lear***

4.1 Wind Model

4.1.1 Mathematical Modelling of Wind Speed

The use of wind speed models plays an important role in dynamic analysis of a wind turbine and its performance. The interaction of the rotor with the wind causes transient torques and moments that drive the dynamics of horizontal-axis wind turbines.

A combination of wind shear, tower shadow, and wind speed turbulence contributes to the structure of the wind-field. Whenever any wind that causes a torque or moment is considered, most of the changes in wind speed over the swept disc are reduced through averaging over the blades. However, the rotation of the rotor causes significant periodic spectral components with frequencies equal to integer multiples of the rotational angular velocity, Ω_0.

Compared to the spectrum of point wind speed, the power in the spectrum of the wind speed at integer multiples of rotational angular velocity is significantly increased but depleted elsewhere. The spectral peaks also have both a deterministic and stochastic component similar to the structure of the wind-field.

The most significant spectral peak is at rotational angular velocity, Ω_0, for the torques and moments acting on a single blade, such as root bending moment, and the most significant is at rotational angular velocity times the number of blades, $n\Omega_0$, for forces and torques acting on the complete rotor, such as axial hub torque.

As the wind-field goes through the rotor disc, the forces acting on a rotating blade-element are determined by wind speed. The total forces acting on the complete rotor or blade are determined by integrating over them.

A wind model is required for design and analysis of control systems and it is represented by simple ordinary differential equations.

In an ideal wind model, the relationship between torque and wind speed and, also, the average of the wind speed over the rotor are very important.

The rotational averaging of the wind speed is modelled using

$$f(s) = \frac{(\sqrt{2}+\sigma(\bar{V})s)}{(\sqrt{2}+\sqrt{a}\sigma(\bar{V})s)(1+\frac{\sigma(\bar{V})s}{\sqrt{a}})} \qquad (4.1)$$

$$= \frac{(\sigma(\bar{V})s+\sqrt{2})}{\sigma^2(\bar{V})^2s^2+\left(\frac{\sqrt{2}\sigma(\bar{V})}{\sqrt{a}}+\sqrt{a}\sigma(\bar{V})\right)s+\sqrt{2}}$$

On dividing the numerator and denominator by $\sqrt{2}$, (4.1) becomes

$$f(s) = \frac{\frac{\sigma(\bar{V})}{\sqrt{2}}s+1}{\frac{\sigma^2(\bar{V})^2}{\sqrt{2}}s^2+\left(\frac{\sigma(\bar{V})}{\sqrt{a}}+\frac{\sqrt{a}\sigma(\bar{V})}{\sqrt{2}}\right)s+1} \qquad a = 0.55$$

where $\bar{V}$ is the 30 seconds mean wind speed and σ is $\frac{\gamma R}{\bar{V}}$, with γ, the turbulent wind speed decay factor. The full mathematical representation for the wind model is given in chapter 5 and included in Appendix B.

The steady wind speed over the rotor that causes the same aerodynamic forces as the non-uniform wind field is the effective wind speed. The effective wind speed model is a filtered point wind speed.

The relationship between torque and wind speed is

$$T = \frac{1}{2}\rho\pi R^3V^2C_q(\lambda) \qquad (4.2)$$

where ρ is the density of air, 1.225 kg/m^2, R is the radius of rotor, which for the wind turbine used here is 16.5 m, V is the filtered wind speed, λ is the tip speed ratio (which is equal to $\frac{\Omega R}{V}$ with Ω, the angular velocity of the rotor), and $C_q(\lambda)$ is the torque coefficient.

The deterministic components such as tower shadow and wind sheer are not represented in the effective wind speed. It is only meant to represent the low frequency turbulent components of the wind field. High frequency spectral peaks, which occur due to rotational sampling of wind field, are not represented by the effective wind speed. The very low frequency components of the turbulent fluctuations in the wind-field are uniform over the rotor disc.

The dynamics of the spatial filter are given by (4.1). The input of this spatial filter is point wind speed.

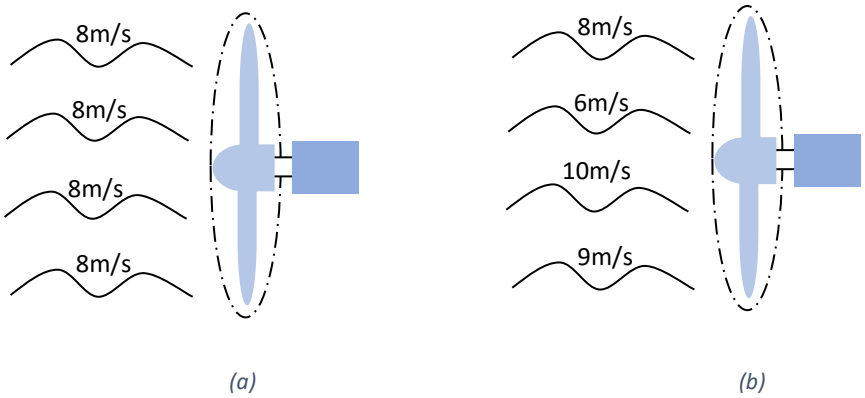

Figure 4.1 – (a) Effective Wind Speed (b) Point Wind Speed

To represent point wind speed fluctuations, many different spectra have been proposed. These spectra are generally of the form:

$$S_v(\omega) = \frac{K_v|\omega|^k}{[1+(\omega T_v)^\alpha]^\delta} \tag{4.3}$$

The parameters α, δ and k depend on the actual spectrum. K_v and T_v are constant with their values dependent on turbulence intensity, roughness of the surface and mean wind speed.

The models of point wind speed generally used are Von Karman, Dryden, Kaimal and the Devenport model. Of the stated models, the most appropriate one for short periods of point wind speed is Von Karman:

$$S_{VK}(\omega) = 0.475\sigma_v^2 \frac{(L/\bar{V})}{(1+(\omega L/\bar{V})^2)^{5/6}} \tag{4.4}$$

where σ_v is the wind turbulence intensity, $\bar{V}$ is the mean wind speed and L is length scale of the turbulence.

The Dryden spectrum is

$$S_D(\omega) = \frac{1}{2\pi}\frac{b_d^2}{(\omega^2+a_d^2)} \quad (4.5)$$

It has the advantage of being a rational polynomial expression such that the wind speed fluctuations, v_d, is modelled by

$$\dot{v}_d = -a_d v_d + b_d \omega \quad (4.6)$$

(4.6) in transfer function form is

$$v_d = \frac{b_d \omega}{s+a_d}$$

where ω is white Gaussian noise. In Appendix B (4.6) is transfer function form.

v_d has zero mean and changes to wind speed. The values of a_d and b_d are determined by

$$a_d = 1.14(\bar{V}/L) \quad ; \quad b_d = \sigma_v\sqrt{2a_d} \quad (4.7)$$

4.1.2 Mean Wind Speed

Filtering the point wind speed by (4.8) estimates the quasi-static mean wind speed, $\bar{V}$.

$$\frac{1}{(\tau s+1)} \quad (4.8)$$

To estimate the axial hub torque generated by the blade, the non-linear torque coefficient can be used in combination with the output from the filter (4.1), Figure 4.2, [19].

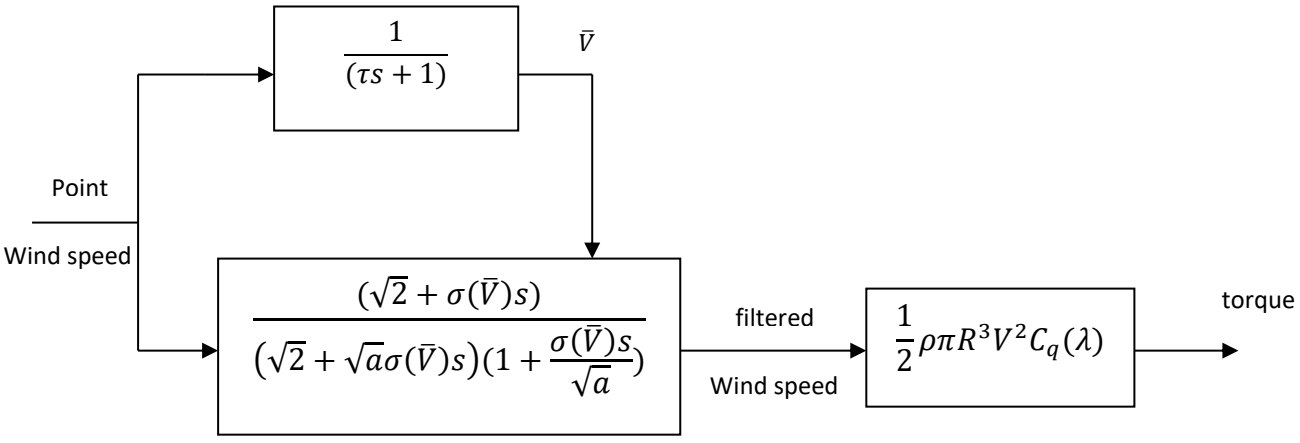

Figure 4.2 – Wind model

The purpose of using (4.8) in the wind speed model, Figure 4.2, is to average the wind speed over τ seconds. τ can be chosen appropriately to be equivalent to a few rotations of the rotor. The model can be expected to be valid for frequencies below $1\Omega_0$.The probability distribution of a long period (5-10 minutes) mean wind speed is the Weibull distribution. In Figure 4.3, [3], a Weibull probability distribution of mean wind speed is shown. The Weibull probability distribution reveals that the larger mean wind speeds rarely occur whereas moderate winds are more frequent. For Figure 4.3, the average wind speed is 7 m/s and the most probable wind speed is 5.5 m/s.

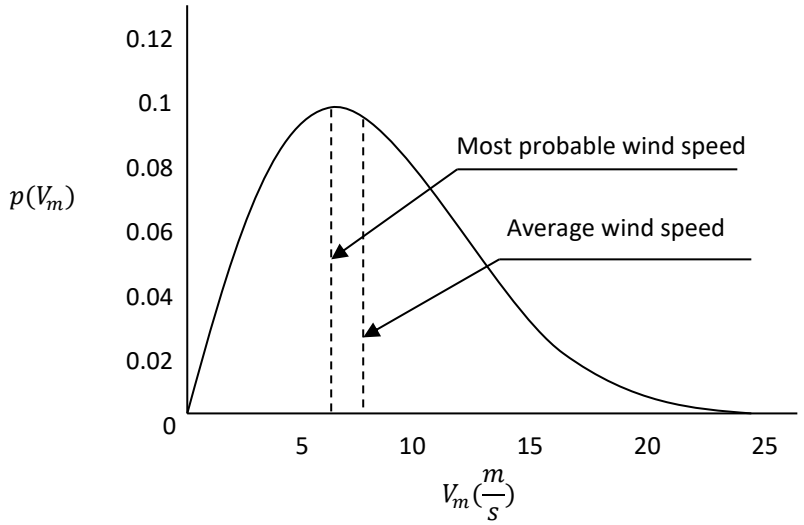

Figure 4.3 - Probability of Weibull distribution of mean wind speed

4.2 Drive-train Model

4.2.1 Drive-train Aspects of Variable-speed Wind Turbines

In all types of wind turbines, the total dynamic behaviour and performance are due to a combination of the structural dynamics, the drive-train and generator dynamics and when necessary, the control system dynamics.

The drive-train dynamics of most types of wind turbines come from a combination of many dynamic modes, including contributions from the tower, blades, low-speed shaft, gearbox, high-speed shaft and mechanical generator.

The drive-train dynamic model of a variable-speed wind turbine is represented in Figure 4.4, [16].

The losses in the drive-train, even very small losses, are important. This is because the mechanical dynamic modes would otherwise be extremely resonant. These losses are viscous damping on the low-speed and high-speed shafts. Generally, most of the damping is related to the rotations of the drive-train, for instance, losses in the gearbox are related to the absolute rotation of the drive-train and losses from shaft twisting, are related to the relative rotation along its length.

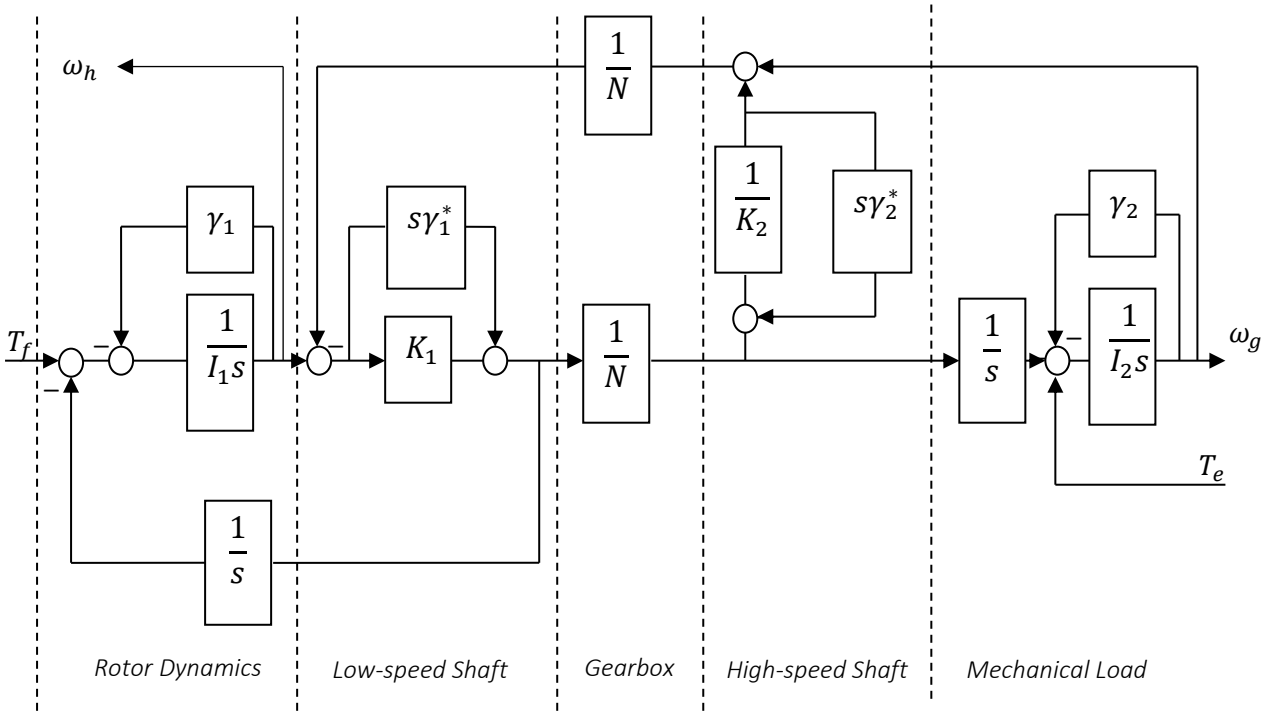

Figure 4.4 – Drive-train model

In this thesis, all parameter values and models chosen are appropriate for a 300 kW three-bladed variable-speed wind turbine. The parameter values of the drive-train model are assumed:

N *Gearbox ratio (38.06:1)*

I_1 *Rotor inertia (100,000 kg.m^2)*

I_2 *Generator inertia (3.8 kg.m^2)*

K_1 *Low-speed Shaft stiffness (1.0 x 10^{6}Nm/rad)*

K_2 *High-speed Shaft stiffness (5.0 x 10^{4}Nm/rad)*

γ_1 *Low-speed Shaft external damping coefficient (980 Nm/rad/s)*

γ_2 *High-speed Shaft external damping coefficient (0.2 Nm/rad/s)*

γ_1^* *Low-speed Shaft internal damping coefficient (9500 Nm/rad/s)*

γ_2^* *High-speed Shaft internal damping coefficient (13 Nm/rad/s)*

The parameter, ω_h, in the drive-train model, Figure 4.4, represents the hub speed and, ω_g, the generator speed. The aerodynamic torque and generator reaction torque are T_f and T_e respectively. The transfer function relating ω_h and ω_g to T_f and T_e is shown in the matrix (4.9).

$$\begin{bmatrix}\omega_h \\ \omega_g\end{bmatrix} = \begin{bmatrix}A(s) & B(s) \\ C(s) & D(s)\end{bmatrix}\begin{bmatrix}T_f \\ T_e\end{bmatrix} \tag{4.9}$$

where:

$$A(s) = \frac{s^2 I_2(K_1+N^2K_2)+s(K_1+N^2K_2)(\gamma_2+(K_1^2\gamma_2^*+N^2K_2^2\gamma_1^*)/K_1+N^2K_2)^2)+K_1K_2}{p(s)}$$

$$B(s) = -\frac{NK_1K_2}{p(s)}$$

$$C(s) = \frac{NK_1K_2}{p(s)}$$

$$D(s) = -\frac{s^2 I_1(K_1+N^2K_2)+s(K_1+N^2K_2)(\gamma_1+N^2(K_1^2\gamma_2^*+N^2K_2^2\gamma_1^*)/K_1+N^2K_2)^2)+N^2K_1K_2}{p(s)}$$

and $p(s)$ is

$$p(s) = s^3 I_1 I_2 (K_1 + N^2 K_2)$$
$$+ s^2((K_1 + N^2 K_2)(I_1 \gamma_2 + I_2 \gamma_1 + (I_1 + N^2 I_2) \text{ X } (K_1^2 \gamma_2^* + N^2 K_2^2 \gamma_1^*)/(K_1 + N^2 K_2)^2))$$
$$+ s(K_1 K_2 (I_1 + N^2 I_2) + (K_1 + N^2 K_2) \text{ X } (\gamma_1 \gamma_2 + (\gamma_1 + N^2 \gamma_2)$$
$$\text{X } (K_1^2 \gamma_2^* + N^2 K_2^2 \gamma_1^*)/(K_1 + N^2 K_2)^2))$$
$$+ K_1 K_2 (\gamma_1 + N^2 \gamma_2)$$

4.3 Power Generation Model

4.3.1 Dynamics of Power Generation Unit (Synchronous Generator)

In variable-speed wind turbines, power is generated by using a synchronous generator, which is connected indirectly to the grid through a rectifier and inverter. The model of electrical characteristics for the dynamics of the power generation unit is shown in Figure 4.5, [16].

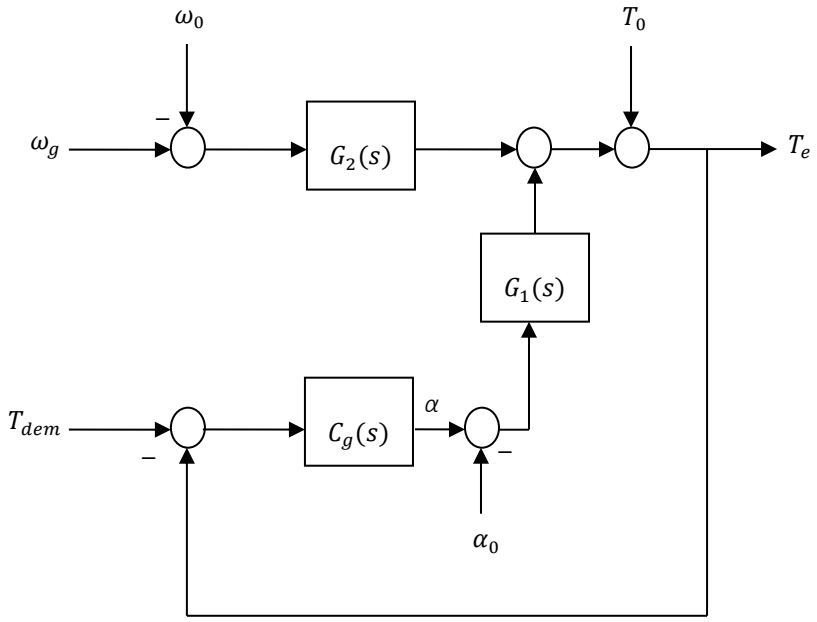

Figure 4.5 - Power generation model

In the model above, α represents rectifier firing angle and α_0, ω_0, T_0 are constants with appropriate values of 0.4697 rad for α_0, 194.5 rad/s for ω_0 and 2154.6 Nm for T_0. The options range from simply open-loop regulation to entirely closed-loop regulation. In open-loop regulation, the power generation unit input values are continuously set to those required to adjust the generator reaction torque to its demanded value. It has the normal problem of all open-loop regulation in being sensitive to disturbances. As shown in Figure 4.5, in closed-loop regulation, generator reaction torque is fedback around the power generation unit. The controller $C_g(s)$ is designed to ensure that the generator reaction torque is set to its demanded torque value, T_{dem}.

For the wind turbine connected here, appropriate transfer functions for $G_1(s)$ and $G_2(s)$, Figure 4.5, the electrical characteristics of the power generation unit, are

$$G_1(s) = \frac{-295.429(s+7.6383)(s-200)(s-644.552)}{(s^2+26.0256s+3314.883)(s+186.6475)} \qquad (4.10)$$

$$G_2(s) = \frac{-42.71111(s+10.3674)(s+23.1307)(s-200)}{(s^2+12.08108s+2189.949)(s+200)} \quad (4.11)$$

The bode plots of the above transfer functions are illustrated in Figure 4.7, [16].

The controller, $C_g(s)$, is chosen as

$$C_g(s) = -\frac{4.2}{s(s+15)^2} \quad (4.12)$$

The Bode plot depicted below in Figure 4.6, [16] represents the open-loop system transfer function $C_g(s)G_1(s)$.

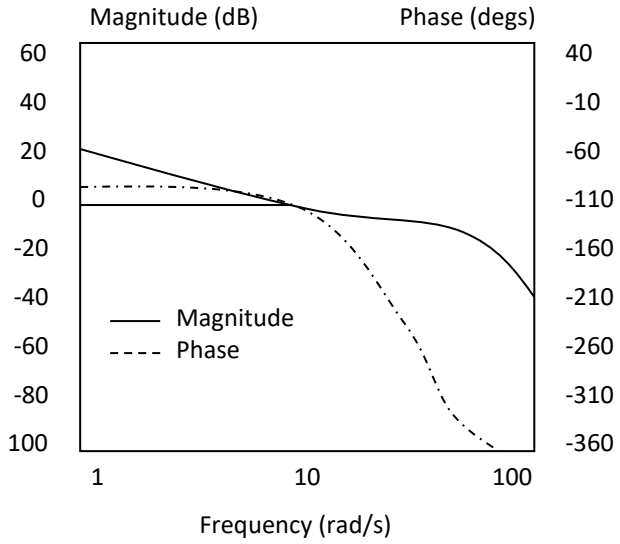

Figure 4.6 - Bode plot representing the open-loop system transfer function $C_g(s)G_1(s)$

Taking account of additional electrical losses in the drive-train model, Figure 4.4, the generated power, P_g, is

$$P_g = E_{ff}\Omega T_D \quad (4.13)$$

where E_{ff} is the efficiency of the electrical aspects of the power generation unit. E_{ff} depends on Ω which is the rotor speed. T_D represents the drive-train torque at the hub.

The relationship of generator reaction torque to generator speed is known for a specific control strategy and so an appropriate E_{ff}, can be defined.

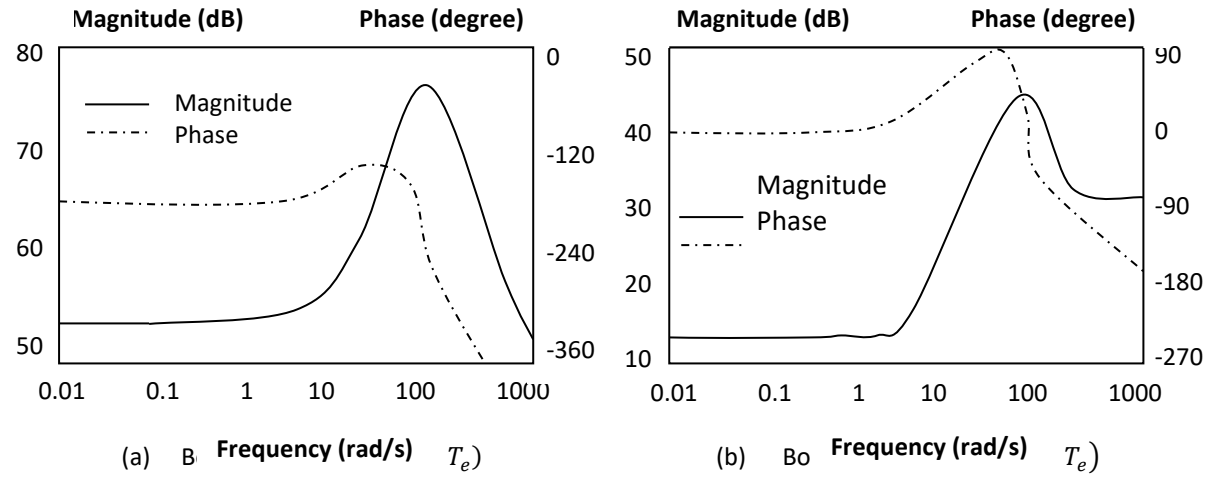

Figure 4.7 - Dynamics model of wind turbine power generation unit

Wind turbine power generation by using synchronous generators is described in more detail in [18].

5. SIMULATION

"The wind moans, like a long wail from some despairing soul shut out in the awful storm."
…… ***W.H. Gibson – Pastoral Days***

5.1 The Use of MATLAB/Simulink

In previous decades, system engineers used high-level languages such as FORTRAN, supported by libraries of numerical algorithms, to design control systems. Today, by using computer systems with advanced operating systems, high resolution displays and superior computer graphics, systems are easily simulated by simulation software. One of the best-known simulation software packages in use today is MATLAB/Simulink.

MATLAB stands for MATrix LABoratory and generally it is used in engineering facilities to programming design a system or analyse system behaviour. This software is also used as a high-level language for technical tasks. MATLAB is interactive software package for numerical computation, symbolic computation and scientific visualization. MATLAB is an interactive environment that allows the user to program as well as to visualise computations. MATLAB also provides for computational calculations. In this content, the client requires better control of graphical output. Other capabilities of MATLAB are to provide a Graphical User Interface (GUI) toolbox, which is not utilized in this project. The GUI toolbox, which also called Guide, is for creation of push buttons, text boxes and similar facilities.

Simulink is an interactive program with a graphical interface that is designed to perform scientific and engineering numerical calculation as well as being used for modelling, simulating and analysing dynamic systems and its fundamental data element is a matrix of arbitrary dimensions. Simulink supports linear and nonlinear systems, and has the ability to model them in continuous time, discrete time or a hybrid of the two. Creating a model block

diagram in Simulink would be done by applying blocks from the comprehensive block libraries and connecting them together. Models Created in Simulink are hierarchical and can be built by constructing subsystem models. This approach gives insight and understanding of how a model is organized and how its parts interact. The simulation results can also be stored in the MATLAB workspace for post processing and visualising. This is possible because MATLAB and Simulink are integrated. In interactive systems using Simulink, menus are more convenient while normally the command-line approach is more helpful for running a batch of simulations. The simulation results can be seen by applying scope blocks and similar display blocks even while the simulation is running. Additionally, parameters can be changed immediately to see the consequences of the system and for visualization and post-processing the simulation results which can then be placed in MATLAB workspace.

Simulink models have been used in this project to represent the wind turbine and its controller.

5.2 Simulation of the Wind Turbine

As explained in Chapter 4 and also shown in Figure 4.2, the input to the wind model is point wind speed. Using the transfer function form of (4.6), the model of point wind speed is that of Figure 5.1.

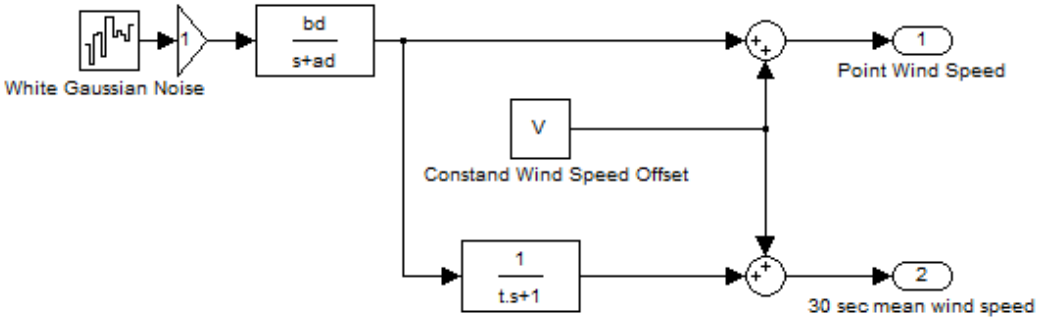

Figure 5.1 - Point wind speed simulation

The plot of the point wind speed for a simulation of 1,000 seconds with a mean of 8 m/s and turbulence intensity of 20% is shown in Figure 5.2.

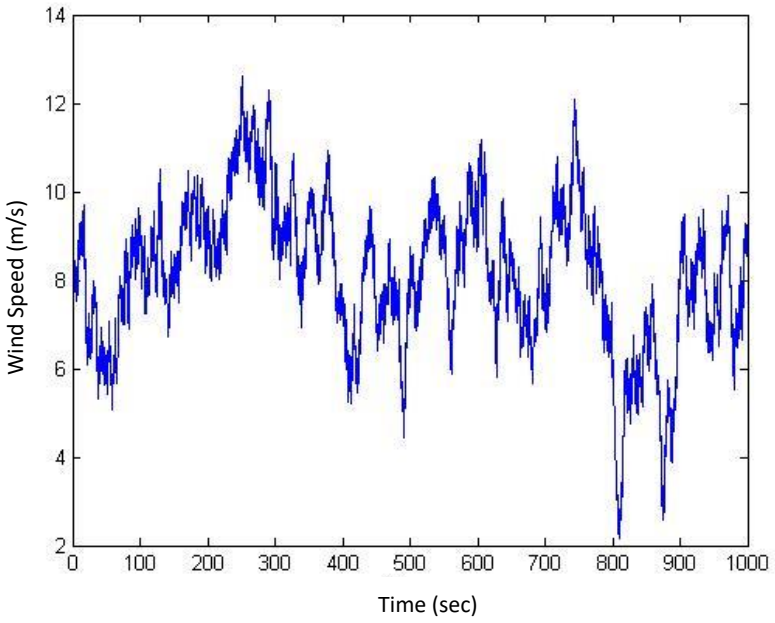

Figure 5.2 - The plot of Point Wind Speed

In the previous chapter, it is explained that a filtered wind speed can be used to estimate the axial hub torque generated by the rotor. Rotational averaging of the wind speed is represented by (4.1), and is modelled by the following transfer function.

$$y = \frac{\sqrt{2}+\sigma(\bar{V})s}{\left(\sqrt{2}+\sqrt{a}\sigma(\bar{V})s\right)\left(1+\sigma(\bar{V})s/\sqrt{a}\right)}$$

The above transfer function is reformulated as an integral equation as below for simulation in Simulink.

$$y = \frac{\left(\sigma(\bar{V})/\sqrt{2}\right)s+1}{\frac{\sigma^2(\bar{V})^2}{\sqrt{2}}s^2+\left(\frac{\sigma(\bar{V})}{\sqrt{a}}+\frac{\sqrt{a}\sigma(\bar{V})}{\sqrt{2}}\right)s+1}$$

$$\frac{\sigma^2(\bar{V})^2}{\sqrt{2}}\ddot{y} + \left(\frac{1}{\sqrt{a}}+\frac{\sqrt{a}}{\sqrt{2}}\right)\sigma(\bar{V})\dot{y} + y = \frac{1}{\sqrt{2}}\sigma(\bar{V})\dot{x} + x$$

$$\frac{\sigma(\bar{V})}{\sqrt{2}}\left(\sigma(\bar{V})\dot{y} - x\right)^{\cdot} = x - y - \left(\frac{1}{\sqrt{a}}+\frac{\sqrt{a}}{\sqrt{2}}\right)\sigma(\bar{V})\dot{y}$$

$$\left(\sigma(\bar{V})\dot{y} - x\right) = \int \frac{\sqrt{2}}{\sigma(\bar{V})}\left[x - y - \left(\frac{1}{\sqrt{a}}+\frac{\sqrt{a}}{\sqrt{2}}\right)\sigma(\bar{V})\dot{y}\right]dt$$

$$\dot{y} = \frac{x}{\sigma(\bar{V})} + \frac{1}{\sigma(\bar{V})}\int \frac{\sqrt{2}}{\sigma(\bar{V})}\left[x - y - \left(\frac{1}{\sqrt{a}}+\frac{\sqrt{a}}{\sqrt{2}}\right)\sigma(\bar{V})\dot{y}\right]dt$$

$$y = \int\left\{\frac{x}{\sigma(\bar{V})} + \sigma^{-1}(\bar{V})\int\sqrt{2}\sigma^{-1}(\bar{V})\left[x - y - \left(\frac{1}{\sqrt{a}}+\frac{\sqrt{a}}{\sqrt{2}}\right)\sigma(\bar{V})\dot{y}\right]dt\right\}dt \qquad (5.1)$$

From (5.1), rotational averaging of the wind speed is simulated as in Figure 5.3, where K is $\left(\frac{1}{\sqrt{a}}+\frac{\sqrt{a}}{\sqrt{2}}\right)$.

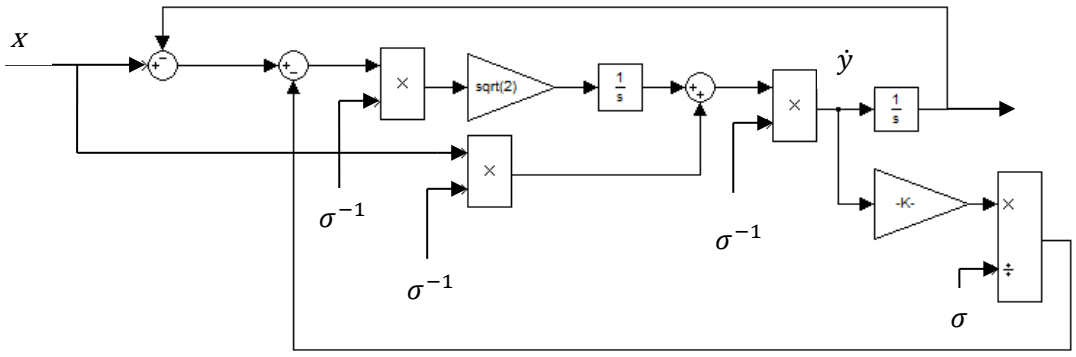

Figure 5.3 - Simulation of rotational averaging of the wind speed

Plots of wind speed for different wind turbulences at mean wind speed of 8 m/s obtained from the simulation in Figure 5.3, are shown in Figure 5.4.

In order to simulate the aerodynamic torque on the rotor, the torque coefficient for the rotor is implemented as a look-up table for the zero degree pitch angle. The values for the

torque coefficient are tabulated in Appendix D and the values for zero pitch shown in Table 2.

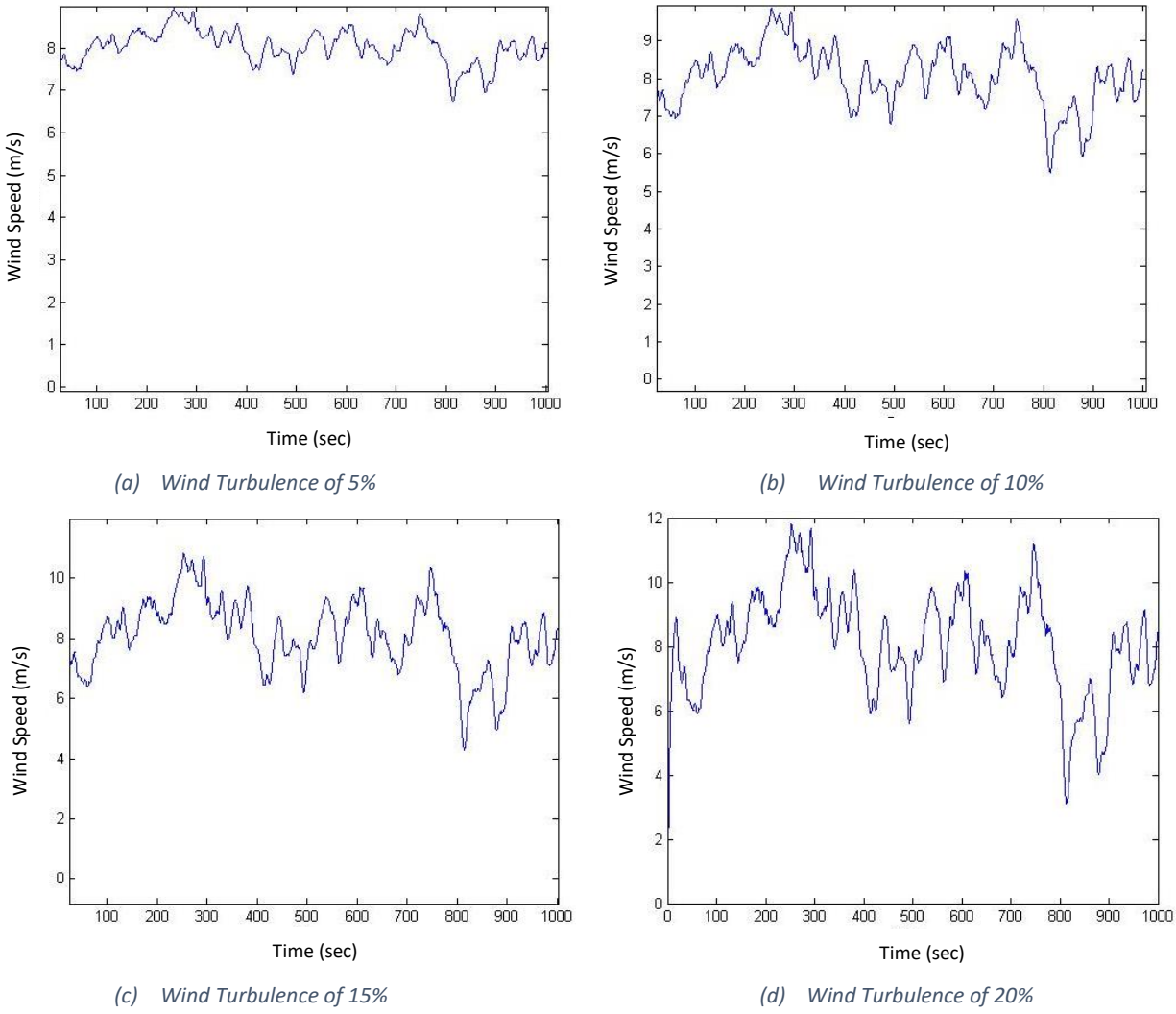

(a) Wind Turbulence of 5%

(b) Wind Turbulence of 10%

(c) Wind Turbulence of 15%

(d) Wind Turbulence of 20%

Figure 5.4 - The plots of wind speed for different wind turbulences

Table 2 - Power Coefficients for the rotor at 0° pitch angle

λ / β	2	3	4	4.5	5	5.5	6	6.25	6.5	7	8	9	12	15
0°	0.058	0.162	0.34	0.4185	0.445	0.4565	0.462	0.4625	0.4615	0.455	0.432	0.396	0.204	- 0.135

The simulation of aerodynamic torque of the rotor, (4.2), is as shown in Figure 5.5.

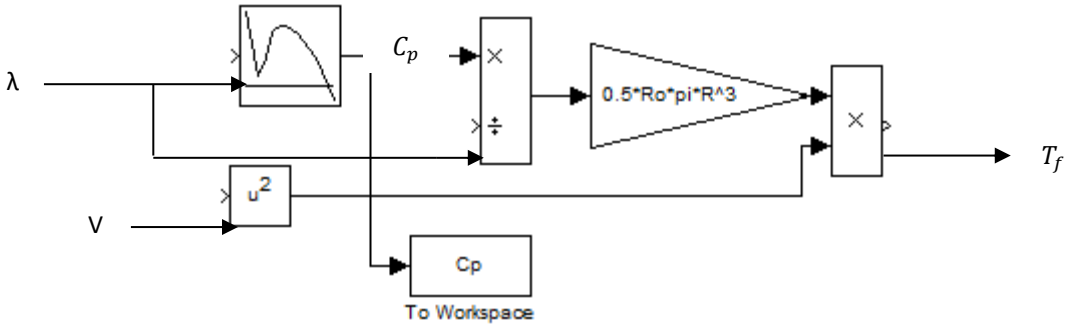

Figure 5.5 - Simulation of the aerodynamic torque

The aerodynamic torque obtained from the simulation in Figure 5.5 depicted in Figure 5.6 for turbulence intensity of 20% and different wind speeds.

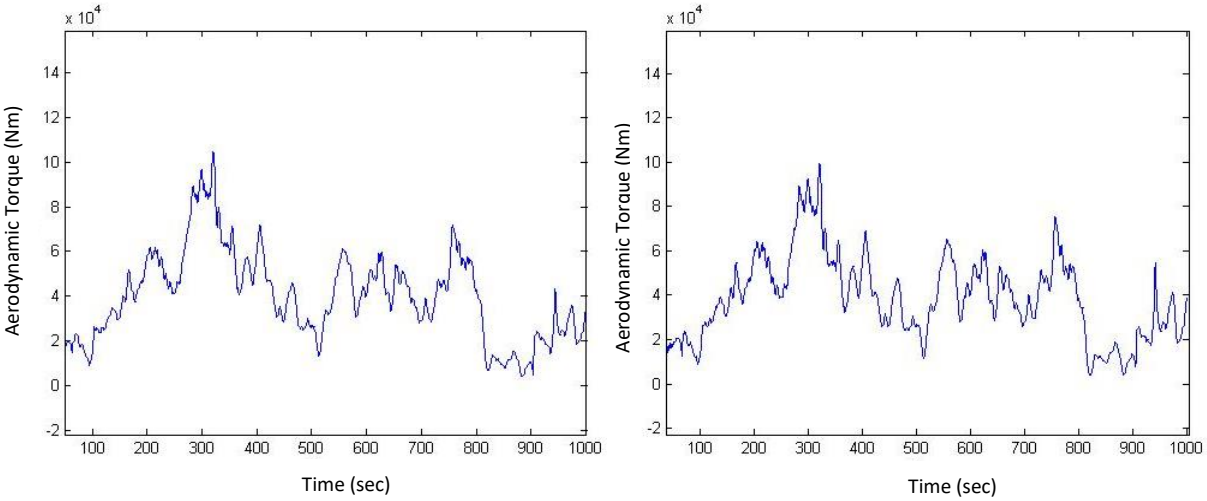

(a) Wind speed of 4 m/s

(b) Wind speed of 6 m/s

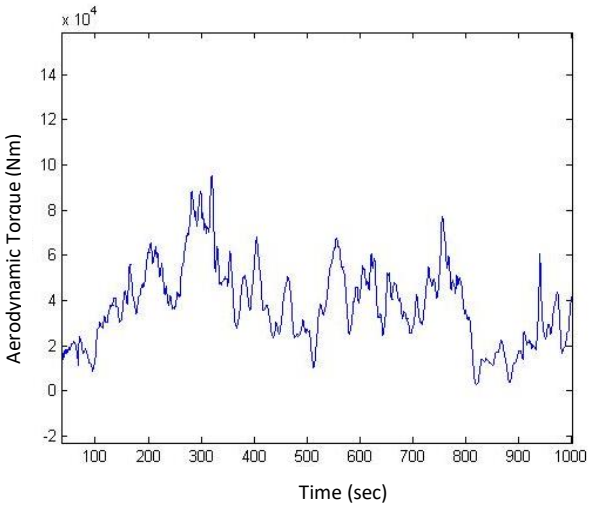

(c) Wind speed of 8 m/s

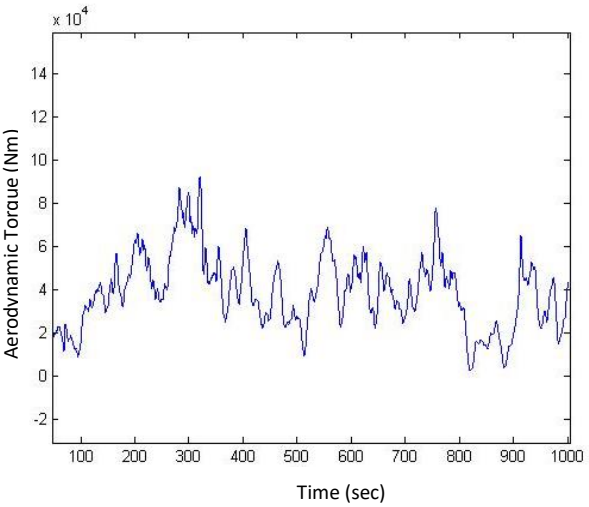

(d) Wind speed of 10 m/s

Figure 5.6 - Aerodynamic torque for different speeds of wind

Combining Figures 5.1, 5.3 and 5.5, the wind model is simulated as depicted in Figure 5.7.

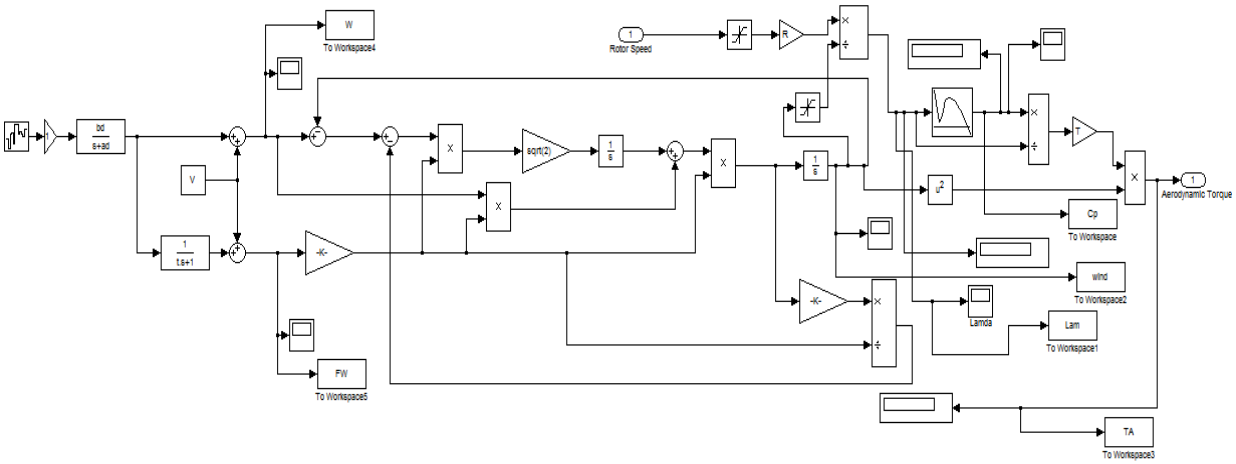

Figure 5.7 - Simulation of the wind model

A first order filter $\frac{1}{\tau s+1}$ is used in Figure 5.7 to average the point wind speed over a short time, τ. The appropriate value to be chosen for τ should be equivalent to a few rotations by rotor; therefore, it was chosen to be 30 seconds. The plot of the filtered wind speed with constant offset of 8 m/s and turbulence intensity of 20% is depicted in Figure 5.8.

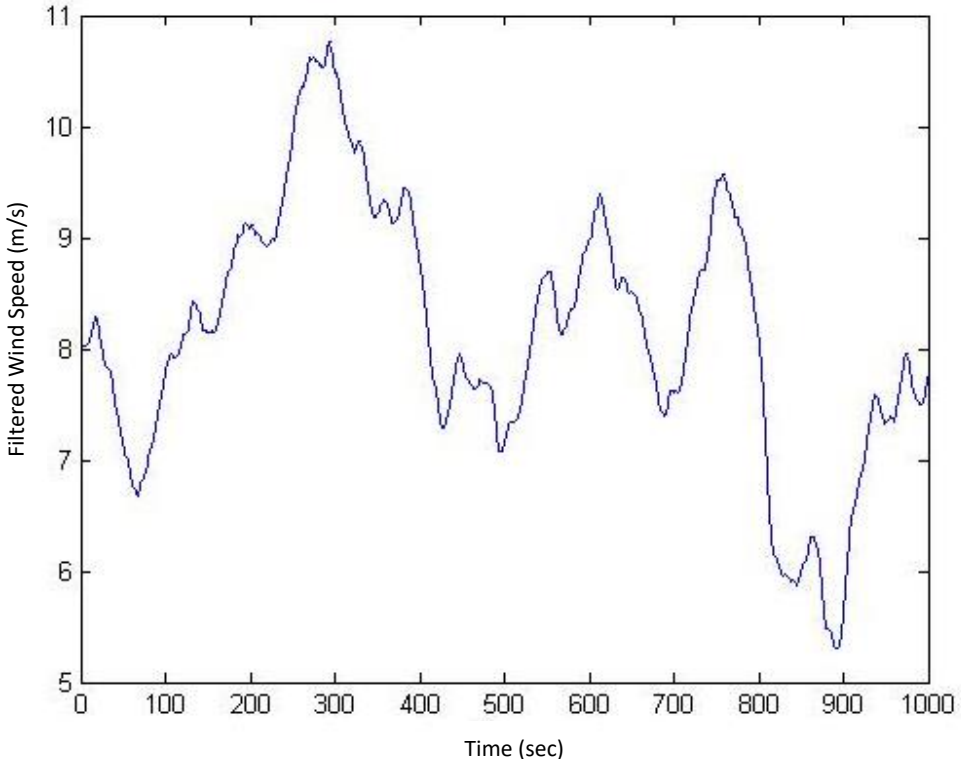

Figure 5.8 - Plot of the filtered wind speed

5.3 Simulation of the Drive-train

5.3.1 Drive-train Dynamics

A simulation of the drive-train is constructed from the dynamic model described in section 4.2.

The dynamics of the drive-train for a wind turbine includes lumped inertia of the rotor, I_1, the external damping coefficient of the low-speed shaft, γ_1, stiffness of low-speed shaft, K_1, which are related to the drive-train physical parameters by

$$I_1 = J + J_H \frac{K_R}{(K_R+K_H)} + \frac{K_1\left[\left(J_S+J_H K_H/(K_R+K_H)\right)\left(K_{GB}+(N-1)^2K_2\right)-N(N-1)J_{GS}K_2\right]}{(K_1+N^2K_2)[K_{GB}+(N-1)^2/N^2k]} \quad (5.2)$$

$$\gamma_1 = B_{G1} + B_s \quad (5.3)$$

$$K_1 = \frac{K_R K_H}{(K_R+K_H)}\left(1+\frac{K_R}{(K_R+K_H)}\frac{J_H}{J}\right) \quad (5.4)$$

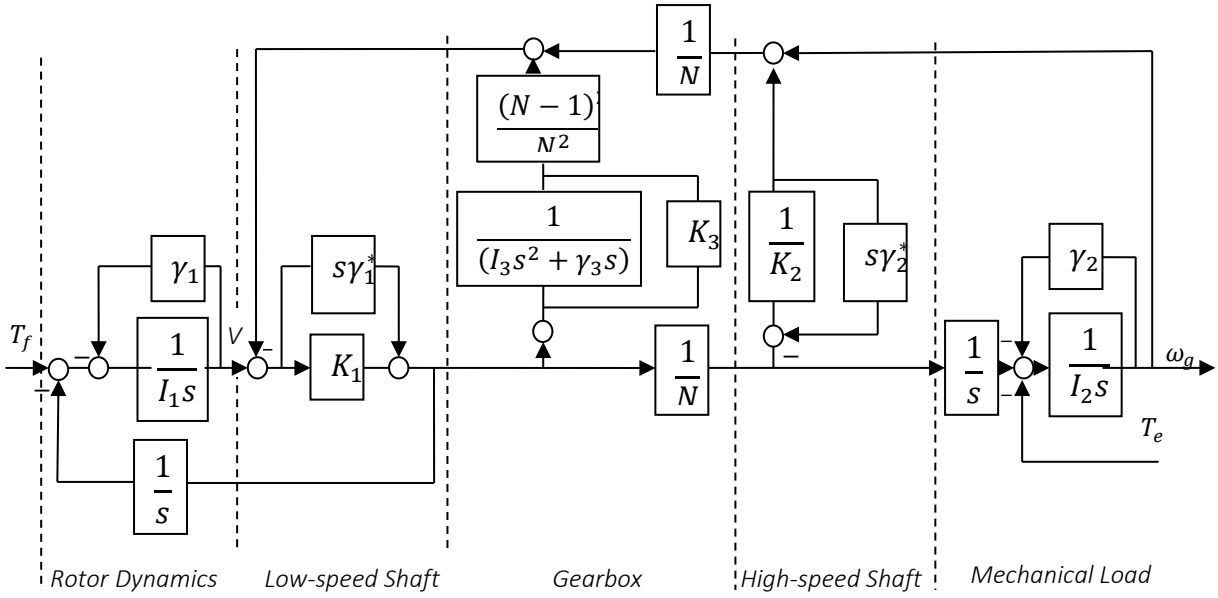

Figure 5.9 - The drive-train dynamics representation

The inertia of the lump generator rotor, I_2, and the external damping coefficient of high-speed shaft, γ_2, are related to the drive-train physical parameters by

$$I_2 = J_G + \frac{K_2(J_S+J_H K_H/(K_R+K_H))(K_{GB}+(N-1)/NJ_{GS}K_1)}{(K_1+N^2K_2)[K_{GB}+(N-1)^2/N^2k]} \quad (5.5)$$

$$\gamma_2 = B_{G2} + B_S \quad (5.6)$$

The stiffness of the high-speed shaft is K_2. The inertia of the lumped gearbox, I_3, the damping of the gearbox, γ_3, and the gearbox mounting stiffness, K_3, are related to the drive-train physical parameters by

$$I_3 = J_{GG} - \frac{J_{GG}^2}{J_S + J_H K_H/(K_R + K_H)} \tag{5.7}$$

$$\gamma_3 = B_{G3} + B_{GB} \tag{5.8}$$

$$K_3 = K_{GB} \tag{5.9}$$

All the parameters of (5.2), (5.3), (5.4), (5.5), (5.6), (5.7), (5.8) and (5.9) are discussed in [21].

Here, the gearbox is not compliantly mounted and the simulation of model depicted in Figure 5.9 is simplified as shown in Figure 5.10.

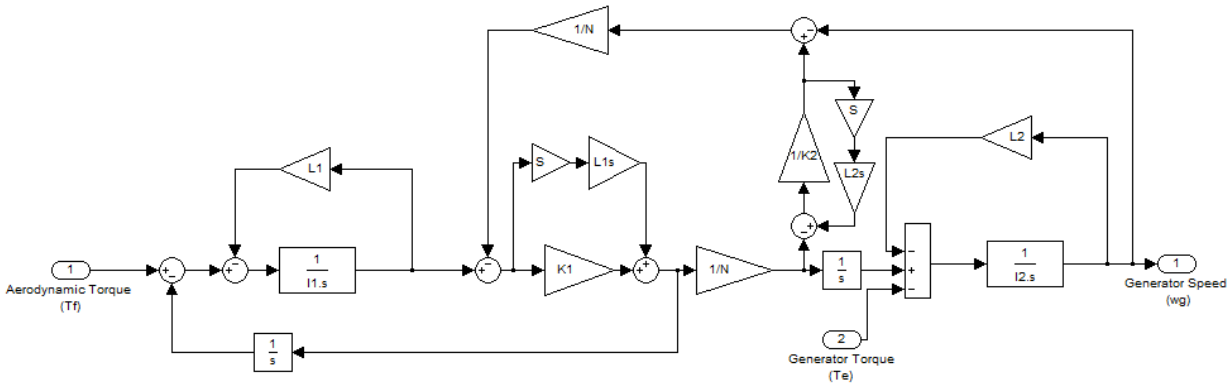

Figure 5.10 - Simulation of drive-train model without mounted gearbox

The low-speed shaft and high-speed shaft in Figure 5.10 contain derivative terms. For better performance of the simulation, the derivative terms should be eliminated. The simulation of drive-train model is now as in Figure 5.11.

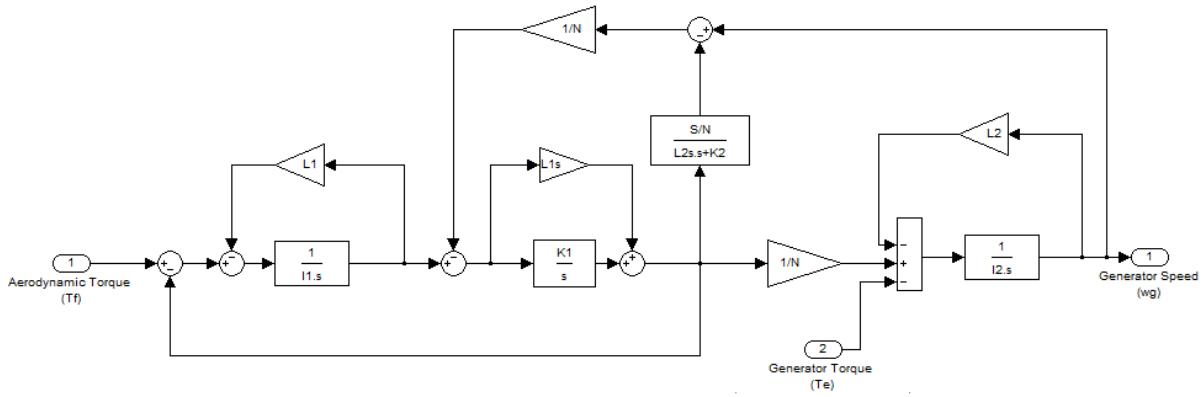

Figure 5.11 - Simulation of drive-train model with eliminated derivative terms

In the above simulation, an algebraic loop exists. This happens when an input port is driven by the output from the same block with direct feedthrough, which means the input depends directly on the value of output port. The mathematical solution of the algebraic loop is discussed in the next section.

5.3.2 Mathematical Representation of Algebraic Loop

The mathematical solution for the algebraic loop existing in Figure 5.11 is discussed below.

After eliminating derivative terms from the model, the section containing the low-speed shaft and high-speed shaft from the simulation in Figure 5.11 becomes as shown in Figure 5.12.

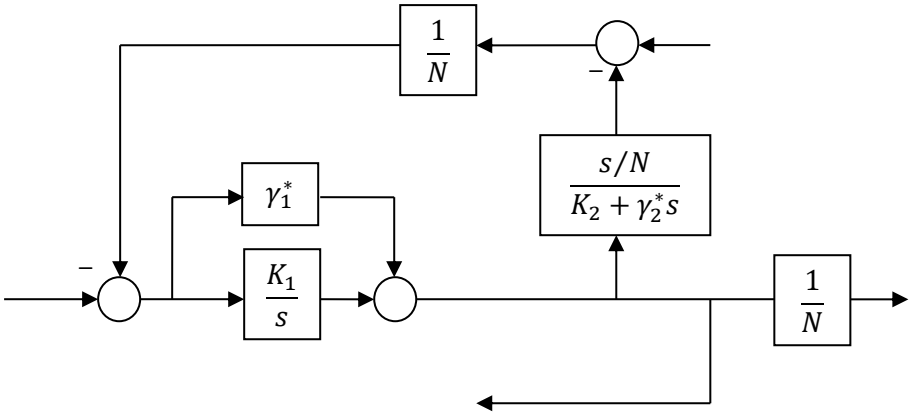

Figure 5.12 - Simulation of low-speed shaft and high-speed shaft

The simplified block diagram simulation and the section with an algebraic loop are clarified in Figure 5.13.

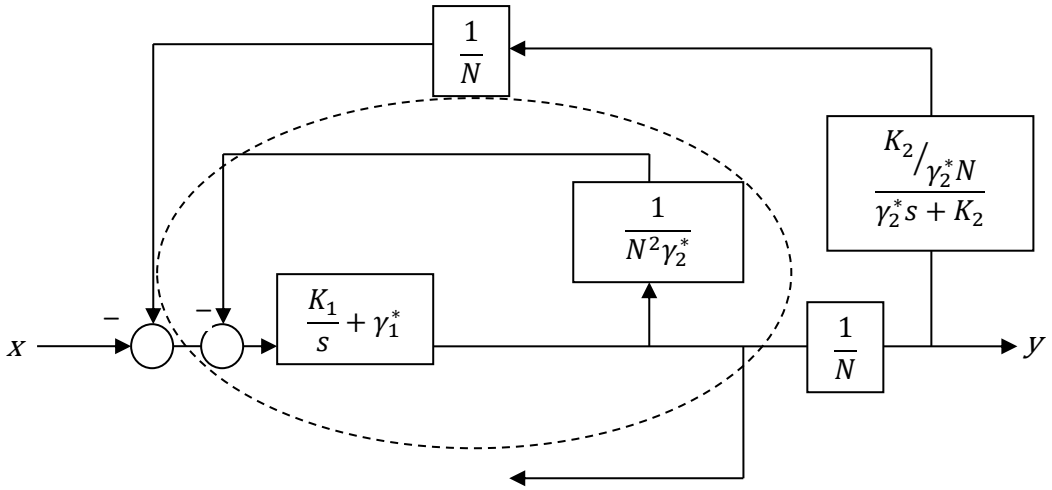

Figure 5.13 - Simplified block diagram simulation with algebraic loop

The inner loop in Figure 5.13, which is separated by the dashed line, contains the algebraic loop and is replaced by G(s) as shown in Figure 5.14.

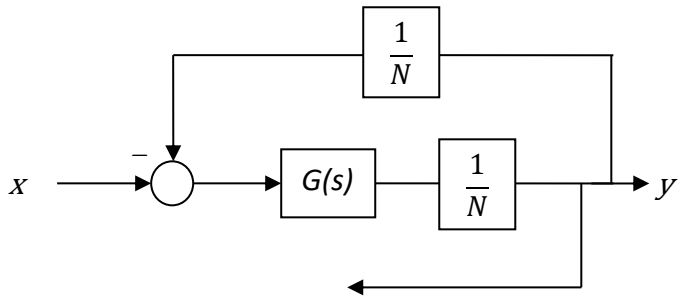

Figure 5.14 - Simplified block diagram with G(s) replaced for algebraic loop

G(s) is determined as below.

$$y = \left(\frac{K_1}{s} + \gamma_1^*\right)\left(x - \left(\frac{1}{N^2\gamma_2^*}\right)y\right)$$

$$\frac{K_1+\gamma_1^* s}{s}x - y\left[\left(\frac{K_1+\gamma_1^* s}{s}\right)\left(\frac{1}{N^2\gamma_2^*}\right)\right] = y$$

$$\frac{K_1+\gamma_1^* s}{s}x - y\left(\frac{K_1+\gamma_1^* s}{N^2\gamma_2^* s}\right) = y$$

$$\frac{K_1+\gamma_1^* s}{s}x = y + y\left(\frac{K_1+\gamma_1^* s}{N^2\gamma_2^* s}\right)$$

$$\frac{K_1+\gamma_1^* s}{s}x = y\left(\frac{K_1+\gamma_1^* s}{N^2\gamma_2^* s} + 1\right)$$

$$y = \frac{\frac{K_1+\gamma_1^* s}{s}}{\frac{K_1+\gamma_1^* s}{N^2\gamma_2^* s}+1} x$$

Multiplying the numerator and denominator by $N^2\gamma_2^* s$, the above transfer function is as follows

$$y = \frac{\frac{(\gamma_1^* s+K_1)\left(N^2\gamma_2^* s\right)}{s}}{\gamma_1^* s+K_1+N^2\gamma_2^* s} x$$

$$y = \frac{\frac{K_1 N^2\gamma_2^* s+N^2\gamma_1^*\gamma_2^* s^2}{s}}{(\gamma_1^*+N^2\gamma_2^*)s+K_1} x$$

$$y = \frac{\gamma_1^*\gamma_2^* N^2 s+K_1 N^2\gamma_2^*}{(\gamma_1^*+N^2\gamma_2^*)s+K_1} x \qquad (5.10)$$

From (5.10) the transfer function, G(s), is

$$G(s) = \frac{\gamma_1^*\gamma_2^* N^2 s+K_1 N^2\gamma_2^*}{(\gamma_1^*+N^2\gamma_2^*)s+K_1}$$

Now the simulation of the drive-train model represented in Figure 4.4 is modified to Figure 5.15.

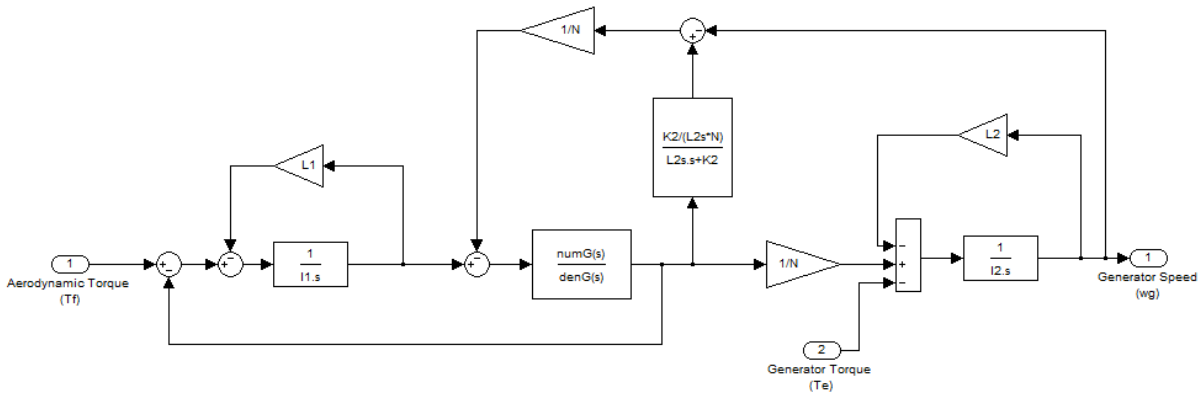

Figure 5.15 - Simulation of the drive-train model

The input to the drive-train model is aerodynamic torque, which is obtained from the output of the wind model. The output of the drive-train simulation is the generator speed. The output of the drive-train model is the input to the synchronous generator which is discussed in the next section.

5.4 Simulation of Power Generation

In section 4.3, the model of power generation is described in detail, see Figure 4.5. The output of the generator is the generator reaction torque, which is controlled through a feedback loop connected around the generator. It is also fedback through the drive-train to balance the aerodynamic torque. The generator speed is an input to the generator. The model depicted in Figure 4.5 is a multi-input single-output (MISO) system. The other input of the system is the demanded torque that is the generator reaction torque set point.

The variables α_0, ω_0 and T_0, as stated in section 4.3, are set to 0.4697 rad, 194.5 rad/s and 2,154.6 Nm, respectively. The Simulink simulation of the model in Figure 4.5 is depicted in Figure 5.16.

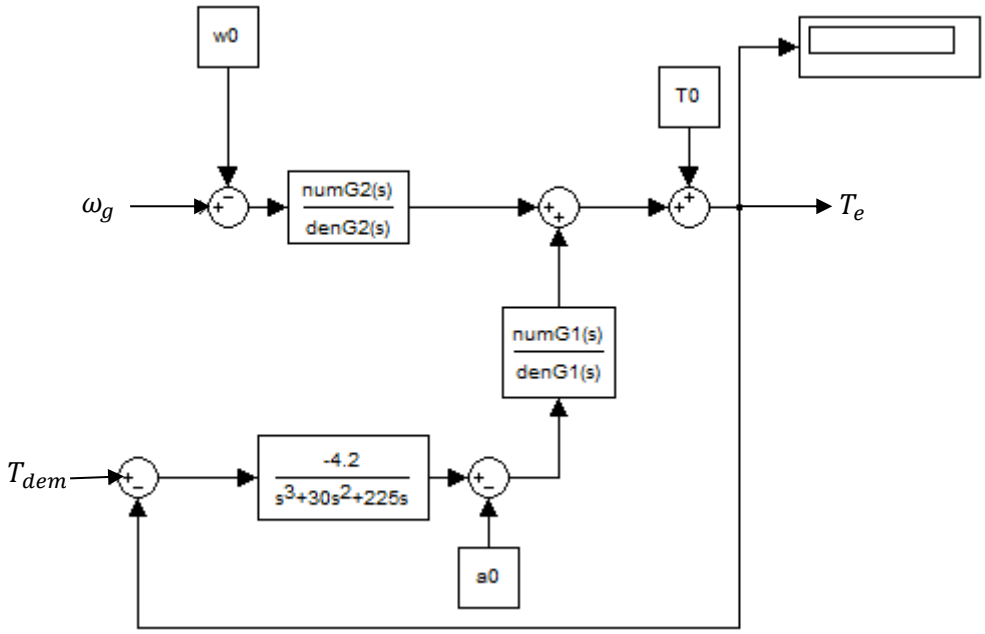

Figure 5.16 - Simulation of synchronous generator

where $\frac{numG1(s)}{denG1(s)}$ and $\frac{numG2(s)}{denG2(s)}$ are respectively the transfer functions of (4.10) and (4.11). Simplified transfer functions, (5.11) and (5.12), are used in the simulation model.

$$G_1(s) = \frac{-295.43s^3+2.52*10^5s^2-3.62*10^7s-2.9*10^8}{s^3+212.67s^2+8.17*10^3s+6.19*10^5} \quad (5.11)$$

$$G_2(s) = \frac{-42.71s^3+7.11*10^3s^2+2.76*10^5s+2.26*10^6}{s^3+212.08s^2+4606s+4.38*10^5} \quad (5.12)$$

The output of the synchronous generator from the simulation, Figure 5.16, is shown in the plots in Figure 5.17.

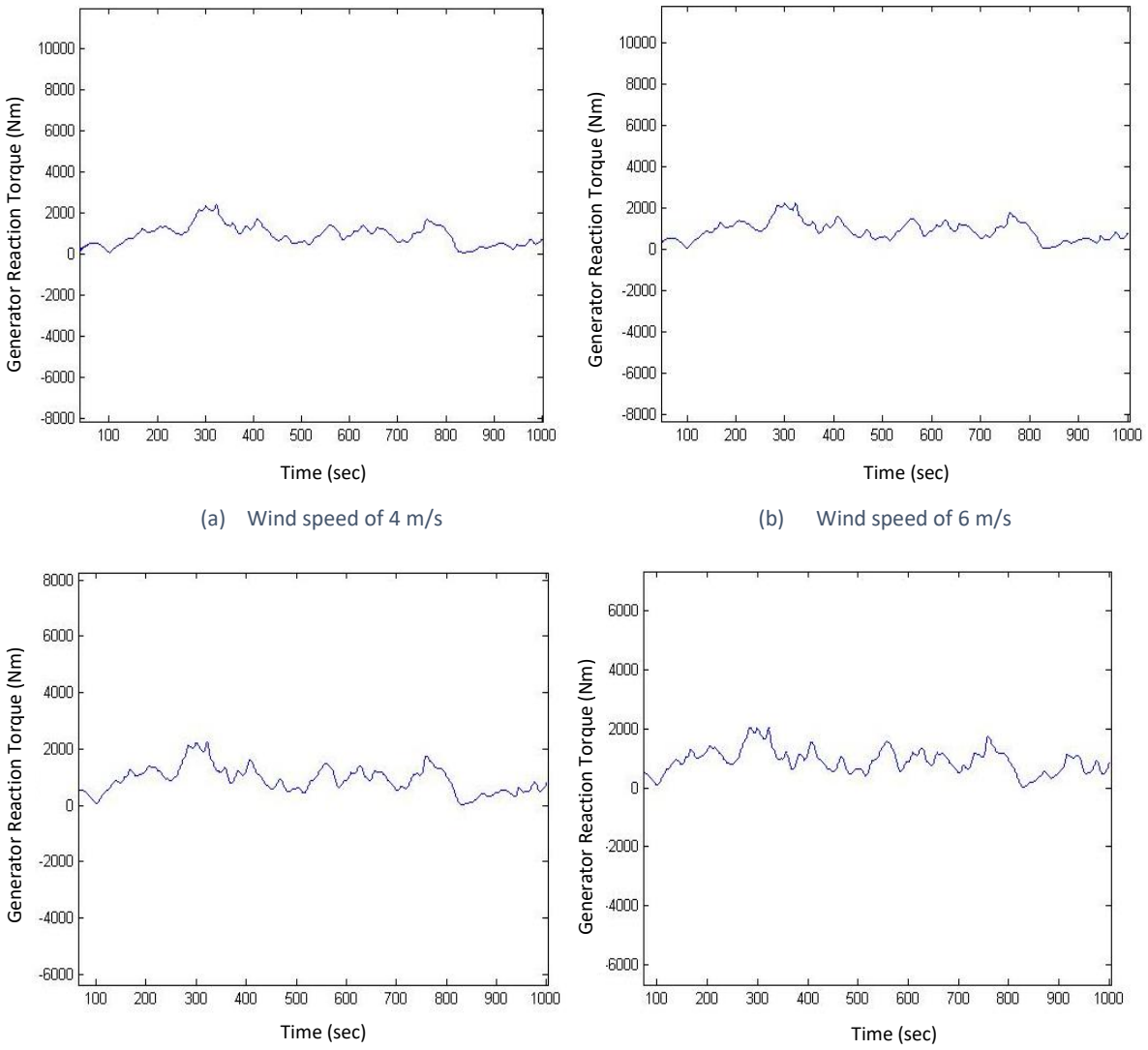

(a) Wind speed of 4 m/s

(b) Wind speed of 6 m/s

(c) Wind speed of 8 m/s

(d) Wind speed of 10 m/s

Figure 5.17 - Plots of the generator reaction torque

In this chapter, the complete simulation of the wind turbine dynamics is described. This models the wind speed model, drive-train model and synchronous generator model. The simulation is as shown in Figure 5.18.

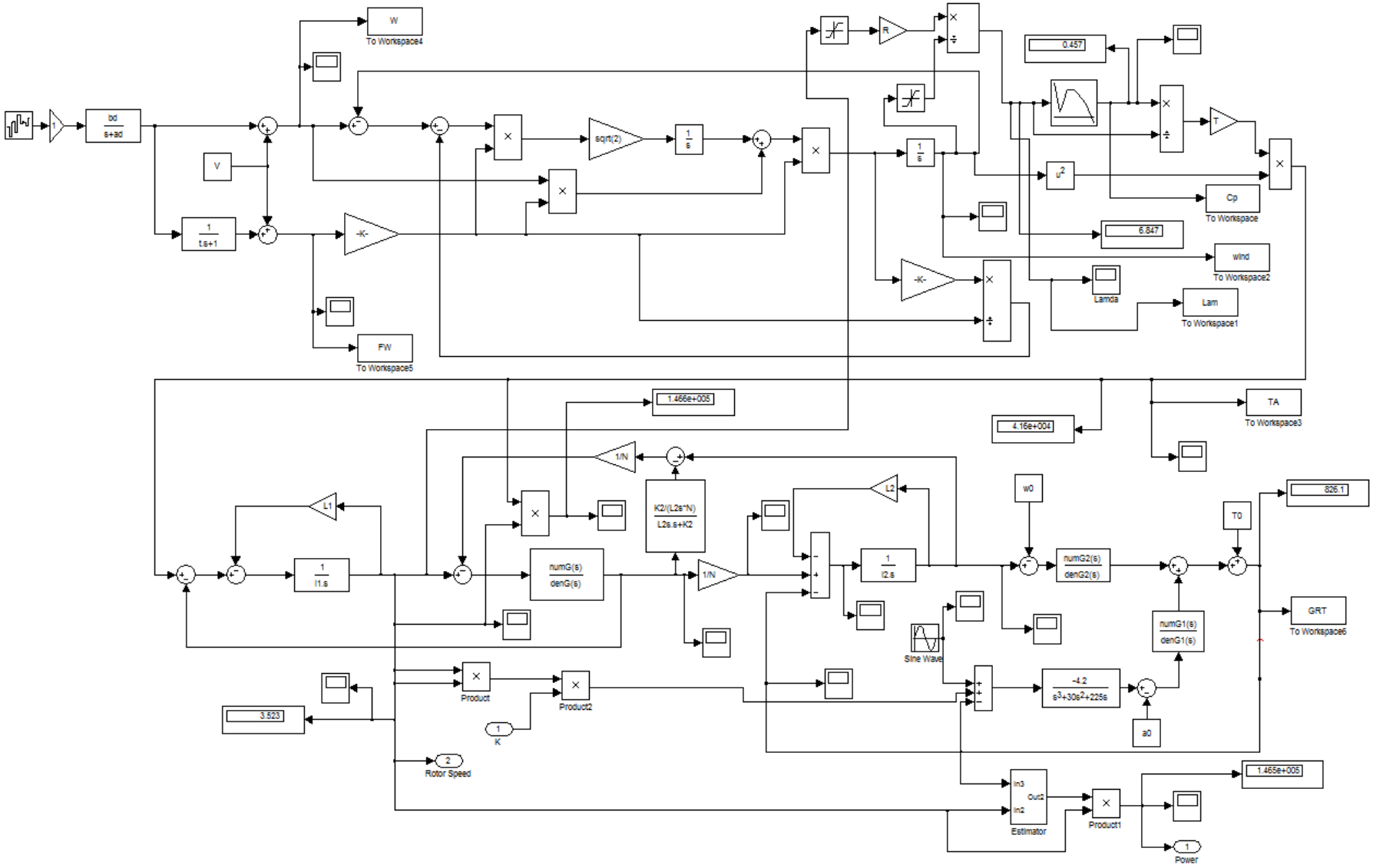

Figure 5.18 - Simulation of wind turbine dynamics

6. GENERAL OBJECTIVE OF CONTROL

"Nature tells man to consult reason. And to
Take it for his guide."
*……. **Paul H.T. D'Holbach***

Separate stages are considered when developing a wind turbine control system. The first stage is defining the control objectives clearly. The next stage is to choose an appropriate control strategy that normally defines the operating point of the wind turbine at each wind speed. The last stage is to determine how the control strategy is to be realized. Each stage is discussed in detail in this chapter.

6.1 Control Objectives

Basically, a wind turbine is a mechanical device that takes some energy from the wind and converts this energy into electric power. The fundamental objective of the control system is to protect the wind turbine from unsafe operation in high wind speed situations. It is done by limiting the power and rotor speed below some particular values.

The general objectives of the control system include alleviating the wind turbine transient loads, smoothing the power generated; providing damping for power-train dynamics and maximizing the energy capture. All these objectives are relevant to the specific case of variable speed wind turbines. Firstly, the wind turbine transient loads are reliant on both the choice of control strategy and effectiveness of the related controller. Secondly, smoothing the power is attained by lessening the load transients. Thirdly, there is extremely low natural damping as the generator is coupled indirectly to the grid. These objectives are explained below in detail.

In control design, the choice of the control strategy and the synthesis of the associated controller, by which it is realised, must be addressed. The former is concerned with global, generally non-linear, aspects of the system dynamics and the latter is concerned with local, essentially linear, aspects.

6.1.1 Energy Capture

The generating capacity, for a wind turbine, specifies how much power can be extracted from the wind, with consideration of both physical and economic constraints. It is often represented as a curve on the generated power-wind speed plane, using the ideal power curve, as shown in Figure 2.11. As indicated in this figure, the range of operational wind speed is bounded by the cut-in and cut-out wind speed. When the wind speed goes above the cut-out wind speed, the turbine is shut down to prevent structural overload. Below cut-in wind speed, the operating costs and losses are higher than the available energy. The wind turbine is stopped beyond cut-in and cut-out wind speed. Even though above cut-out wind speed has massive energy, constructing turbines strong enough to extract this energy is uneconomic and the contribution to annual average energy is negligible.

According to section 2.4.2, the ideal power curve has different regions with different objectives. When wind speed is low, the available power is lower than rated power. The available power is defined as:

$$P_{av} = \frac{1}{2}\rho\pi R^2 C_{pmax} V^3 \qquad (6.1)$$

where C_{pmax} is the maximum power coefficient. So, the objective in below rated region is to extract all available power.

6.1.2 Mechanical Loads

There are two types of mechanical loads, static and dynamic. Static loads are due to the mean wind speed. The dynamic loads are caused by spatial and temporal distribution of the wind speed field over the area swept by the rotor. The net dynamic load is propagated down the drive-train giving rise to the drive-train loads. The dynamic loads, also, comprise variations in the aerodynamic loads that impact on the mechanical structure giving rise to the structural load.

When the control system operates perfectly, the loads track their steady state values while the wind speed changes. The loads in this situation are called on-design loads. Obviously, the control system does not operate perfectly resulting in additional transient loads on the wind turbine, called off-design loads. The on-design drive-train loads are a function of the choice of control strategy while the off-design drive-train loads are a function of the associated controller. When designing the drive-train components, such as gearbox, both the on-design and off-design loads play an important role. Therefore, both the choice of the control strategy and the synthesis of the associated controller are relevant to achieving the control objective to reduce the drive-train transient loads. The associated controller is required to reduce the low-frequency off-design drive-train loads whilst the high-frequency off-design loads are not increased.

Essential to determining component rating is the transient loads in high wind speeds. Strong transient loads might occur with inappropriate control strategies, thus, when selecting control strategy, they should be considered. Additionally, design of the controller influences the transient loads.

It is noted, [17], that the structural component design is driven by the extreme loads and by dynamically induced fatigue. In many situations, the former are caused by events outwith the control system influence; for instance, in edge-wise mode, the extreme blade load is totally dominated by the weight of the blade itself and in flap-wise mode, the extreme blade root bending moment occurs when the blade is vertical and the turbine is yawed at 90° towards the wind direction. Only through the dynamically induced fatigue does the control system affect the structural components design. Generally, the contribution of the off-design structural loads is considerably less than the on-design loads. While the choice of the control strategy has considerably influence on the dynamically induced fatigue of the structural loads, the effectiveness of the associated controller has weak influence. It follows that the control objective attainment to alleviate the structural load mainly depends on selection of the control strategy but not the synthesis of the associated controller, although, when possible, the low frequency off-design structural loads must be reduced. Because excitation of structural modes by the controller should be avoided, the most important requirement on the associated controller is to avoid increasing the high-frequency off-design loads. For instance, it is possible that the excitation of the edge-wise natural mode

would make the extreme edge-wise blade root bending moment increase. Therefore, similarly to the drive-train loads, the on-design structural loads are only a function of the choice of control strategy while the off-design structural loads are a function of the effectiveness of the associated controller. Nevertheless, unlike the drive-train loads, the design of the structural elements, such as rotor and tower, are only influenced by the on-design structural loads.

The on-design energy capture is that accruing with ideal control operation and the difference between the on-design energy capture and that accruing with imperfect control operation is the off-design energy discrepancy. Also, like the drive-train transient loads, the off-design energy discrepancy is a function of the effectiveness of the associated controller while the on-design energy capture is only a function the control strategy choice. Thus, the control objective to maximise the energy capture depends on both aspects of the control design task.

The high frequency cyclic loads are caused by rotational sampling. These cyclic loads are concentrated around spectral peaks at multiples of rotor speed. Cyclic loads are influenced by the control strategy. Hence, inappropriate control designs might accentuate structural modes and possibly cause fatigue damage to some mechanical parts such as gearbox or blades. To mitigate high-frequency loads and bring down the fatigue damage rates, the controller should, whenever possible, provide damping of structural modes.

It should be considered that the behaviour of the wind turbine, in terms of the on-design transient loads and energy capture, are related. The desired state of the machine in all conditions is determined by the selection of control strategy fundamentally specifying the on-design transient loads and energy capture. The strategy itself is chosen to attain some purpose related to the transient loads or energy capture or a combination of both. The role of the associated controller is to make the local deviations from the desired state to be minimized at any time. Accordingly, since many design objectives are essentially a function of the global non-linear aspects of the wind turbine dynamics, any attempt to trade them off by means of local synthesis method is basically pointless.

6.1.3 Power Quality

In many ways, power quality influences the cost of energy. For example, poor power quality demands an extra investment in power lines. Traditionally, wind generation facilities are considered as poor quality power suppliers because of the variability in long and short time scales of the energy resources and the interaction with the power network. Therefore, in control system design, power conditioning should be taken into account.

Generally, frequency is stable. Frequency variations in an electric power network occur when power is unbalanced. For example, when the supplied power exceeds the consumption, the generators accelerate and the frequency increases. Analogously, the frequency decreases when generators slow down due to not be capable of converting the power demand. Usually, the frequency will not be affected by single wind turbines or by small-scale wind farms when connected to the bulk network.

As mentioned earlier, rotational sampling creates cyclic loads. The rotational sampling propagated down the drive-train towards the grid generates fast fluctuations of grid voltage. The frequency of these cyclic loads induce flicker as they may fall into the range of human eye sensitivity. In engineering, flicker is defined as an impression of an unsteadiness sensation caused by a fluctuating light stimulus. By containing passive or active filters, these voltage fluctuations and flicker are attenuated in the case of variable-speed wind energy conversion systems, by controlling the reactive power handled by the electronic converters.

6.2 Control Strategies

6.2.1 Control Strategy Definition

In variable-speed wind turbines the rotor speed can be changed with wind speed. This relationship is precisely defined by the choices of controller strategy. Obviously, in the definition of control strategy, the rotor speed is specified as a function of wind speed; that is, the strategies are defined in the context of the rotor speed/wind speed plane. However, the local dynamics and the operating point (the nominal rotor speed, torque, etc.) change with wind speed. The measurement of the wind speed experienced by the wind turbine cannot be achieved directly. Hence, from the measurements made on the wind turbine itself such as electrical power, rotor speed and the operating point, the wind speed could perhaps be estimated. Unfortunately, this is not a practical approach. One of the difficulties is that the aerodynamics are non-linear and not uniquely related to the wind speed. There may be more than one operating point for a given wind speed and more than one wind speed for a given operating point. Hence, relying on the wind speed knowledge, to determine the operating point of the wind turbine must be avoided.

As discussed above, the control strategy is defined in the context of rotor speed/wind speed plane. An alternative context to this is the torque/rotor speed plane. There are some doubts about the identity of the torque, whether it is aerodynamic torque, T_f, drive-train torque, T_D, or the combination of both since the control strategy may be defined with respect to all. The torques in the steady-state, assuming the drive-train torque to be the low-speed shaft torque, are equivalent. In the torque/rotor speed plane, all control strategies correspond to a curve which the wind turbine tracks through the control system. The curve is implicitly parameterized by wind speed. Concerning the estimation of the state of the wind turbine, only an estimate of aerodynamic torque is needed instead of an estimate of wind speed. In fact, the knowledge of the wind speed is not necessary.

In some particular strategies, i.e. for a particular choice of curve in the torque/rotor speed plane, the on-design loads and on-design energy capture are those that are encountered on the curve. Since the state of the wind turbine caused to track the curve more tightly, the on-design loads and on-design energy capture does not change, however, the off-design loads and off-design energy discrepancy reduce. Thus, for the wind turbine operating state, to track the curve as tightly as possible, the associated controller is needed. For this purpose,

the output of the plant is chosen to be the tracking error with the controller synthesized to obtain the highest possible crossover frequency for the resulting open-loop system. In the control loop, the aerodynamic loads act as disturbance, so the high-frequency components must not be enhanced i.e. the sensitivity function gain must not be much greater than one at the spectral peak frequencies.

In Figure 6.1, [17], the torque/speed curves and operational strategy for a variable speed wind turbine is depicted. It can be observed that the relation of the operating point to the wind speed is not unique and that is due to the curve defining a control strategy being cut more than once by the constant wind speed curves. In addition, non-uniqueness is not only due to the constant wind speed curves but in some conditions may occur dynamically from stall hysteresis and unsteady effects such as dynamic stall (Figure 6.1 represents steady state condition only and this condition is not depicted).

The control strategies for pitch regulated wind turbines can be defined in similar way. The appropriate context is the torque/rotor speed/pitch angle space. In this space, all the control strategies are defined as a curve and to cause the state of the wind turbine to track the curve with highest possible accuracy, the associated controller is needed.

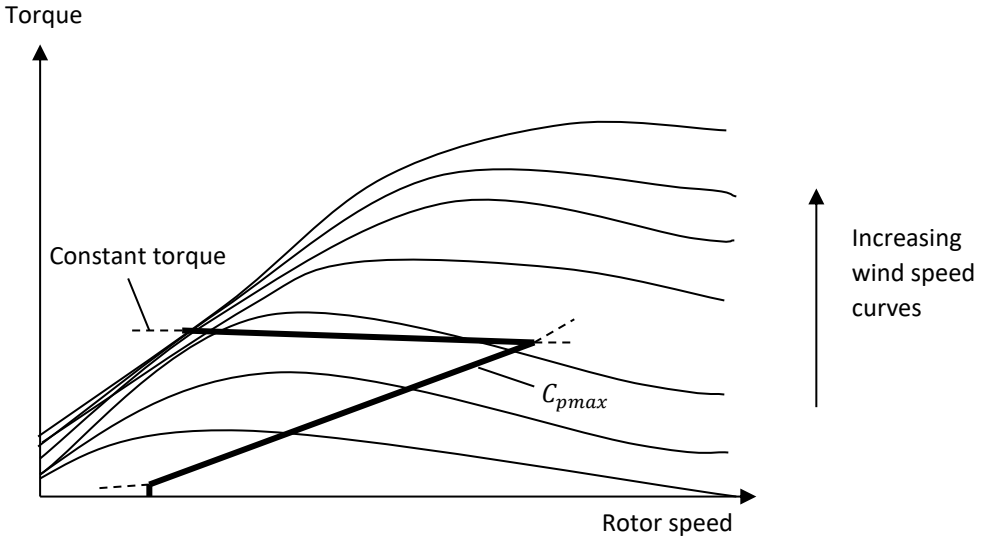

Figure 6.1 - Effective strategy for a variable speed wind turbine

6.3 Control Strategy to Improve Power Capture for Variable-speed Wind Turbine in Below Rated Wind Speed

The control system in below rated wind speed is single-input single-output (SISO) as illustrated in Figure 6.2. The input of the plant is, for example, the rectifier firing angle, α.

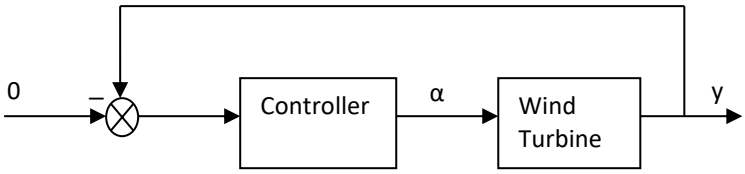

Figure 6.2 - SISO system in below rated

No distinction is made between the rectifier firing angle and its demand value since the dynamics of the electrical aspects of the power generation unit are fast enough that no difference is needed in this context. The output, y, is the function of measurements of rotor speed and drive-train torque variables, which accomplishes a particular strategy defined in the torque/rotor speed plane.

In below rated wind speed, the main objective of using a control system is to maximize the energy capture. The aerodynamic efficiency changes with rotor speed, and a unique point on the torque/rotor speed exists when the maximum efficiency is attained. The constant wind speed curve together with the locus of the points, which have the maximum aerodynamic efficiency, is depicted in Figure 6.3, [17], for both flat and peaked $C_p - \lambda$ curves. The maximum aerodynamic efficiency corresponds to the maximum value of the aerodynamic power coefficient, C_p. Therefore, in Figure 6.3, the locus of maximum aerodynamic efficiency is referred to as the C_{pmax} curve. To maximize energy capture the aerodynamic torque should be controlled to track the C_{pmax} curve.

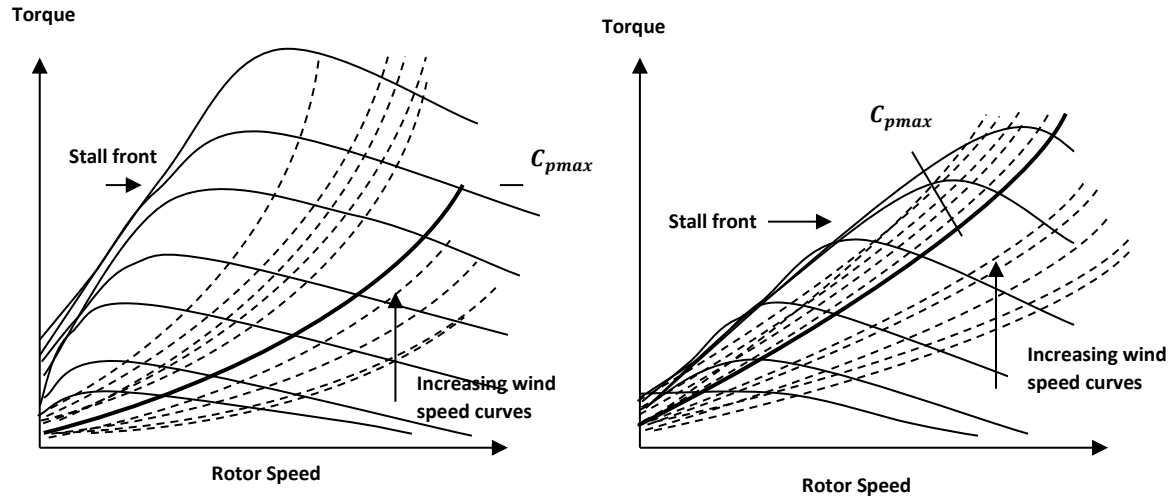

(a) Flat $C_p - \lambda$ curve *(b) Peaked $C_p - \lambda$ curve*

Figure 6.3 - Different efficiencies on torque/speed curves

The system is dynamically stable for any equilibrium operating point on the C_{pmax} curve. Figure 6.4, [17], shows the stability of below rated tracking. The wind turbine is considered to be experiencing a constant wind speed, U, for situation (a). In this situation the wind turbine is operating on the C_{pmax} curve in equilibrium, i.e. at point *a*, the drive-train torque and the aerodynamic torque are T_a with rotor speed Ω_a. The turbine operating state changes to a different point when the rotor speed is displaced. For example, at point *b,* the aerodynamic torque increases to T_b when the rotor speed relocates to Ω_b. Similarly, at point *c,* the aerodynamic torque decreases to T_c when the rotor speed relocates to Ω_c. The system is stable if the rotor speed is displaced from Ω_a then the wind turbine operating point returns to point *a*.

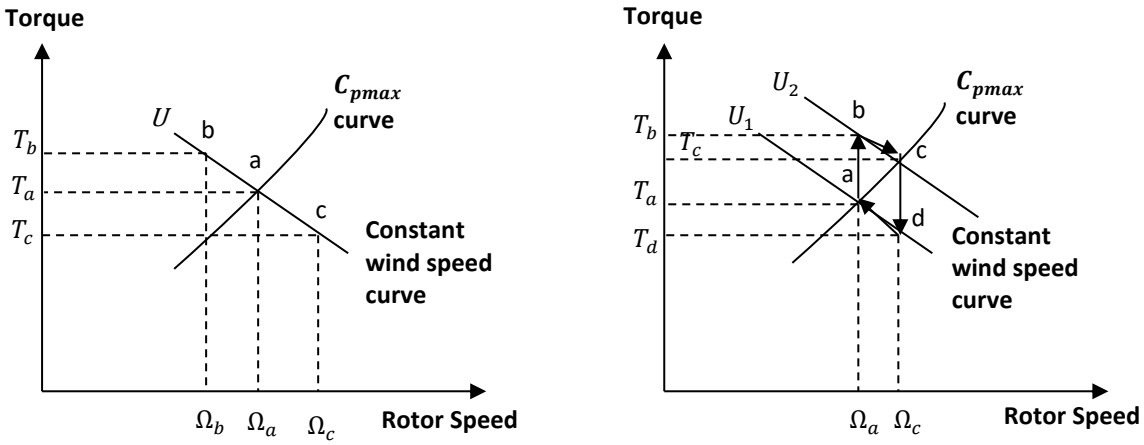

Figure 6.4 - Stability of tracking in below rated

6.3.1 Tracking by Drive-train Torque

From stability, the wind turbine operating state, in particular the aerodynamic torque, can be made to follow the C_{pmax} curve as the wind speed fluctuates by causing the drive-train torque to track the C_{pmax} curve. Consider the situation (b) depicted in Figure 6.4, the losses in drive-train are disregarded. Assuming the drive-train torque is continuously set at any rotor speed to the value of the C_{pmax} curve. That is, perfect or infinite bandwidth control is assumed. The wind turbine is considered to experience a wind speed, U_1. In this situation the wind turbine is operating on the C_{pmax} curve at point *a*, with the aerodynamic torque, T_a, and rotor speed, Ω_a. When the wind speed increases and changes quickly from U_1 to U_2, the wind turbine operating point changes to *b*. In this state, the drive-train torque is exceeded and the aerodynamic torque increases to T_b and rotor speed rises. The drive-train torque continues to be exceeded by the aerodynamic torque and the rotor speed keeps increasing until the operating state reaches *c*. As before, when the wind speed decreases and changes to U_1, the rotor speed also decreases to Ω_a from Ω_c. It is obvious that the wind turbine operating state tracks the C_{pmax} curve.

Hence, one of the control strategy choices in below rated wind speed is to track the C_{pmax} curve by the drive-train torque, T_D. Since the C_{pmax} curve is proportional to Ω^2, the related output y in Figure 6.2 is

$$y = T_D - k\Omega^2 \qquad (6.2)$$

where, k is constant with an appropriate value. Initially, by increasing the effectiveness of the controller acting on y, i.e. increasing the crossover frequency of the open-loop system,

both the aerodynamic torque and the drive-train torque are caused to track the C_{pmax} curve more tightly. Therefore, the energy capture increases since the off-design drive-train loads and the off-design energy discrepancy are decreasing. However, there is a limit to the extent to which the aerodynamic torque can be made to track the C_{pmax} curve, and so to the extent, to which the off-design energy discrepancy can be decreased. This approach is discussed more in [17], where the generator reaction torque is directly set to $k\Omega^2$.

The loss of energy capture, which is incurred by sluggish tracking of the C_{pmax} curve by aerodynamic torque, is dependent on the aerodynamics. In Figure 6.3, the closest curve to the C_{pmax} curve is the 99% efficiency curve, along which the power extracted at any wind speed is 99% of the maximum possible. The farther curves from the C_{pmax} curve are 98%, 97%, 96% and 95% curves respectively. Generally, for a peaked $C_{p-\lambda}$ curve, these curves are symmetric around the C_{pmax} curve with those above the C_{pmax} curve closer together. Referring to Figure 6.3, since the aerodynamic efficiency is significantly decreased in the stalling front (the upper boundary on the torque/rotor speed plane of the operational envelope), it must be avoided. In addition, the control system becomes ineffective and the wind turbine recovers slowly. In stall front, the constant wind speed curves are almost parallel to the C_{pmax} curve. Subsequently, changing the drive-train torque and so the rotor speed has slight influence on the tracking error merely causing the operating point to move along the stalling front.

6.3.2 Tracking by Aerodynamic Torque

The limit on the extent, to which the off-design energy discrepancy can be reduced, may be overcome by causing the aerodynamic torque or an estimate of aerodynamic torque, $\hat{T}_f$, to track the C_{pmax} curve directly. The responding output *y* in Figure 6.2 is

$$y = \hat{T}_f - k\Omega^2 = T_D + h(s)\Omega - k\Omega^2 \qquad (6.3)$$

with the appropriate transfer function *h(s),* see [17]. As the control action is attained through the generator reaction torque, this strategy improves tracking of the C_{pmax} curve by the aerodynamic torque but degrades tracking of the C_{pmax} curve by the drive-train torque. Increasing off-design drive-train loads and so increasing controller activity is required to reduce the off-design aerodynamic reaction torque. The energy capture below

rated wind speed, however, is not necessarily maximized by controlling on (6.3) since the transfer function from wind speed disturbance to output y has a zero in the right half plane, which means it is inevitably non-minimum phase. Being higher frequency, the non-minimum phase zero does not affect stability but the system responds in an inappropriate manner. For instance, the state of the system may have larger transients due to the non-minimum phase zero and temporarily deviate further from the curve to be tracked, resulting in a loss of aerodynamic efficiency. The rotor characterized by a peaked $C_{p-\lambda}$ curve has greater effect. Consequently, adopting an alternative strategy, which avoids the non-minimum phase behaviour and decreases controller activity, is more sensible.

6.3.3 Tracking by Combined Drive-train and Aerodynamic Torque

A compromise, between tracking by drive-train torque, T_D, or by aerodynamic torque, $\hat{T}_f$, is tracking by a linear combination. In this case, the responding output *y* in Figure 6.2 is

$$y = (1-\varepsilon)(T_D + h(0)\Omega) + \varepsilon\hat{T}_f - k\Omega^2 = T_D + H_\varepsilon(s)\Omega - k\Omega^2 \qquad (6.4)$$

where $H_\varepsilon(s) = [(1-\varepsilon)h(0) + \varepsilon h(s)]\Omega$, and ε is a constant in the range of $0 \le \varepsilon \le 1$. When ε is 1, (6.4) reduces to (6.3), which means tracking by aerodynamic torque, $\hat{T}_f$, and when ε is 0, (6.4) reduces to

$$y = (T_D + h(0)\Omega) - k\Omega^2 \qquad (6.5)$$

Comparing (6.5) with (6.2), the extra term of $h(0)\Omega$ signifies the drive-train losses and (6.5) is equivalent to tracking by the low-speed shaft torque. For a particular wind turbine, the most proper choice, in terms of energy capture and level of control activity, is determined by changing the value of ε. Generally, the energy capture increases by increasing ε, at least until the disturbance transfer function becomes significantly non-minimum phase. The activity of the controller increases, in particular the drive-train off-design transient loads. The most appropriate value of ε results in better energy capture than with value ε to 1, but detuning the controller until its level of activity is the same since the gain of the open-loop system for the former is greater at low frequencies. According [12] and [9], the cost of a gearbox is almost proportional to its equivalent infinite life torque rating. Referring to the application of British Standard BS 436 part 3, 1986, discussed in [12], except in some cases when the below rated transient loads are as large as the above rated transient loads, drive-

train loads have only slight influence on the gearbox rating. The extent of the off-design transient loads is restricted by the necessity to keep the generated power positive and prevent it becoming negative. In other respects, due to uncertainty concerning the higher frequency plant dynamics and by restrictions on the rate of change of the firing angle, the controller performance is constrained. So, the choice of control strategy is essentially driven by the necessity to maximize energy capture with only a little consideration of the extent of the drive-train off-design transient loads.

6.3.4 Other Continuous Strategies

In below rated wind speed, several other continuous strategies are available. Any of the prior strategies might be used to track a different curve other than C_{pmax} curve in order to prevent the stalling front. For instance, since the wind turbine is operated further away from the stall front, the efficiency of tracking the 99% curve below the C_{pmax} curve might be higher than tracking the C_{pmax} curve. When the turbulence intensity is high, the energy capture might be increased, and likely, when the turbulence intensity is low, the energy capture might be decreased. Therefore, this choice of strategy is dependent on the wind conditions at a particular site.

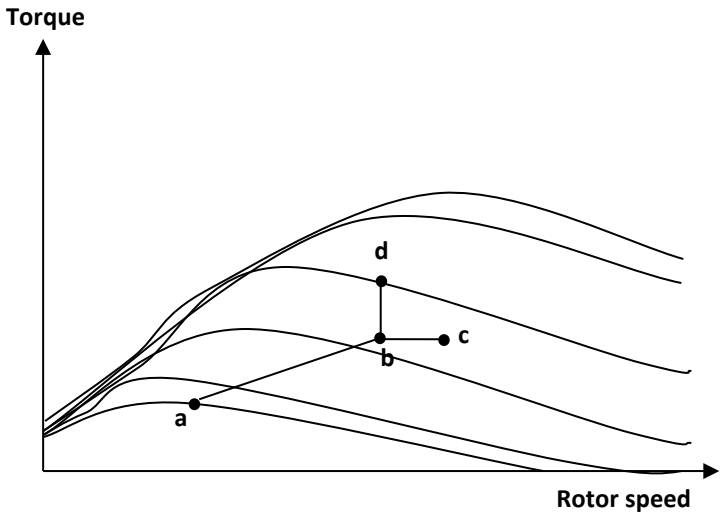

Figure 6.5 - Other continuous strategies in below rated

Figure 6.5, [17], shows two other strategies by the curves *abc* and *abd*. The wind turbine operating state is tracking the C_{pmax} curve until some maximum permitted torque or rotor speed reached at point *b*. It is caused to track a constant torque curve, which is represented by *bc*, or a constant speed curve, which represented by *bd*.

6.3.5 Discrete Speed Operation

Discrete speed operation is used in some wind energy conversion systems (WECS) to improve the conversion efficiency of control strategies in below rated wind speed. Basically, it consists of switching between two operating speeds. Operation of wind turbines over a continuous range of rotor speed has similar potential advantage to operation at two discrete rotor speeds. Although, discrete speed operation is implemented, in practice as constant speed operation with the ability to switch speeds to minimize the costs. It is assumed that, the power generation unit stays unchanged from continuous variable speed operation, thereby facilitating a fair comparison.

Figure 6.6, [17], compares the two speed strategy. The wind turbine is regulated to keep the rotor speed constant in two situations. The first situation is in low wind speed, Ω_1, and the second situation is in high wind speed but still below rated wind speed. The corresponding output *y* in Figure 6.2 for the first situation is

$$y = \Omega - \Omega_1 \tag{6.6}$$

And the corresponding output *y* for the second situation in Figure 6.2 is

$$y = \Omega - \Omega_2 \tag{6.7}$$

Rather than drive-train torque, an estimate of aerodynamic torque, $\hat{T}_f$, should trigger switching between rotor speed Ω_1 and rotor speed Ω_2 as the regulation is enacted through the generator reaction torque.

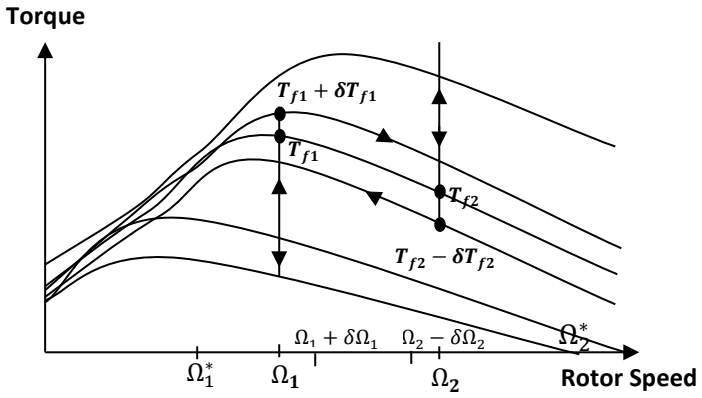

Figure 6.6 - Discrete speed operation in below rated

When $\widehat{T}_f > T_{f1} + \delta T_{f1}$, the switch is triggered from Ω_1 to Ω_2 and when $\widehat{T}_f < T_{f2} + \delta T_{f2}$, the switch is triggered from Ω_2 to Ω_1. When a switch has been triggered once, it must be completed to avoid dither of the rotor speed between Ω_1 to Ω_2. The conversion between Ω_1 to Ω_2 is done by merely substituting of the outputs (6.6) and (6.7) but otherwise not changing the controller. Rotor speeds Ω_1^* and Ω_2^*, as shown in Figure 6.6, are used respectively instead of Ω_1 and Ω_2 to increase the errors in an artificial manner, which speed up the conversions until it is completed; that is, in Figure 6.6, rotor speed is close to its target speed as indicated by $\Omega_1 + \delta\Omega_1$ and $\Omega_2 - \delta\Omega_2$. T_{f1} and T_{f2} correspond to the same wind speed, and Ω_1 to Ω_2 are chosen to optimize the aerodynamic efficiency in below rated wind speed. To prevent excursion into the stall region, care should be taken over the choice of $T_{f1} + \delta T_{f1}$ and Ω_1. To prevent too frequent switching, δT_{f1} and δT_{f2} define a hysteresis loop.

6.3.6 Discontinuous Speed Operation

To realise the advantages of variable speed operation in below rated wind speed, changing the rotational speed over a wide range should be considered. This operation mode tends to excite some structural mode since the frequency of the cyclic loads varies in proportion to rotational speed. The extent of allowed rotational speeds should be limited in some way to avoid structural resonance.

The rotor speed, or a harmonic of it, could pass through the frequency of a structural mode, such as tower frequency, in variable speed operation. Restricting the extent to which the rotor speed can be close to its frequency is required to avoid excitation of the structural mode. To accomplish this, requires two speed operation to be combined with tracking the C_{pmax} curve as depicted in Figure 6.7, [17]. In this figure, the frequency of the structural mode is considered to be between Ω_1 and Ω_2 and by switching between the two constant speed sections, it is avoided.

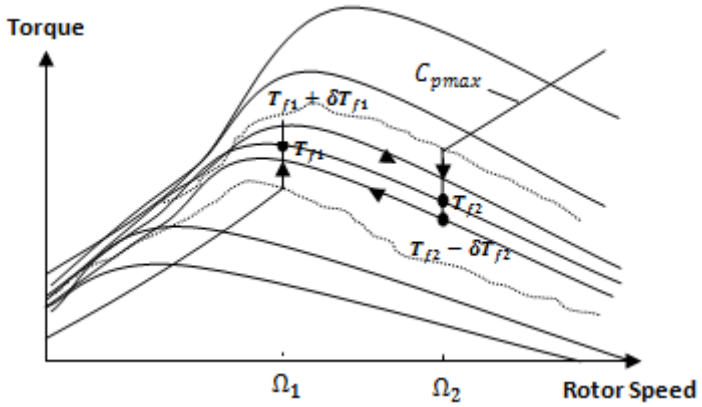

Figure 6.7 - Preventing structural resonance in flat $C_p - \lambda$ curve

According to above discussion, speed up is not necessary in transition between Ω_1 and Ω_2 since, generally, the interval between Ω_1 and Ω_2 is less than the interval needed in discrete speed operation.

Figure 6.7 is not appropriate for a rotor with a sharp $C_p - \lambda$ curve as the point $(\Omega_1, T_{f1} + \delta T_{f1)}$ may be in the stall region but it is appropriate for a rotor speed with a flat $C_p - \lambda$ curve. For a sharp $C_p - \lambda$ curve a more appropriate strategy is shown in Figure 6.8, [17]. The Figure 6.8 indicates the frequency of the structural mode is considered to be between $\Omega_1 + \delta\Omega$ and Ω_2, and by switching between the low wind speed section of the C_{pmax} curve and the constant speed section of the Ω_2, it is avoided. When $\Omega > \Omega_1 + \delta\Omega$, the switch is triggered from $\Omega_1 + \delta\Omega$ to Ω_2 and when $\widehat{T}_f < T_{f2} + \delta T_{f2}$, the switch is triggered from Ω_2 to Ω_1. As in the two speed strategy, when a switch has been triggered, it must be completed to avoid dither of the rotor speed between $\Omega_1 + \delta\Omega$ and Ω_2. The transition is done by substitution of the output (6.2), (or (6.4) for some value of ε) and (6.7). To prevent too frequent switching, δT_{f2} and $\delta\Omega$ are defined as a hysteresis loop.

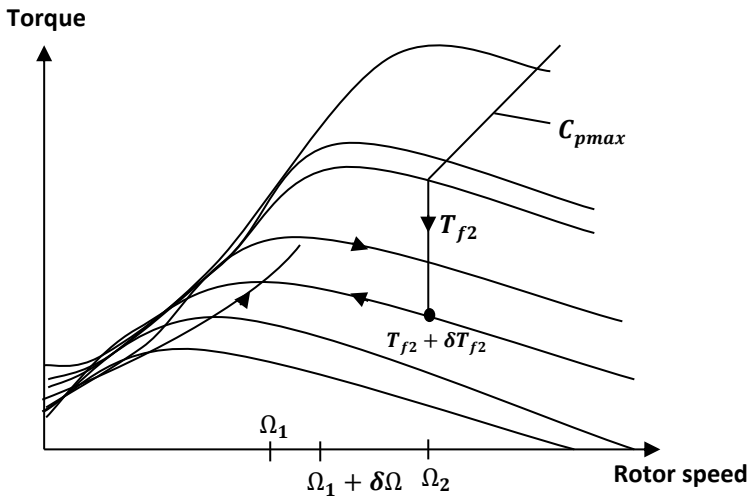

Figure 6.8 - Preventing structural resonance in peaked $C_p - \lambda$ curve

7. OPTIMISING CONTROL SYSTEM

"He that troubleth his own house shall inherit the world"
*……. **Proverb 11:29***

7.1 Controller for Tracking C_{p-max} Curve

In variable speed wind turbines, the aerodynamic efficiency of the wind turbine is related to the tip-speed ratio, λ, which is the ratio of rotor speed to wind speed. When wind speed varies, provided the rotor speed could be controlled, then the tip-speed ratio would be adjusted to optimise the power coefficient, C_p, which results in the energy capture being increased. The capability to change the rotor speed with wind speed is usually exploited only in below rated wind speed.

The major objective for a variable speed wind turbine is to maximise energy capture. The purpose of this part of the project is to investigate a control strategy and apply a controller to achieve this objective for a medium scale wind turbine with characteristics stated below:

Type of Rotor:	*Three-bladed Horizontal Axis*
Rotor speed:	*Variable*
Generator:	*Synchronous*
Rated power:	*330 KW*

The generated power from the wind, *P*, is

$$P = \frac{1}{2}\rho A C_p(\lambda) V^3 \qquad (7.1)$$

with power coefficient, C_p, and the tip-speed ratio, λ.

Maintaining the correct relationship between the rotor speed and wind speed is performed by a control system. In control terms, the state of the wind turbine must be caused to track the C_{pmax} curve in order to maximise energy capture. The control strategy used here is to minimise the error $T_D - k\Omega^2$, see (6.2).

The block diagram for the controller (6.2), is shown below in Figure 7.1.

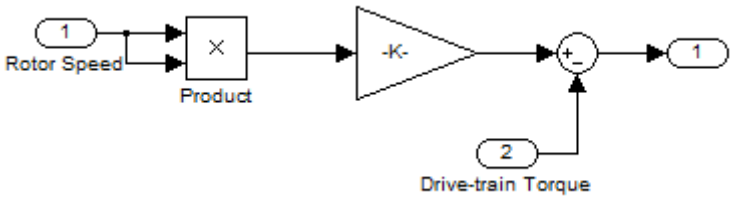

Figure 7.1 - Controller for tracking C_{pmax} curve

Variation of power, when the rotor speed is varied so that the tip speed/ratio, λ, varies about a mean value centred on its maximum value λ_0, below λ_0 and above λ_0, is shown in Figure 7.2. When varied centred on λ_0, the frequency of variation of the power is double the frequency of λ. When the variation of drive-train torque is below λ_0 the variation of the power is in phase and with same frequency as λ. When the drive-train torque is varying above λ_0 the variation of the power is in anti-phase with λ with same frequency.

The discussion in the above paragraph is dependent on the value of *k* in (6.2), which is obtained from

$$k = \frac{{}^1\!/_2 \rho \pi R^5 C_q(\lambda_0,0)}{\lambda_0^2} \qquad (7.2)$$

The expression (7.2) is obtained from the expression for aerodynamic torque together with $k = \frac{T_D}{\Omega^2}$, (6.2), and $V = \frac{\Omega R}{\lambda_0}$. According to Table 2 (which obtained from Table 3 in Appendix D), C_p is 0.4625 for zero pitch angle when λ_0 is 6.25. In this case $\lambda = \lambda_0$, therefore C_q is 0.074 since $C_q = \frac{C_p}{\lambda}$. The value of *k* is determined to be 72.75 to keep the variation of λ centred on λ_0. The full mathematical calculation to obtain value of *k* is given in Appendix B.

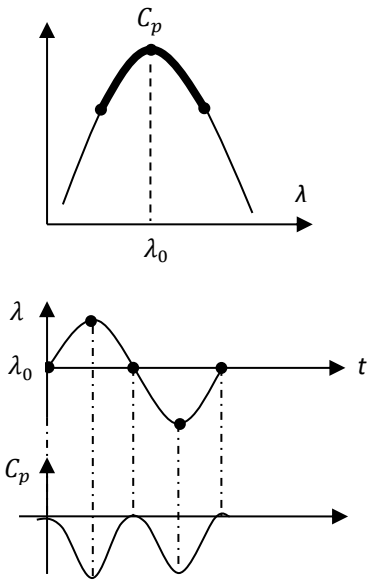

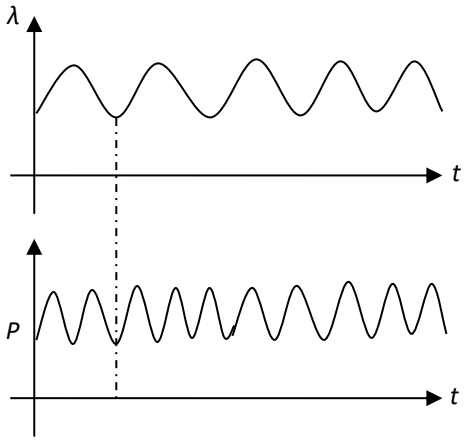

(a) Variation of torque centred on λ_0

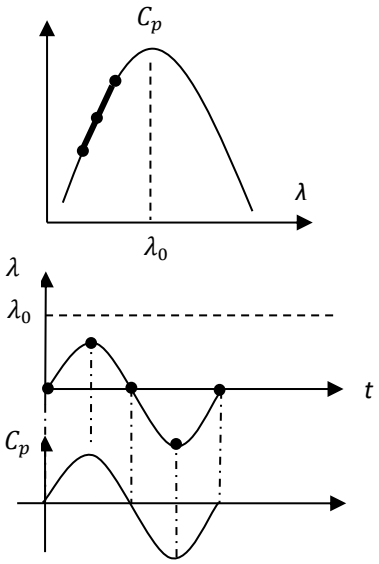

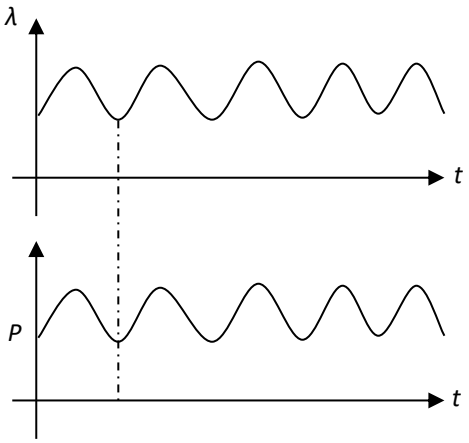

(b) Variation of torque below λ_0

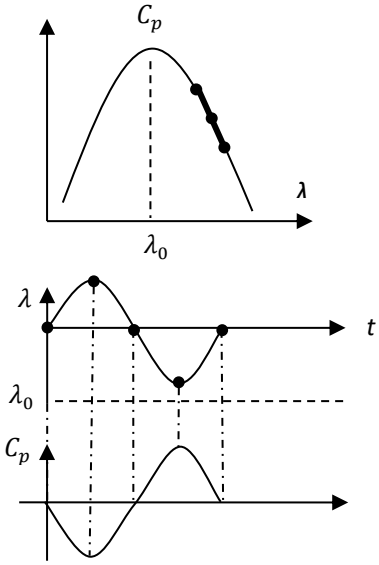

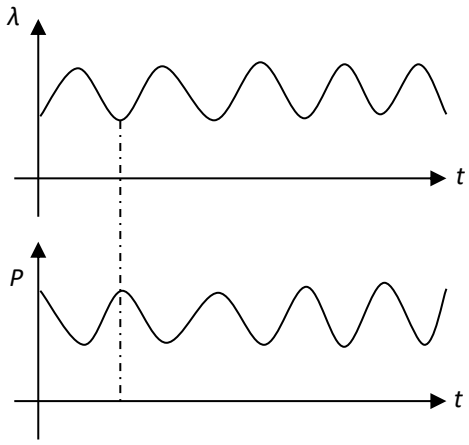

(c) Variation of torque above λ_0

Figure 7.2 - Variation of T_D on C_P - λ curve

Due to drive-train losses, the variation is not exactly centred on λ_0, so the controller is re-tuned to set *k* to a value of 105. When drive-train losses increase, the value of *k* also increases. A sinusoidal perturbation is added to the control demanded torque with amplitude, A, and frequency, ω, i.e. $A\sin(\omega t)$.

Increasing or decreasing the value of *k* from 105 by approximately $\pm$40% moves the centre of variation of λ to below or above λ_0. Figure 7.3 illustrates the simulation results equivalent to Figure 7.2 by setting the amplitude and the frequency of the perturbation to the controller (6.2) demand to 500Nm and 0.05 rad/s, respectively.

Figure 7.3 (a) shows the frequency of the power is doubled with respect to the frequency of tip-speed ratio when the value of *k* is 105. When *k* is set to 160 (40% increment of 105) the frequency of the power is the same as frequency of the tip-speed ratio, Figure 7.3 (b), and similarly, the frequency of the power is the same but with opposite phase relative to tip-speed ratio when the value of *k* is set to 50 (40% decrement of 105) as depicted in Figure 7.3 (c).

The power discussed above is an aerodynamic power and since it cannot be measured it must be estimated. A simple estimation is discussed in section 7.2 and an estimation of correlation factor is discussed in section 7.3.

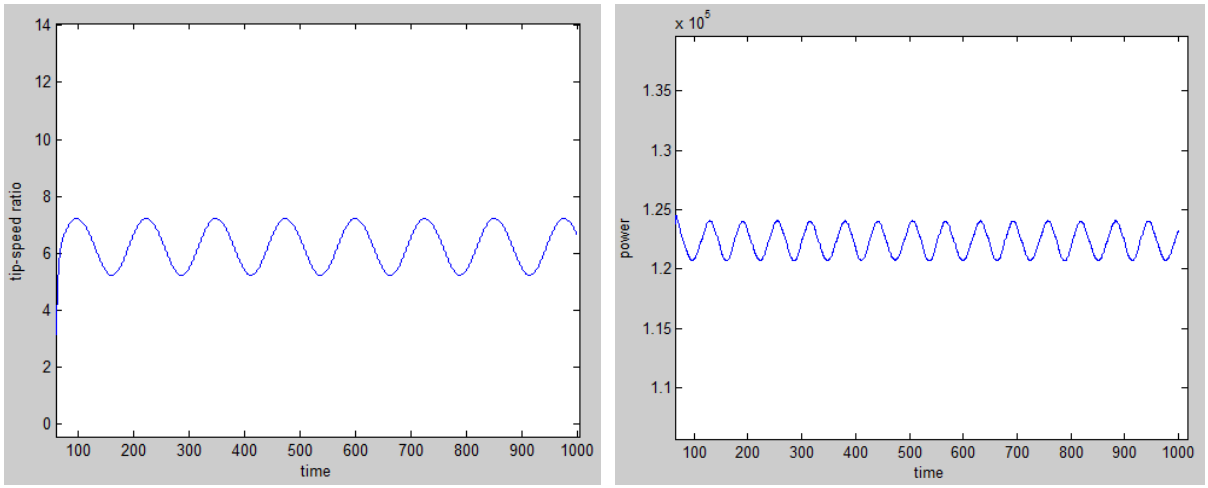

(a) Oscillation at peak with k=105

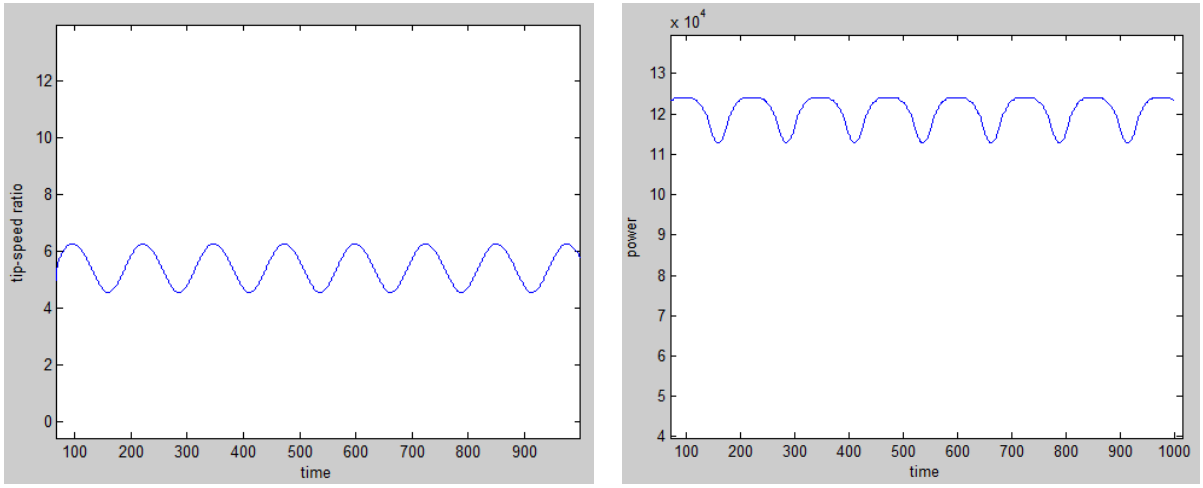

(b) Oscillation at left hand side with k=160

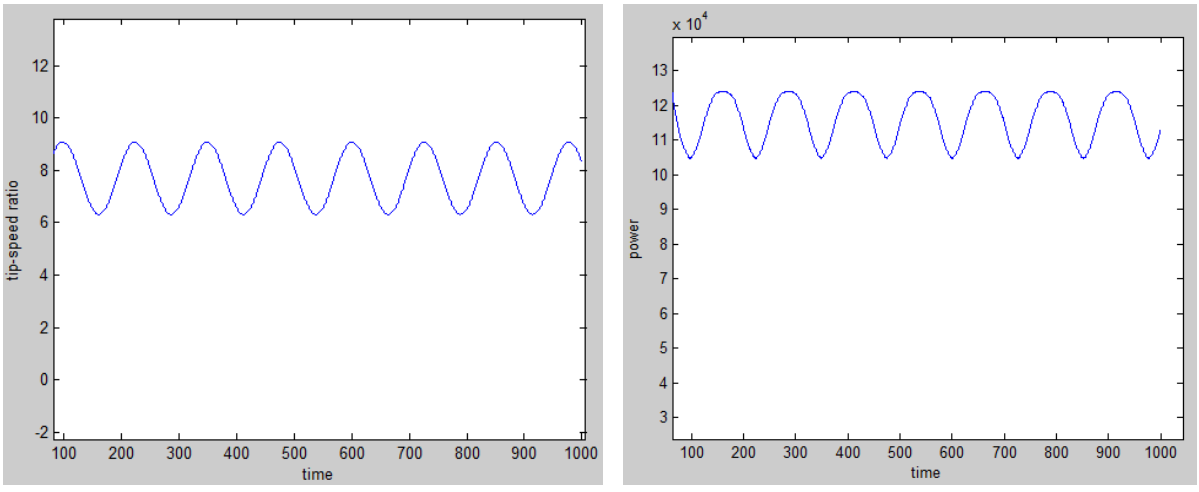

(c) Oscillation at right hand side with k=50

Figure 7.3 - Oscillation of tip-speed ratio and power with different values of k

7.2 Aerodynamic Estimator

Section 6.5 discusses the control strategy for below rated operation. It is single-input single-output with demanded generator reaction torque the input to the plant. This strategy is defined in terms of rotor speed, Ω, and the hub torque, T_D, or aerodynamic torque, T_f. Obviously, the aerodynamic torque, T_f, cannot be measured so it must be estimated from T_D and Ω, i.e. $\hat{T}_f$, the estimate of T_f, is

$$\hat{T}_f = NT_e + \psi \tag{7.3}$$

where ψ is dynamically linearly related to Ω by

$$I\frac{d\Omega}{dt} + B\Omega = T_f - T_D \tag{7.4}$$

where, the total inertia and the total viscous damping in the drive-train are represented by I and $B\Omega$ respectively. In this case, the hub torque, T_D, is the generator reaction torque, T_e, scaled by the gearbox ratio, *N*. Therefore, a possible estimator for T_f is:

$$\hat{T}_f = NT_e + Q$$

$$Q = (I_1 + N^2 I_2)\frac{dV}{dt} + (\gamma_1 + N^2\gamma_2)V_H \tag{7.5}$$

Because the total inertia of the drive-train is $(I_1 + N^2 I_2)$ and the total viscous damping coefficient is $(\gamma_1 + N^2\gamma_2)$,

$$h(s) = (I_1 + N^2 I_2)s + (\gamma_1 + N^2\gamma_2) \tag{7.6}$$

The simulation of the estimator to measure aerodynamic torque is shown in Figure 7.4.

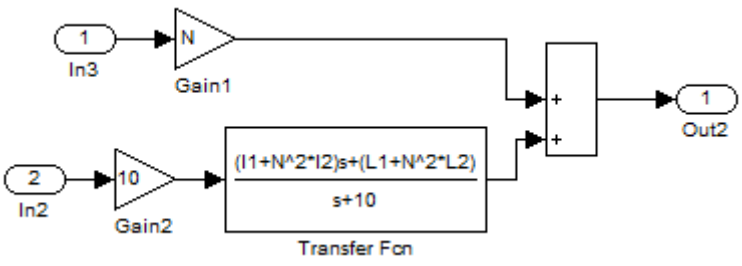

Figure 7.4 - Simulation of the estimator

Comparison of aerodynamic torque and the estimated aerodynamic torque, obtained as in Figure 7.4, is depicted in Figure 7.5.

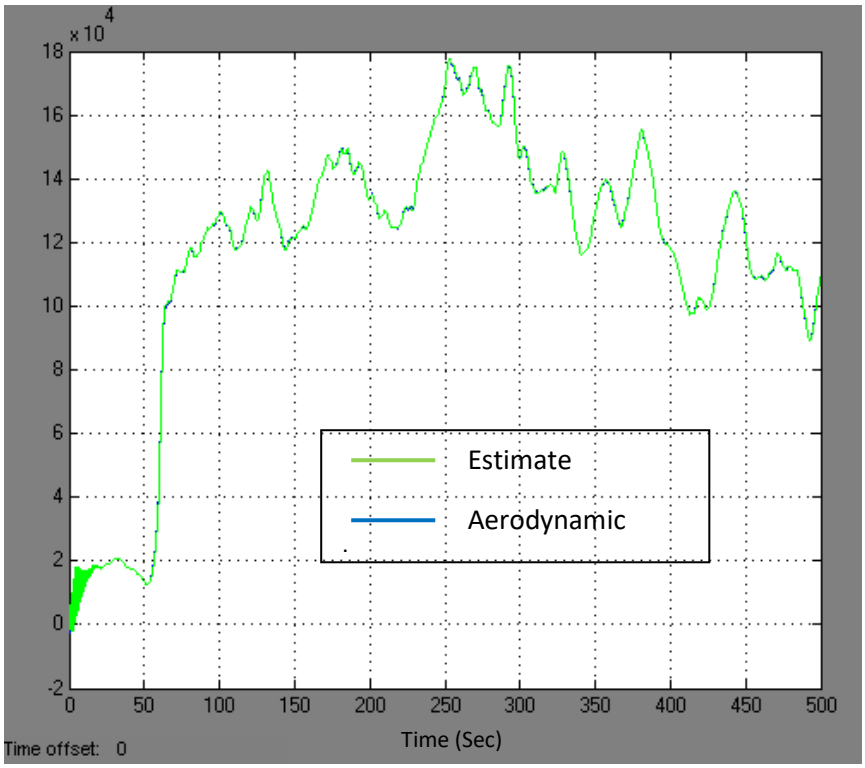

Figure 7.5 - Aerodynamic torque and estimate

As can clearly be seen in Figure 7.5, the estimated output and the aerodynamic torque are virtually equivalent to each other.

Figure 7.6 depicts the simulation of the drive-train including the controller and the aerodynamic estimator. As represented in Figure 7.6, a sine wave is added to the system to perturb the control input.

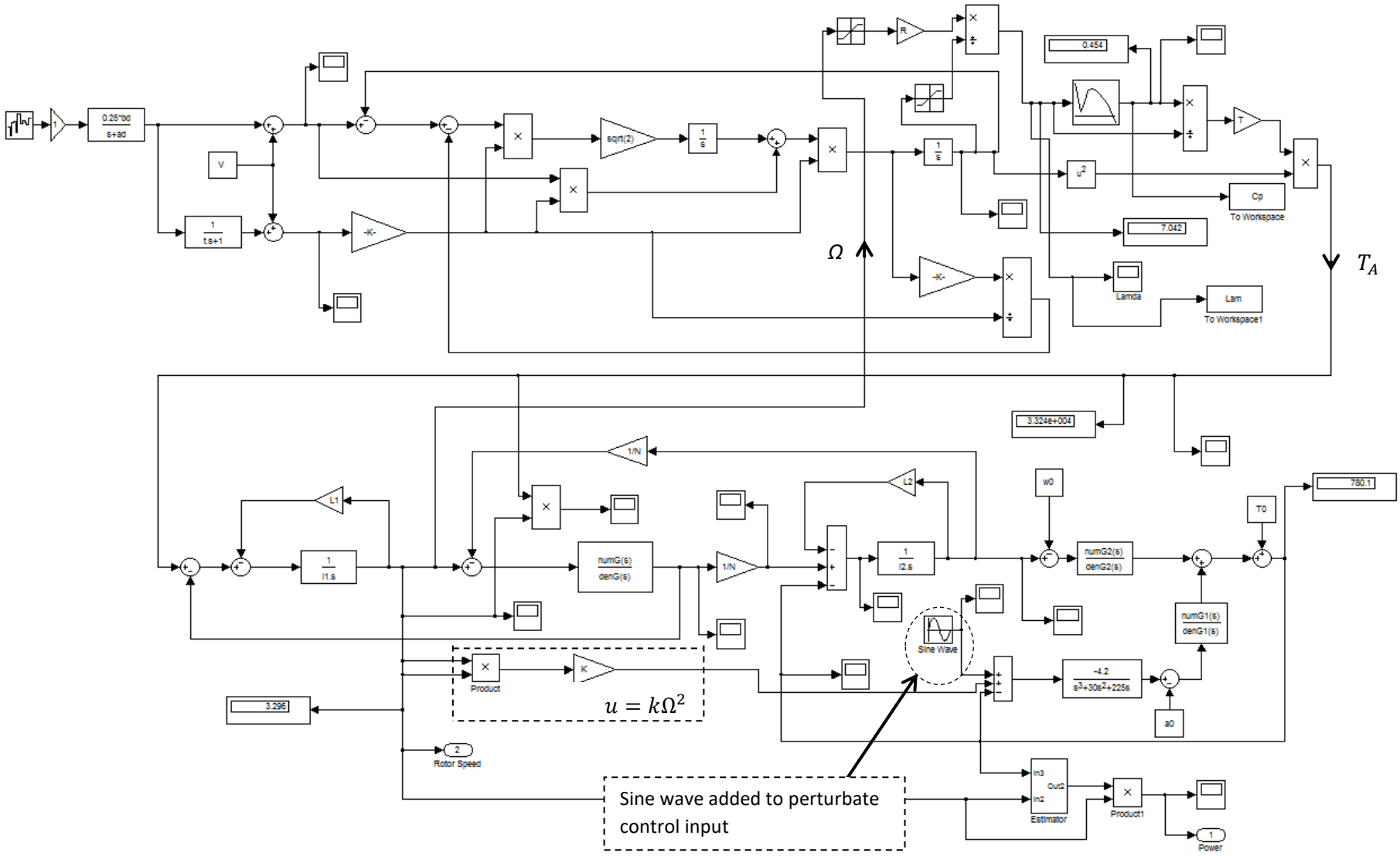

Figure 7.6 - Simulation of the plant

7.3 Correlation Estimator

The correlation of power, P, and rotor speed, Ω, over N cycles of the perturbation in control demand is

$$\frac{C_{P\Omega}-NT\bar{P}\bar{\Omega}}{\sqrt{(C_{PP}-NT\bar{P}^2)(C_{\Omega\Omega}-NT\bar{\Omega}^2)}} \tag{7.9}$$

where:

$$C_{P\Omega}(t)=\int_{t-NT}^{t}P(\acute{t})\Omega(\acute{t})\,d\acute{t},\ C_{PP}(t)=\int_{t-NT}^{t}P^2(\acute{t})\,d\acute{t},\quad C_{\Omega\Omega}(t)=\int_{t-NT}^{t}\Omega^2(\acute{t})\,d\acute{t}$$

$$\bar{P}(t)=(NT)^{-1}\int_{t-NT}^{t}P(\acute{t})\,d\acute{t},\ \ \bar{\Omega}(t)=(NT)^{-1}\int_{t-NT}^{t}\Omega(\acute{t})\,d\acute{t}$$

The estimations for $C_{P\Omega}(t)$, $C_{PP}(t)$, $C_{\Omega\Omega}(t)$, $\bar{P}(t)$, $\bar{\Omega}(t)$ are all calculated continuously as functions of time. In simulation, the above definite integrals are calculated as the indefinite integrals minus their values delayed by 1440 (*NT*) time steps; that is, 12 periods of the oscillating perturbation.

When calculating the correlation, the outputs of the plant are filtered using the transfer function in (7.10).

$$\frac{2*0.1*0.05s}{s^2+2*0.1*0.05s+0.05^2} \tag{7.10}$$

The calculation of the correlation between power and rotor speed is shown in the block diagram in Figure 7.7.

The indicated section A in Figure 7.7 shows the transfer functions (7.10). Section B in Figure 7.7 converts power and rotor speed signals from continuous to discrete time with sample time of $\frac{2\pi}{5}$. Figure 7.8 and Figure 7.9 illustrate the power and rotor speed respectively in continuous and discrete time. As discussed earlier in this chapter, the *P* and Ω signals are delayed by 12 cycles in indicated section C. Indicated section D in Figure 7.7 is the discrete-time integrators.

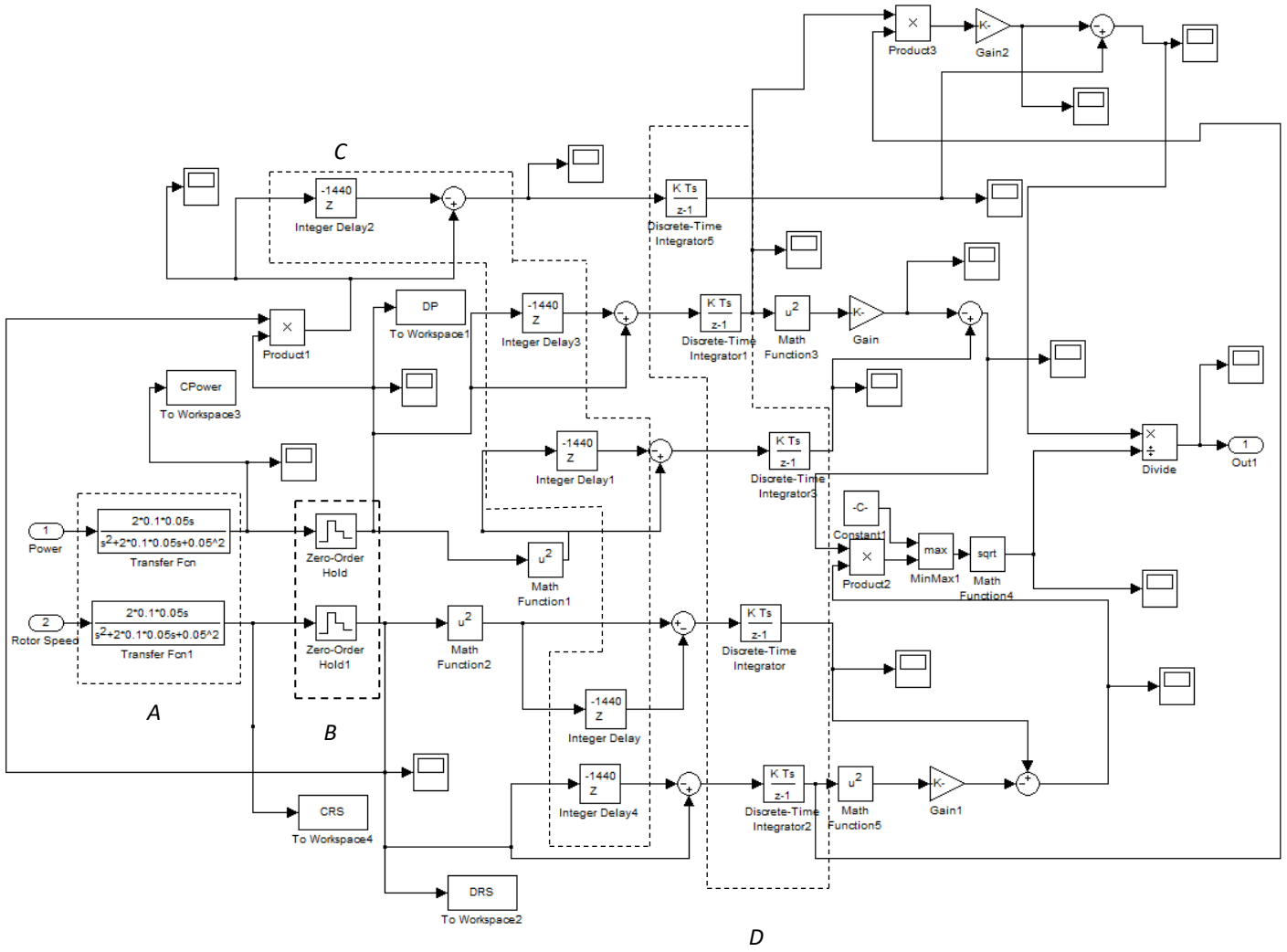

Figure 7.7 - Block diagram of Power and Rotor speed correlation

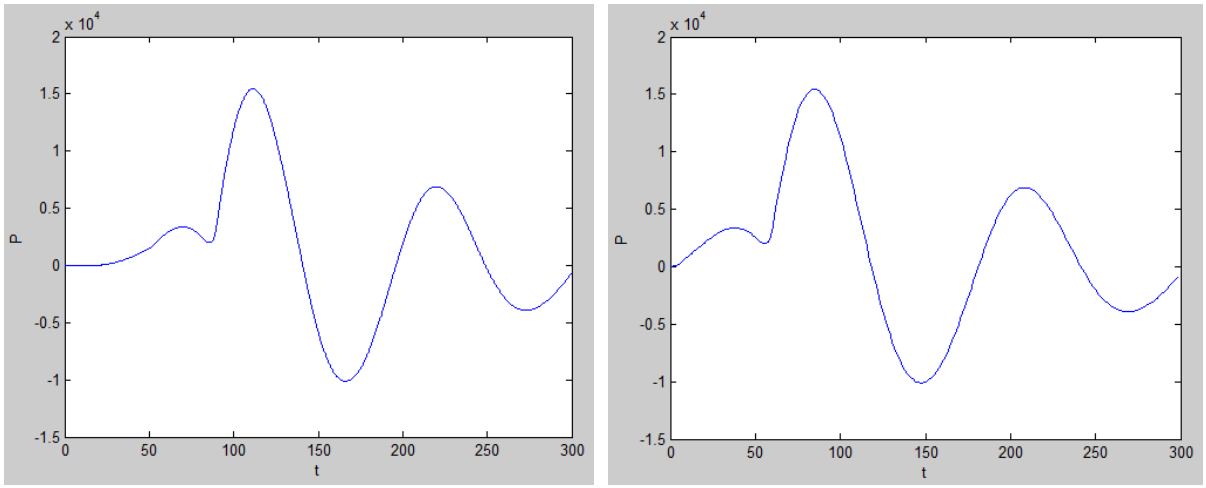

(a) *(b)*

Figure 7.8 - Power in (a) Continuous time (b) Discrete time

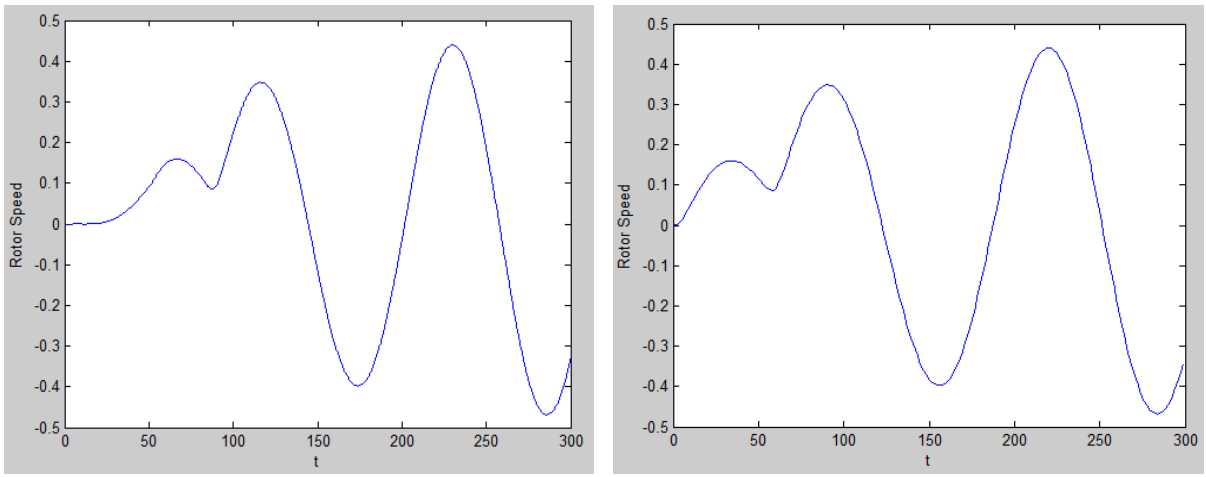

(a) *(b)*

Figure 7.9 - Rotor Speed in (a) Continuous time (b) Discrete time

When the simulated variation of the drive-train torque is centred at λ_0, the average of the correlation of the output in Figure 7.7, i.e. correlation fraction, should be around zero. The average of the variations of the correlation would change to 1 or -1 if the torque variation is moved to below or above λ_0, respectively. Figure 7.10 shows the correlation for these situations with the value of k 105 (at λ_0). The average value is approximately at 0. Similarly, the correlation is approximately 0.8 and -0.9 for the value of k 160 (above λ_0) and 50 (below λ_0), respectively.

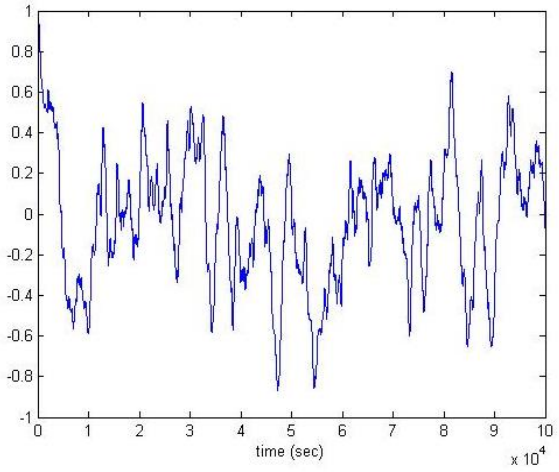

(a) Correlation for k = 105

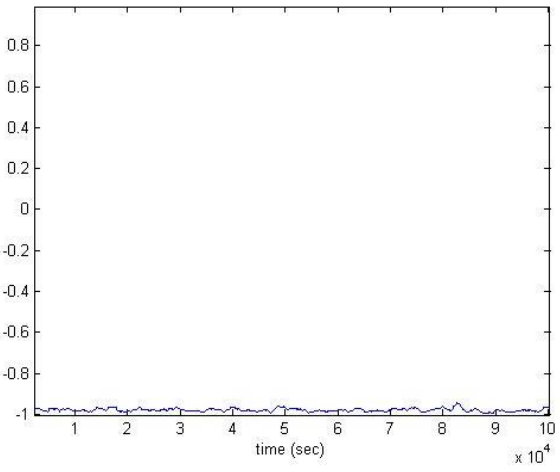

(b) Correlation for k = 50

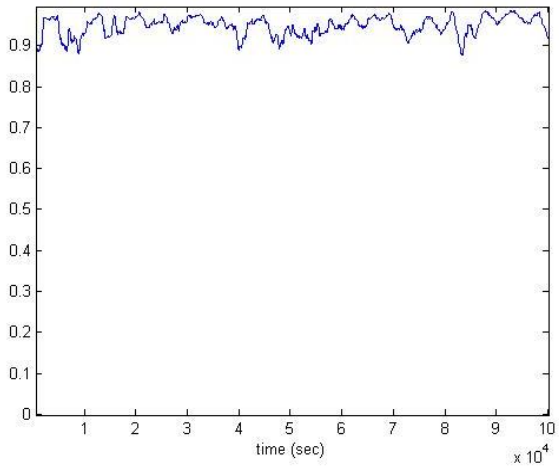

(c) Correlation for k = 160

Figure 7.10 - Correlation when the torque variation is on (a) centred (b) below and (c) above λ_0

7.4 Design of Auto-tuning Controller

A PI controller is added to the model to adjust the value of *k* in Figure 7.11, which is the constant of proportionality that corresponds to maximum aerodynamic efficiency, to keep the variation of the torque centred at λ_0, and so, to keep the averaging value of the correlation around 0. The PI controller was tuned to have an integral gain value of 0.003 and proportional gain value of 1.5.

Figure 7.11 shows the block diagram for the control system and the value of the gain k is plotted against time in Figure 7.12.

As shown in Figure 7.12, the value of the gain *k* against time starts very low but reaches the desired value of 105 and after going higher the value of 105, it goes back to 105 again. The controller in Figure 7.6 acts on an estimation of correlation to adjust the value of k in (6.2).

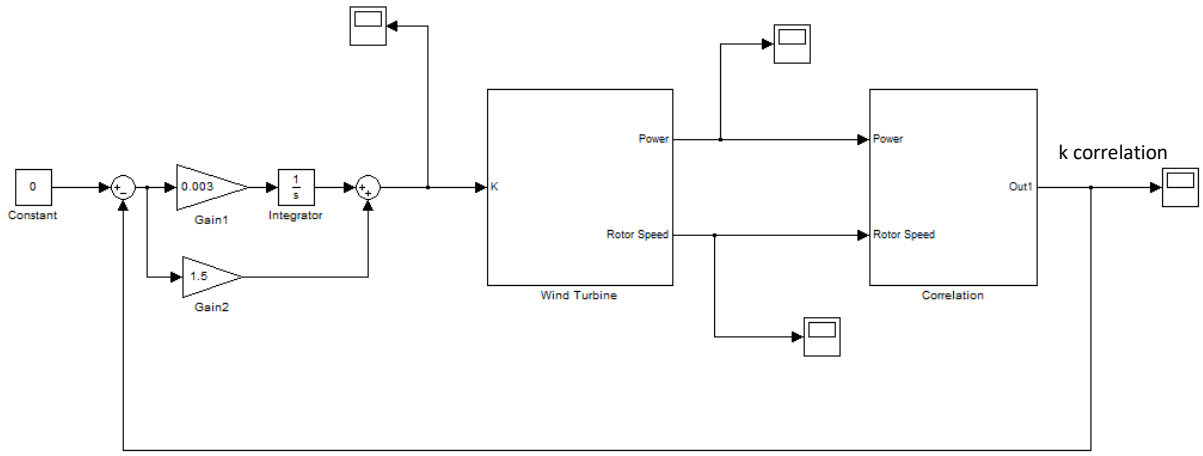

Figure 7.11 - Control strategy simulation

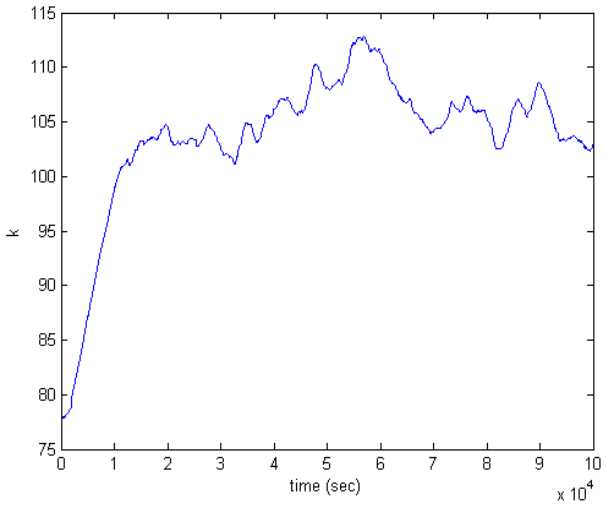

Figure 7.12 - Graph of k against time

The results for different wind speeds and turbulences are shown below. Figure 7.13 represents the correlation results for the mean wind speed of 4 m/s with turbulences from 5% to 20%. As shown in Figure 7.13, the average value of the correlation is around 0, which means the variation of the torque is kept centred at λ_0.

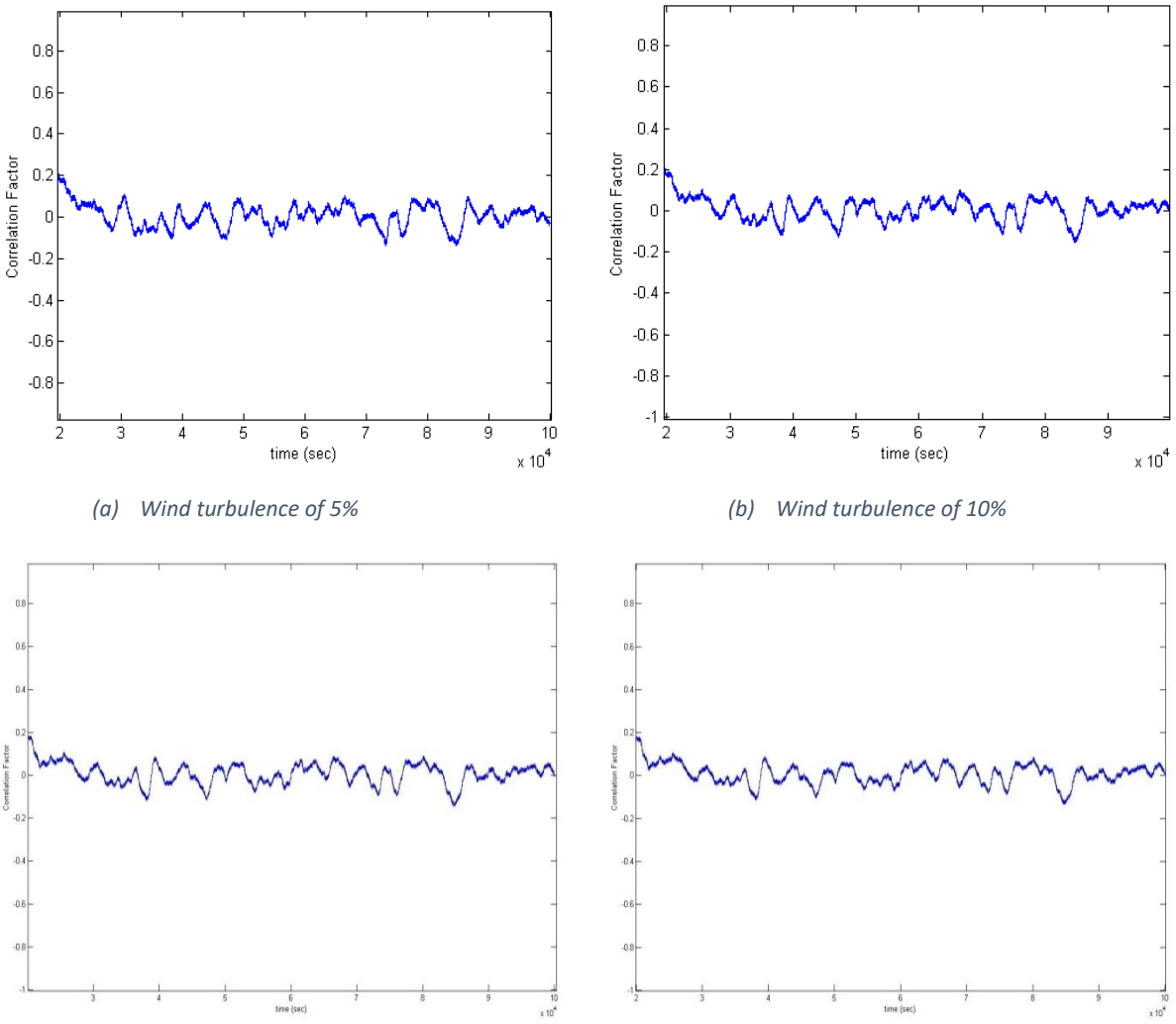

(a) Wind turbulence of 5%

(b) Wind turbulence of 10%

(c) Wind turbulence of 15%

(d) Wind turbulence of 20%

Figure 7.13 - Correlation results for mean wind speed of 4 m/s

Figure 7.14 represents the results for the mean wind speed of 6 m/s with turbulences from 5% to 20%. As shown in Figure 7.14, the average value of the correlation is around 0, which means the variation of the torque is kept centred at λ_0.

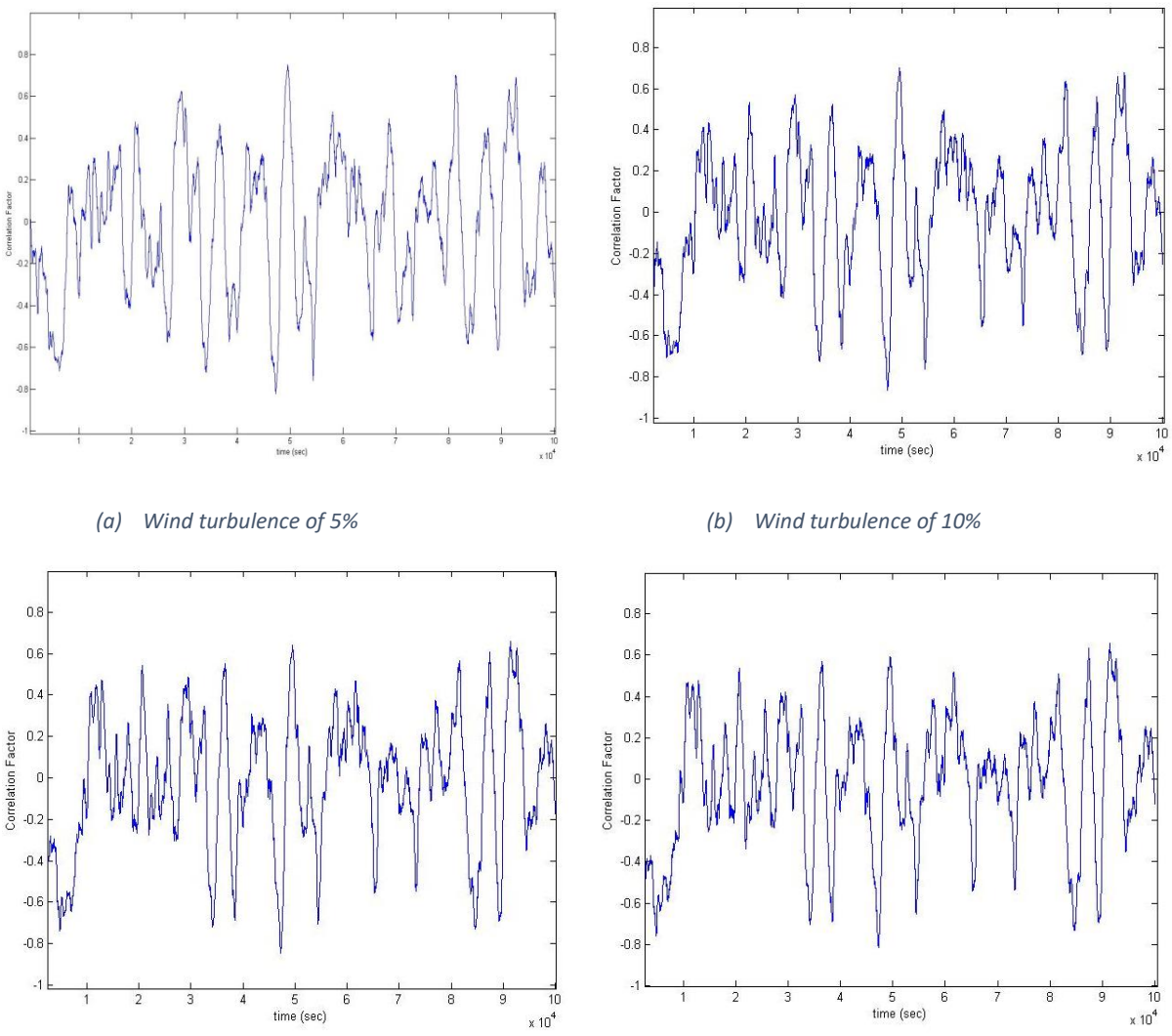

(a) Wind turbulence of 5%

(b) Wind turbulence of 10%

(c) Wind turbulence of 15%

(d) Wind turbulence of 20%

Figure 7.14 - Correlation results for mean wind speed of 6 m/s

Figure 7.15 represents the results for the mean wind speed of 8 m/s with turbulences from 5% to 20%. As shown in Figure 7.15, the average value of the correlation is around 0, which means the variation of the torque is kept centred at λ_0.

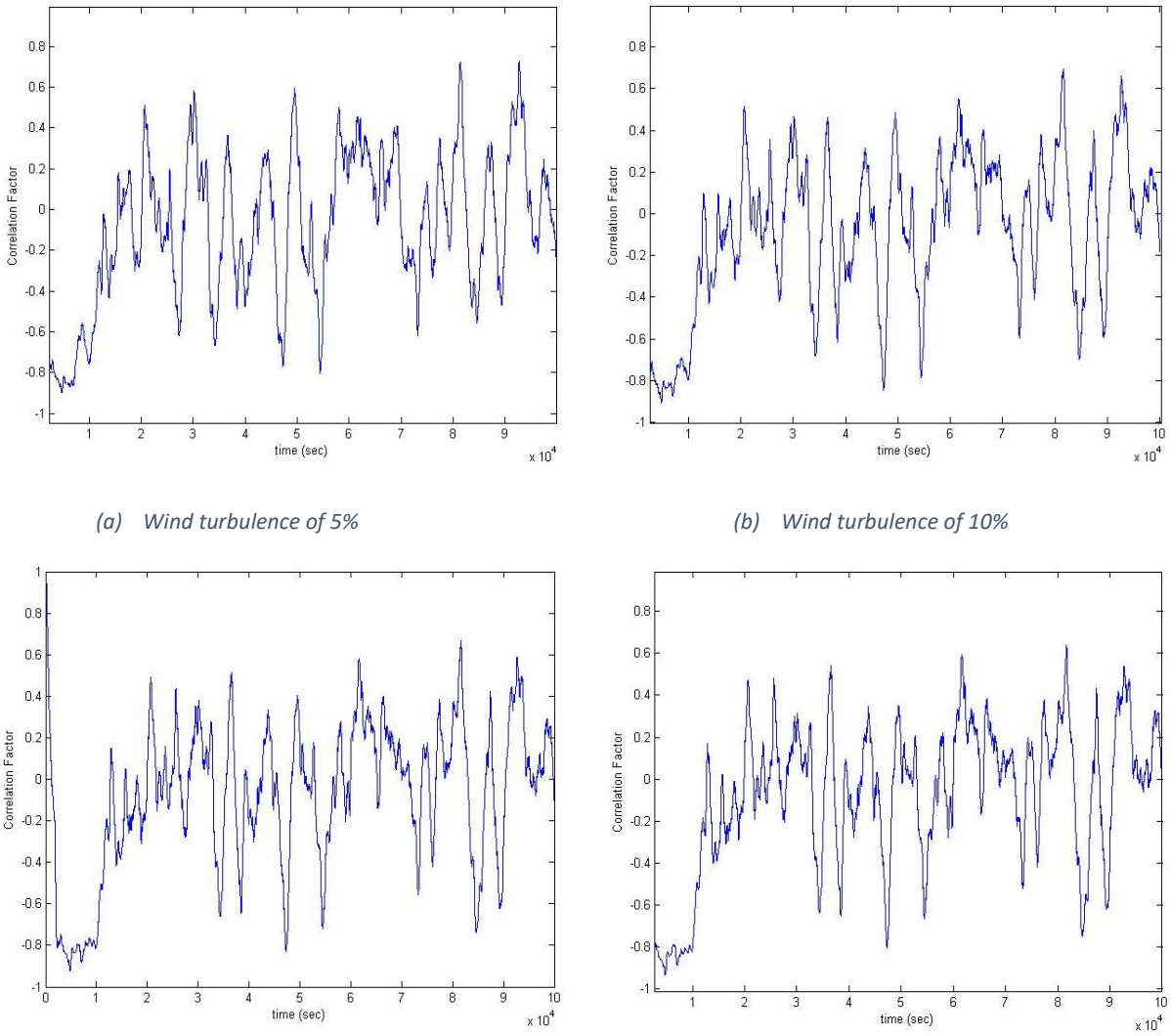

(a) Wind turbulence of 5%

(b) Wind turbulence of 10%

(c) Wind turbulence of 15%

(d) Wind turbulence of 20%

Figure 7.15 - Correlation results for mean wind speed of 8 m/s

Figure 7.16 represents the results for the mean wind speed of 10 m/s with turbulences from 5% to 20%. As shown in Figure 7.16, the average value of the correlation is around 0 (and -0.1 for higher wind turbulence), which means the variation of the torque is kept centred at λ_0.

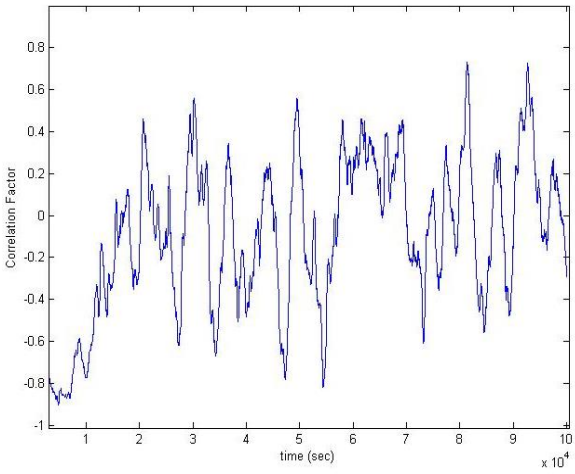

(a) Wind turbulence of 5%

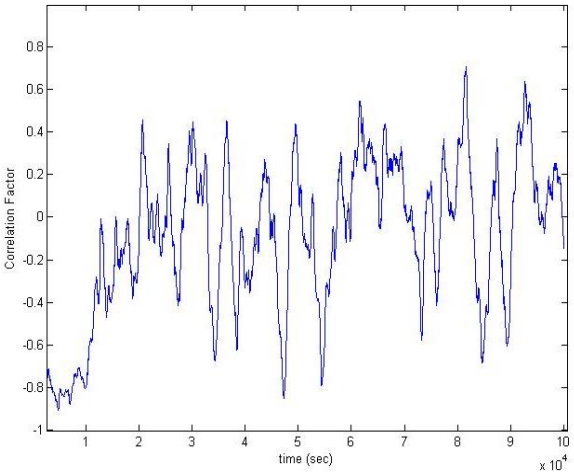

(b) Wind turbulence of 10%

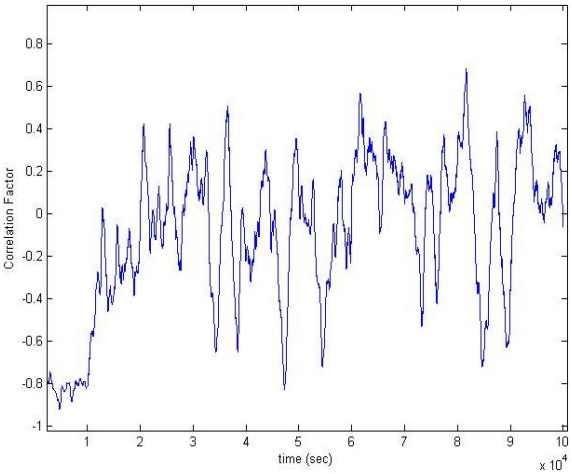

(c) Wind turbulence of 15%

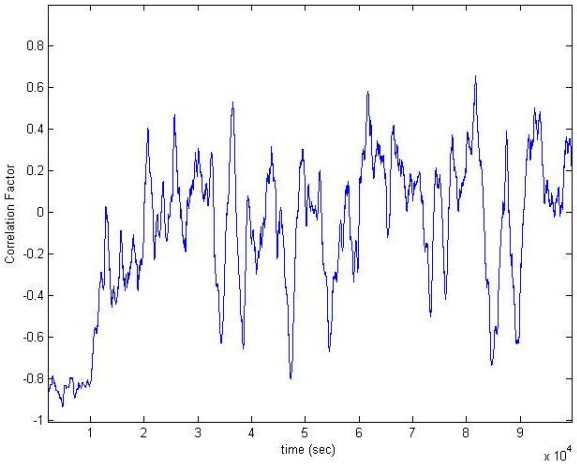

(d) Wind turbulence of 20%

Figure 7.16 - Correlation results for mean wind speed of 10 m/s

Figure 7.17 represents the results for the mean wind speed of 12 m/s with turbulences from 5% to 20%. As shown in Figure 7.17, the average value of the correlation is around -0.1, which means the variation of the torque is kept centred at λ_0.

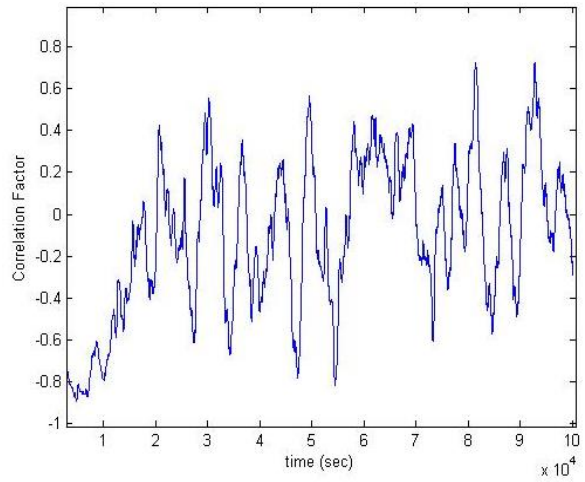

(a) Wind turbulence of 5%

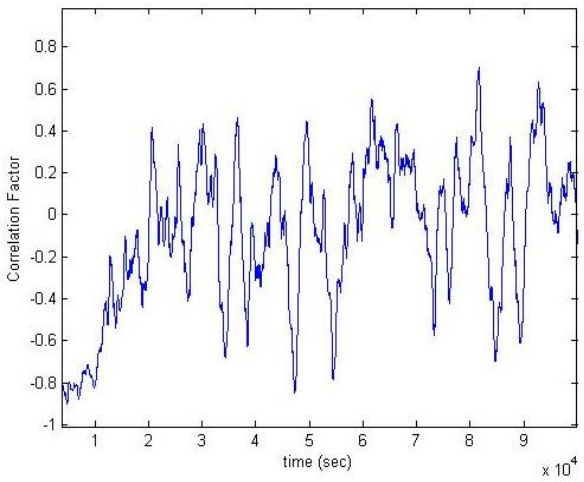

(b) Wind turbulence of 10%

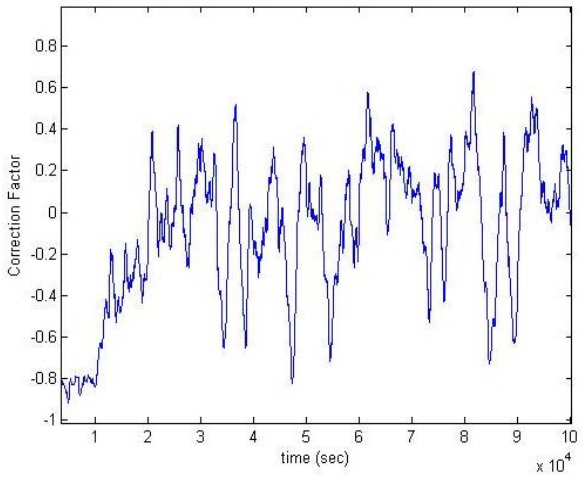

(c) Wind turbulence of 15%

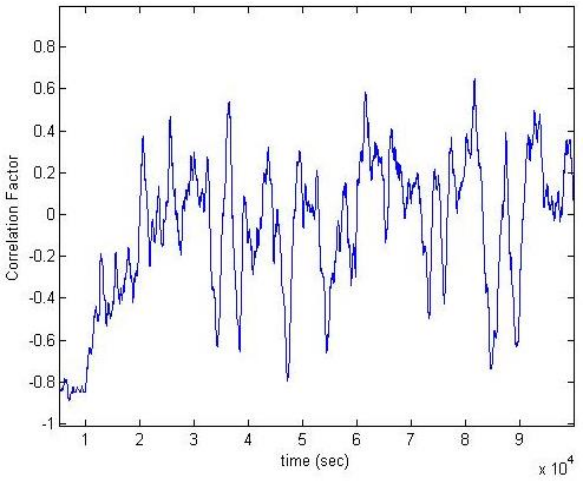

(d) Wind turbulence of 20%

Figure 7.17 - Correlation results for mean wind speed of 12 m/s

Figure 7.18 (a) shows the performance of the gain value of k for a mean wind speed of 8 m/s and a turbulence intensity of 10%. As can be seen, the average value of the gain is around 109. Figure 7.18 (b) shows the correlation of the system. The average value of the correlation in Figure 7.18 (b) is around 0.

From Figure 7.18, it can be concluded that the variation of the drive-train torque is kept centred at λ_0 as described in section 7.1.

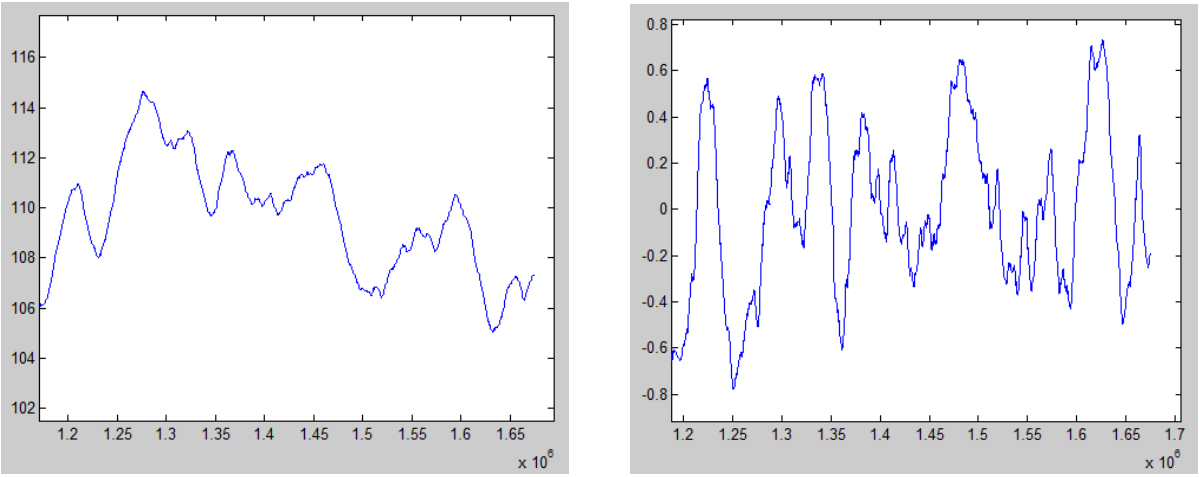

(a) *(b)*

Figure 7.18 - The graph of (a) k value and (b) its related correlation

8. CONCLUSION

"When we analyze a mechanism, we tend to overestimate its complexity. In the uphill process of analysis, a given degree of complexity offers more resistance to the workings of our mind than it would if we encountered it downhill, in the process of invention."
***Valentino Braitenberg**, Vehicles*

In variable speed wind turbines, the operational strategy is regularly selected to maximise the energy capture. For this purpose, the operating state of the wind turbine is caused to track the C_{pmax} curve, which is the maximum aerodynamic efficiency curve. The accuracy of this tracking depends on the controller designed for the wind turbine and the control strategy used.

An auto-tuning controller to maximise the energy capture of a variable speed wind turbine in below rated wind conditions is developed. In below rated conditions, the control strategy is to maximise energy capture by causing the operated state of the turbine to track the C_{pmax} curve. This is achieved by setting the generator reaction torque proportional to generator speed squared.

The auto-tuning controller determines the value of the constant of proportionality that corresponds to maximum aerodynamic efficiency. It acts on an estimation of the correlation factor between aerodynamic power and rotor speed when the generator reaction torque is perturbated by a sinusoidal.

Maximum aerodynamic efficiency corresponds to a value of zero for the correlation factor. The controller is validated using a Simulink model developed to the wind turbine. From the results it shows that the controller achieves the objective of driving the correlation factor to

zero. This happens when the variation of the drive-train torque is centred at λ_0 with the value of controller gain, *k,* 105 at λ_0.

The result from the Simulink model illustrate the controller gain against time starts very low but reaches the desired value of 105 and after going higher the value of 105, it goes back to 105 again. The auto-tuning controller acts on an estimation of correlation to adjust the controller gain value.

The Simulink model tested for different wind speeds from 4 m/s to 12 m/s and different turbulences from 5% to 20%. For all these scenarios the average value of the correlation is around zero, which means the variation of the torque is kept centred at λ_0.

REFERENCES

[1] British Wind Energy Association: *Annual Review 2009.*

[2] E. Iyassere, M. Salah, D. Dawson and J. Wagner, Nonlinear robust control to maximize energy capture in a variable speed wind turbine. *American Control Conference, Washington, USA, June 11-13, 2008, pp. 1824-1829.*

[3] F. D. Bianchi, H. De Battista and R. J. Mantz, Wind turbine control systems: Principles, modelling and gain scheduling design, *2007.*

[4] G. Boyle, Renewable energy: power for a sustainable future, *Second Edition, 2004.*

[5] H. Li, K. L. Shi and P. G. McLaren, Neural-Network-Based sensorless maximum wind energy capture with compensated power coefficient. *IEEE Transaction on industry applications, VOL. 41, 2005, pp. 1548-1556.*

[6] J. Creaby, Y. Li and J. E. Seem, Maximizing wind turbine energy capture using multivariable extremum seeking control. *Wind Engineering, VOL. 33, 2009, pp. 361-388.*

[7] K. E. Johanson, L. J. Fingersh, M. J. Balas and L. Y. Pao, Methods for increasing region 2 power capture on a variable speed HAWT. *23rd ASME Wind Energy Symposium, Reno, Nevada, January 5-8, 2004.*

[8] M. G. SimÕes, B. K. Bose and R. J. Spiegel, Fuzzy logic based intelligent control of a variable speed cage machine wind generation system. *IEEE Transaction on power electronics, VOL. 12, January 1997, pp. 87-95.*

[9] N. D. P. Barltrop, I. P. Ward and D. S. Daw, A fatigue costing study of horizontal axis wind turbines, *DTI Report No. ETSU W/44/00259/REP, 1993.*

[10] N. P. Cheremisinoff , Fundamentals of wind energy, *1978.*

[11] National renewable energy action plan for the United Kingdom (NREAP for UK): *Article 4 of the Renewable Energy Directive, 2009.*

[12] P. R. D. Agius, C. G. Anderson, D. R. R. Green, W. M. R. Smith and N. J. Urwin, Machine for the nineties: study for a cost effective HAWT. *D. En. Report prepared for DTI by windharvester Ltd. Report No. ETSU WN/6110, 1993.*

[13] Renewables 2010: Global Status Report (REN21, GSR), *Renewable Energy Policy Network for the 21st Century, 2010.*

[14] UK Renewable Energy Industry: Introduction and overview, ***STEM*** *Choices 7. Industry Focus, 2009, pp. 7.17-7.29.*

[15] V. Galdi, A. Piccolo, P. Siano, Exploiting maximum energy from variable speed wind power generation systems by using an adaptive Takagi-Sugeno-Kang fuzzy model. *Energy Conversion and Management, 2009, pp. 413-421.*

[16] W. E. Leithead and B. Connor, Control of variable speed wind turbines: dynamic models, *International Journal of Control, VOL. 73, 2000, pp. 1173-1188.*

[17] W. E. Leithead and B. Connor, Control of variable speed wind turbines: design task, *International Journal of Control, VOL. 73, 2000, pp. 1189-1212.*

[18] W. E. Leithead and B. Connor, Investigation of a fundamental trade-off in tracking the C_{pmax} curve of a variable speed wind turbine, *pp. 313-319.*

[19] W. E. Leithead and D. M. Robb, Derivation and validation of simple correlated wind speed models.

[20] W. E. Leithead and M. C. M. Rogers, Drive-train characteristics of constant speed HAWT's: Part I – Representation by simple dynamic models, *Wind Engineering, VOL. 20, 1996, pp. 149-174.*

[21] W. E. Leithead and M. C. M. Rogers, Drive-train characteristics of constant speed HAWT's: Part II – Simple characterisation of dynamics, *Wind Engineering, VOL. 20, 1996, pp. 175-201.*

[22] W. E. Leithead, A. Chatzopoulos, Assessing the energy capture capability of a MW scale wind turbine during below rated operation. ***EWEC 2010*** *Scientific Proceedings, pp. 251-254.*

[23] W. E. Leithead, Lecture notes of basic wind turbine technology, University of Strathclyde, Glasgow.

BIBLIOGRAPHY

A. Grauers, Synchronous generator and frequency converter in wind turbine applications: System design and efficiency, *Technical Report No. 175L, Department of Electrical Machines and Power Electronics, Chalmers University of Technology, Göteborg, Sweden, May 1994.*

A. Mullane, G. Lightbody and R. Yacamini, Adaptive Control of Variable Speed Wind Turbine, *Rev. Energ. Ren.: Power Engineering, 2001, pp. 101-110.*

Bonus Energy Info Newsletter, *The Wind Turbine: Components and Operation, Autumn 1999.*

C. Ghiţă, A. –I. Chirilă, I. –D. Deaconu and D. –I. Ilina, Wind turbine permanent magnet synchronous generator magnetic field study, *Department of Electrical Engineering, University Politehnica of Bucharest.*

D. Aouzellag, K. Ghedamsi, E. M. Berkouk, Power control of a variable speed wind turbine driving an DFIG, *Electrical Engineering department, A. Mira University, Bejaïa, Algeria.*

D. Wu and Z. Wang, The study of multimode power control system for MW variable-speed wind turbine, *WSEAS Transactions on Systems, China.*

Digest of United Kingdom energy statistics 2010, *Department of Energy and Climate Change, London, 2010.*

E. L. Van der Hooft and T. G. Van Engelen, Estimated wind speed feed forward control for wind turbine optimisation, *European Wind Energy Conference, London, November 22-25, 2004.*

E. L. Van der Hooft, P. Schaak, T. G. Van Engelen, Wind turbine control algorithms, *December 2003.*

E. Muljadi and C. P. Butterfield, Pitch-controlled variable-speed wind turbine generation, *IEEE Industry Applications, Society Annual Meeting, Phoenix, Arizona, October 3-7, 1999.*

E. Muljadi, K. Pierce and P. Migliore, Control strategy for variable-speed, stall-regulated wind turbines, *American Control Conference, Philadelphia, PA, June 24-26, 1998.*

E. Muljadi, K. Pierce, P. Migliore, Soft-stall control for variable-speed stall-regulated wind turbines, *Journal of Wind Engineering and Industrial Aerodynamics, VOL. 85,2000, pp. 277-291.*

G. L. Johnson, Wind turbine power, energy and torque, *Wind Energy System, Chapter 4, pp. 4.1-4.53, November 2001.*

H. Binder, Active control: Wind turbine model, *Risø National Laboratory, Roskilde, Denmark, July 1999.*

H. Imamura, Aerodynamics of wind turbines, *Department of Mechanical Engineering and Material Science, Yokohama National University, Yokohama, Japan.*

I. Munteanu, A. I. Bratcu, E. Ceangă, Wind turbulence used as searching signal for MPPT in variable-speed wind energy conversion systems, *International Journal of Renewable Energy, VOL. 34, 2009, pp. 322-327.*

Implications of the UK meeting its 2020 renewable energy target, *A report to WWF-UK and greenpeace UK, August 2008.*

J. Marques, H. Pinheiro, H. A. Gründling, J. R. Pinheiro and H. L. Hey, A survey on variable-speed wind turbine system, *UFSM/CT/GEPOC/NUPEDEE, Campus Universitário, Camobi, Santa Maria, Brazil.*

J. R. Connell, The spectrum of wind speed fluctuations encountered by a rotating blade of a wind energy conversion system, *Solar Energy, VOL. 29, 1982, pp. 363-375.*

J. Twidell and T. Weir, Renewable energy resources, *Second Edition, 2006.*

J. Watson, J. Hertin, T. Randall and C. Gough, Renewable energy and combined heat and power resources in the UK, *Tyndall Centre for Climate Change Research, Paper No. 22, April 2002.*

J. Zhang, M. Cheng, Z. Chen and X. Fu, Pitch angle control for variable speed wind turbines, *DRPT2008, April 6-9, 2008, China.*

K. A. Stol, Disturbance tracking and blade load control of wind turbines in variable-speed operation, *AIAA/ASME Wind Symposium, Reno, Nevada, January 6-9, 2003.*

K. Pierce and L. J. Fingersh, Wind turbine control system modelling capabilities, *American Controls Conference, Philadelphia, June 24-26, 1998.*

K. Pierce, Control method for improved energy capture below rated power, *3rd ASME/JSME Joint Fluids Engineering Conference, San Francisco, California, July 18-23, 1999.*

L. Greco, C. Testa and F. Salvatore, Design oriented aerodynamic modelling of wind turbine performance, *Journal of Physics: Conference Series **75**, 2007.*

M. C. Robinson, M. M. Hand, D. A. Simms and S. J. Schreck, Horizontal axis wind turbine aerodynamics: Three-dimentional, unsteady and separated flow influences, *3rd ASME/JSME Joint Fluids Engineering Conference, San Francisco, California, July 18-23, 1999.*

M. H. Hansen, A. Hansen, T. J. Larsen, S. Øye, P. Sørensen and P. Fuglsang, Control design for a pitch-regulated variable speed wind turbine, *Risø National Laboratory, Roskilde, Denmark, 2005.*

M. H. J. Cuijpers, System identification of a synchronous wind turbine generator using a modified MIMO ARX structure.

M. Lindholm, Doubly fed drives for variable speed wind turbines, *A 40KW laboratory setup, Technical University of Denmark, Denmark.*

M. Rasila, Torque and speed control of a pitch regulated wind turbine, *Department of Electronic Power Engineering, Chalmers University of Technology, Göteborg, Sweden, 2003.*

M. V. A. Nunes, J. P. A. Vieira, U. H. Bezerra and J. A. Peças Lopes, New mathematical models to represent variable speed wind turbine systems in transient stability studies, *15th PSCC, Liege, August 22-26, 2005.*

P. Aree and E. Acha, Block diagram model for fundamental studies of a synchronous generator-static VAr compensator system, *IEEE Proceedings-Gener. Transm. Distrib., VOL. 146, September 1999, pp. 507-514.*

P. M. M. Bongers and S. Dijkstra, A filter controller for a flexible wind turbine in partial load.

P. Novak, T. Ekelund, I. Jovik and B. Schmidtbauer, Modeling and control of variable-speed wind-turbine drive-system dynamics, *IEEE Control systems, August 1995, pp. 28-38.*

P. W. Carlin, A. S. Laxson and E. B. Muljadi, The history and state of the art of variable-speed wind turbine technology, *Wind Energy, VOL. 6, 2003, pp. 129-159.*

P. W. Carlin, A. S. Laxson and E. B. Muljadi, The history and state of the art of variable-speed wind turbine technology, *National Renewable Energy Laboratory, February 2001.*

R. L. Ottinger, Experience with promotion of renewable energy: Successes and lessons learned, *Parliamentarian Forum on Energy Legislation and Sustainable Development, Cape Town, South Africa, October 5-7, 2005.*

S. A. Papathanassiou, Models for variable speed wind turbines, *Contribution to the analysis of variable speed wind turbines with induction generator, Athens, 1997.*

S. Arnaltes, Comparison of variable speed wind turbine control strategies.

S. B. Papaefthimiou and S. A. Papaefthimiou, Simulation and control of a variable speed wind turbine with synchronous generator.

S. M. Barakati, Wind Turbine Systems: History, Structure and Dynamic Model, *Handbook of Renewable Energy Technology, Chapter 2, pp. 21-51, University of Sistan and Baluchestan, Iran.*

T. Burton, D. Sharpe, N. Jenkins and E, Bossanyi, Wind Energy Handbook.

The UK Renewable Energy Strategy, *Parliament by the Secretary of State for Energy and Climate Change, July 2009.*

V. Ramakrishan and S. K. Srivasta, Mathematical modelling of wind turbine systems, *Asian Journal of Information Technology, 2007, pp. 1160-1166.*

W. E. Leithead and B. Conner, Control of a variable speed wind turbine with induction generator, *IEE Conference Publication No. 389, March 1994, pp. 1215-1220.*

W. E. Leithead and D. J. Leith, Implementation of wind turbine controllers, *International Journal of Control, VOL. 66, 1997, pp. 349-380.*

W. E. Leithead and S. Dominguez, Active regulation of multi-MW turbines: an overview

W. E. Leithead, Lecture notes of wind turbine control, University of Strathclyde, Glasgow.

W. E. Leithead, S. A. De la Salle, D. Reardon and M. J. Grimble, Wind turbine modelling and control, *University of Strathclyde, UK.*

W. E. Leithead, S. De la Salle, D. Reardon, Role and objective of control for wind turbine, *IEE Proceedings, VOL. 138, March 1991, pp. 135-148.*

W. E. Leithead, V. Neilson and S. Dominguez, Alleviation of unbalanced rotor loads by single blade controllers.

Y. D. Song, B. Dhinakaran, X. Y. Bao, Variable speed control of wind turbine using nonlinear and adaptive algorithms, *Journal of Wind Engineering and Industrial Aerodynamics, VOL. 85, 2000, pp. 293-308.*

APPENDIX A: EQUATIONS

The equations of motion of the rotor:

$$J\ddot{\theta}_R = -(K_E + J\Omega_0^2)[(\theta_R - \theta_H)\cos\beta - (\emptyset_R - \emptyset_T)\sin\beta]\cos\beta - (K_F + J\Omega_0^2)[(\theta_R - \theta_H)\sin\beta + (\emptyset_R - \emptyset_T)\cos\beta]\sin\beta + F_1 \quad \text{(A.1)}$$

$$\frac{(1-J_C^2/JJ_T)}{(1+J_C/J_T)}J\ddot{\emptyset}_R = (K_E + J\Omega_0^2)[(\theta_R - \theta_H)\cos\beta - (\emptyset_R - \emptyset_T)\sin\beta]\sin\beta - (K_F + J\Omega_0^2)[(\theta_R - \theta_H)\sin\beta + (\emptyset_R - \emptyset_T)\cos\beta]\cos\beta + \left[F_2 - \frac{J_C}{J_T}D_T + \frac{J_C}{J_T}K_T\emptyset_T\right]/(1 + J_C/J_T) \quad \text{(A.2)}$$

Where θ_R stands for in-plane rotor rotational displacement, $\emptyset_R$ represents out-of-plane rotor rotational displacement, β is the angle between the plane of the blade edge-wise mode and the plane of the rotor.

The equations of motion of the tower:

$$(1 - J_{GS}^2/J_{GG}J_{SS} - J_X^2/J_TJ_{GG})J_T\ddot{\theta}_T = -K_{GB}(1 + J_X/J_{GG} - J_{GS}^2/J_{GG}J_{SS}).(\theta_T - \theta_{GB}) - K_T(1 - J_{GS}^2/J_{GG}J_{SS})\theta_T + (N-1)J_X/J_{GG}.T_2 - J_XJ_{GS}/J_{GG}J_{SS}.(T_1 + NT_2) - (1 - J_{GS}^2/J_{GG}J_{SS})B_T\dot{\theta}_T + J_X/J_{GG}.\left((N-1)B_{G2}\dot{\theta}_2 + B_{G3}\dot{\theta}_{GB} + B_{GB}\dot{\theta}_{GB}\right) - J_XJ_{GS}/J_{GG}J_{SS}.\left(B_{G1}\dot{\theta}_1 + NB_{G2}\dot{\theta}_2\right) \quad \text{(A.3)}$$

$$\frac{(1-J_C^2/JJ_T)}{(1+J_C/J)}J_T\ddot{\emptyset}_T = -(K_E + J\Omega_0^2).[(\theta_R - \theta_H)\cos\beta - (\emptyset_R - \emptyset_T)\sin\beta]\sin\beta + (K_F + J\Omega_0^2).[(\theta_R - \theta_H)\sin\beta + (\emptyset_R - \emptyset_T)\cos\beta]\cos\beta - \left[B_T\emptyset_T + K_T\emptyset_T + \frac{J_C}{J}F_2\right]/(1 + J_C/J) \quad \text{(A.4)}$$

The equations of motion of the hub and low-speed shaft:

$$J_H\ddot{\theta}_H = T_H - T_1\ ;\ T_1 = K_H(\theta_H - \theta_1) \quad \text{(A.5)}$$

$$T_H = (K_E + J\Omega_0^2)[(\theta_R - \theta_H)\cos\beta - (\emptyset_R - \emptyset_T)\sin\beta]\cos\beta + (K_F + J\Omega_0^2)[(\theta_R - \theta_H)\sin\beta + (\emptyset_R - \emptyset_T)\cos\beta]\sin\beta \quad \text{(A.6)}$$

Where θ_H is represented as the hub rotational displacement.

The equations of motion of the gearbox:

$$J_{SS}\ddot{\theta}_1 - J_{GS}\ddot{\theta}_{GB} = T_1 + NT_2 - B_{G1}\dot{\theta}_1 - NB_{G2}\dot{\theta}_2 \quad \text{(A.7)}$$

$$J_{GG}(1 - J_X^2/J_T J_{GG})\ddot{\theta}_{GB} - J_{GS}\ddot{\theta}_1 = -K_{GB}(1 + J_X/J_T)(\theta_{GB} - \theta_T) + K_T J_X/J_T\theta_T - (N-1)T_2 - (N-1)B_{G2}\dot{\theta}_2 - B_{G3}\dot{\theta}_{GB} - B_{GB}\dot{\theta}_{GB} + J_X/J_T B_T\dot{\theta}_T \quad \text{(A.8)}$$

Where θ_2 is the rotational displacement of the input shaft and θ_G is the rotational displacement of the gearbox casing.

The equations of motion of the generator rotor and high-speed shaft:

$$J_G\ddot{\theta}_G = T_G - T_2 \;;\; T_2 = K_2(\theta_G - \theta_2) \quad \text{(A.9)}$$

$$\theta_2 = N\theta_1 - (N-1)\theta_{GB} \quad \text{(A.10)}$$

Kinetic Energy:

$$KE\ (J) = \frac{1}{2} * mass\ (kg) * Velovity^2\ (ms^{-1}) \quad \text{(A.11)}$$

Power in wind:

$$P\ (w) = \frac{1}{2} * \text{density of air } (\rho = 1.2256\ \text{kg}m^{-3}) * \text{Area } (\text{m}^2) * \text{ Velocity}^3\ (\text{ms}^{-1}) \quad \text{(A.12)}$$

The force on the rotor:

$$F = \frac{1}{2}\rho\pi\text{R}^2\text{V}^2\text{C}_\text{T}(\lambda, \beta) \quad \text{(A.13)}$$

The relationship between torque and wind speed:

$$T = \frac{1}{2}\rho\pi\text{R}^3\text{V}^2\text{C}_\text{Q}(\lambda, \beta) \quad \text{(A.14)}$$

The Power delivered:

$$P = \frac{1}{2}\rho\pi\text{R}^2\text{V}^3\text{C}_\text{P}(\lambda, \beta) \quad \text{(A.15)}$$

Where ρ is the density of air, which is 1.2256 $\text{kg}m^{-3}$, R is the radius of rotor, V is the wind speed, C_P is the power coefficient, C_Q is the torque coefficient, which is $C_Q = {C_P}/{\lambda}$, λ is the tip-speed ration, which is $\lambda = \frac{\Omega R}{V}$ and Ω represents as rotor speed.

Model of the point wind speed:

$$S_v(\omega) = \frac{K_v|\omega|^k}{[1+(\omega T_v)^\alpha]^\delta} \quad \text{(A.16)}$$

The parameters of α, δ and k are representing power which depend on the actual spectrum. K_v and T_v are constant and normally their values rely on turbulence intensity, roughness of the surface and mean wind speed.

The inertia of the lump rotor:

$$I_1 = J + J_H \frac{K_R}{(K_R+K_H)} + \frac{K_1\left[\left(J_S+J_H K_H/(K_R+K_H)\right)\left(K_{GB}+(N-1)^2K_2\right)-N(N-1)J_{GS}K_2\right]}{(K_1+N^2K_2)[K_{GB}+(N-1)^2/N^2k]} \quad \text{(A.17)}$$

The external damping coefficient of low-speed shaft:

$$\gamma_1 = B_{G1} + B_s \quad \text{(A.18)}$$

The stiffness of low-speed shaft:

$$K_1 = \frac{K_R K_H}{(K_R+K_H)}\left(1 + \frac{K_R}{(K_R+K_H)}\frac{J_H}{J}\right) \quad \text{(A.19)}$$

The inertia of the lump generator rotor:

$$I_2 = J_G + \frac{K_2(J_S+J_H K_H/(K_R+K_H))(K_{GB}+(N-1)/NJ_{GS}K_1)}{(K_1+N^2K_2)[K_{GB}+(N-1)^2/N^2k]} \quad \text{(A.20)}$$

The external damping coefficient of high-speed shaft:

$$\gamma_2 = B_{G2} + B_S \quad \text{(A.21)}$$

The inertia of the inertia of the lumped gearbox:

$$I_3 = J_{GG} - \frac{J_{GG}^2}{J_S+J_H K_H/(K_R+K_H)} \quad \text{(A.22)}$$

The damping of the gearbox:

$$\gamma_3 = B_{G3} + B_{GB} \quad \text{(A.23)}$$

The gearbox mounting stiffness:

$$K_3 = K_{GB} \tag{A.24}$$

Correlation for continuous functions, f and g:

$$(f * g)(t) \stackrel{\text{def}}{=} \int_{-\infty}^{\infty} f^* g(t+\tau) d\tau \tag{A.25}$$

$$(f * g)[n] \stackrel{\text{def}}{=} \sum_{m=-\infty}^{\infty} f^*[m] g[n+m] \tag{A.26}$$

Where f^* is denoting the complex conjugate of f.

APPENDIX B: MATHEMATICAL DERIVATIONS

The rotational averaging of the wind speed:

$$f(s) = \frac{(\sqrt{2}+\sigma(\bar{V})s)}{(\sqrt{2}+\sqrt{a}\sigma(\bar{V})s)(1+\frac{\sigma(\bar{V})s}{\sqrt{a}})}$$

$$= \frac{(\sigma(\bar{V})s+\sqrt{2})}{\sqrt{2}+\frac{\sqrt{2}\sigma(\bar{V})s}{\sqrt{a}}+\sqrt{a}\sigma(\bar{V})+\frac{\sqrt{a}\sigma^2(\bar{V})^2s^2}{\sqrt{a}}}$$

$$= \frac{(\sigma(\bar{V})s+\sqrt{2})}{\sigma^2(\bar{V})^2s^2+\left(\frac{\sqrt{2}\sigma(\bar{V})}{\sqrt{a}}+\sqrt{a}\sigma(\bar{V})\right)s+\sqrt{2}}$$

Now the top and bottom of the above equation can be dividing by $\sqrt{2}$, thus we have

$$= \frac{\frac{\sigma(\bar{V})}{\sqrt{2}}s+1}{\frac{\sigma^2(\bar{V})^2}{\sqrt{2}}s^2+\left(\frac{\sigma(\bar{V})}{\sqrt{a}}+\frac{\sqrt{a}\sigma(\bar{V})}{\sqrt{2}}\right)s+1} \quad \text{(B.1)}$$

Where σ is represented by $\frac{\gamma R}{\bar{V}}$, which γ is being the turbulent wind speed decay factor.

The model of the wind speed fluctuations:

$$\dot{v}_d = -a_d v_d + b_d \omega$$

$$\dot{v}_d + +a_d v_d = b_d \omega$$

$$s v_d + a_d v_d = b_d \omega$$

$$v_d(s + a_d) = b_d \omega$$

$$v_d = \frac{b_d \omega}{s+a_d} \quad \text{(B.2)}$$

Where v_d represent the wind speed, ω is white Gaussian noise.

Simplification of the rotational averaging of the wind speed:

$$y = \frac{\sqrt{2}+\sigma(\bar{V})s}{\left(\sqrt{2}+\sqrt{a}\sigma(\bar{V})s\right)\left(1+\sigma(\bar{V})s/\sqrt{a}\right)}$$

$$y = \frac{\left(\sigma(\bar{V})/\sqrt{2}\right)s+1}{\frac{\sigma^2(\bar{V})^2}{\sqrt{2}}s^2+\left(\frac{\sigma(\bar{V})}{\sqrt{a}}+\frac{\sqrt{a}\sigma(\bar{V})}{\sqrt{2}}\right)s+1}$$

$$\frac{\sigma^2(\bar{V})^2}{\sqrt{2}}\ddot{y} + \left(\frac{1}{\sqrt{a}}+\frac{\sqrt{a}}{\sqrt{2}}\right)\sigma(\bar{V})\dot{y} + y = \frac{1}{\sqrt{2}}\sigma(\bar{V})\dot{x} + x$$

$$\frac{\sigma(\bar{V})}{\sqrt{2}}\left(\sigma(\bar{V})\dot{y} - x\right)^{\cdot} = x - y - \left(\frac{1}{\sqrt{a}}+\frac{\sqrt{a}}{\sqrt{2}}\right)\sigma(\bar{V})\dot{y}$$

$$\left(\sigma(\bar{V})\dot{y} - x\right) = \int \frac{\sqrt{2}}{\sigma(\bar{V})}\left[x - y - \left(\frac{1}{\sqrt{a}}+\frac{\sqrt{a}}{\sqrt{2}}\right)\sigma(\bar{V})\dot{y}\right]dt$$

$$\dot{y} = \frac{x}{\sigma(\bar{V})} + \frac{1}{\sigma(\bar{V})}\int \frac{\sqrt{2}}{\sigma(\bar{V})}\left[x - y - \left(\frac{1}{\sqrt{a}}+\frac{\sqrt{a}}{\sqrt{2}}\right)\sigma(\bar{V})\dot{y}\right]dt$$

$$y = \int\left\{\frac{x}{\sigma(\bar{V})} + \sigma^{-1}(\bar{V})\int \sqrt{2}\sigma^{-1}(\bar{V})\left[x - y - \left(\frac{1}{\sqrt{a}}+\frac{\sqrt{a}}{\sqrt{2}}\right)\sigma(\bar{V})\dot{y}\right]dt\right\}dt \qquad \text{(B.3)}$$

The mathematical process to solve the algebraic loop appeared in drive-train simulation:

$$y = \left(\frac{K_1}{s}+\gamma_1^*\right)\left(x - \left(\frac{{}^{s}/_{N^2}}{K_2+\gamma_2^* s}\right)y\right)$$

$$\frac{K_1+\gamma_1^* s}{s}x - y\left[\left(\frac{K_1+\gamma_1^* s}{s}\right)\left(\frac{{}^{s}/_{N^2}}{K_2+\gamma_2^* s}\right)\right] = y$$

$$\frac{K_1+\gamma_1^* s}{s}x - y\left[\left(\frac{K_1+\gamma_1^* s}{s}\right)\left(\frac{s}{N^2(K_2+\gamma_2^* s)}\right)\right] = y$$

$$\frac{K_1+\gamma_1^{8} s}{s}x - y\left(\frac{K_1+\gamma_1^*}{N^2(K_2+\gamma_2^* s)}\right) = y$$

$$\frac{K_1+\gamma_1^* s}{s}x = y + y\left(\frac{K_1+\gamma_1^* s}{N^2(K_2+\gamma_2^* s)}\right)$$

$$\frac{K_1+\gamma_1^* s}{s}x = y\left(\frac{K_1+\gamma_1^* s}{N^2(K_2+\gamma_2^* s)}\right) + 1$$

$$y = \frac{\frac{K_1+\gamma_1^* s}{s}}{\frac{K_1+\gamma_1^* s}{N^2(K_2+\gamma_2^* s)}+1}x$$

To simplify the above relation, top and bottom are multiplied by $N^2(\gamma_2^* s + K_2)$.

$$y = \frac{\frac{(\gamma_1^* s+K_1)(\gamma_2^* s+K_2)N^2}{s}}{\gamma_1^* s+K_1+(\gamma_2^* s+K_2)N^2}$$

$$y = \frac{\frac{\gamma_1^*\gamma_2^* N^2 s^2+(\gamma_1^* K_2 N^2+\gamma_2^* K_1 N^2)s+K_1 K_2 N^2}{s}}{(\gamma_1^*+\gamma_2^* N^2)s+(K_1+K_2 N^2)}$$

$$y = \frac{\gamma_1^*\gamma_2^* N^2 s^2+(\gamma_1^* K_2 N^2+\gamma_2^* K_1 N^2)s+K_1 K_2 N^2}{(\gamma_1^*+\gamma_2^* N^2)s^2+(K_1+K_2 N^2)s} \quad \text{(B.4)}$$

Determination of the gain value of *k*:

$$T_A = \frac{1}{2}\rho\pi R^3 V^2 C_q(\lambda_0, \beta)$$

β=0 and $\lambda = \lambda_0$. Since $C_q = \frac{C_p}{\lambda_0}$ and $\lambda_0 = \frac{\Omega R}{V} \Longrightarrow V = \frac{\Omega R}{\lambda_0}$ the above equation can substitute to:

$$T_A = \frac{1}{2}\rho\pi R^3 \left(\frac{\Omega R}{\lambda_0}\right)^2 C_q(\lambda_0, 0)$$

$$T_A = \frac{{}^1/_2 \rho\pi R^3 \Omega^2 R^2 C_q(\lambda_0,0)}{\lambda_0^2}$$

$$T_A = \frac{{}^1/_2 \rho\pi R^5 C_q(\lambda_0,0)}{\lambda_0^2}\Omega^2$$

From Equation (6.2) we have $T = k\Omega^2$, therefore

$$k = \frac{{}^1/_2 \rho\pi R^5 C_q(\lambda_0)}{\lambda_0^2} \quad \text{(B.5)}$$

APPENDIX C: MATLAB M-FILE

```
% Parameter Values for variable-speed Wind Turbine

N = 38.06;       % Gearbox Ratio
I1 = 100000;     % Rotor Inertia
I2 = 3.8;        % Generator Inertia
K1 = 1.0*10^6;   % Low-speed shaft stiffness
K2 = 5.0*10^4;   % High-speed shaft stiffness
L1 = 980;        % Low-speed shaft external damping coefficient
L2 = 0.2;        % High-speed shaft external damping coefficient
L1s = 9500;      % Low-speed shaft internal damping coefficient
L2s = 13;        % High-speed shaft internal damping coefficient

a = 0.55;
t = 30;
gamma = 1.3;

Ro = 1.225;                % Density of air
R = 16.5;                  % Radius of rotor
V = 8;                     % Wind Speed
om = 4.187;                % Angular velocity of the rotor
T = 0.5*Ro*pi*R^3;         % relationship between torque and wind speed

Vbar = 8;
L = 200;
ad = 1.14*(Vbar/L);

sigmav = 1.8;
bd = sigmav*sqrt(2*ad);

a0 = 0.4697;
w0 = 194.5;
T0 = 2154.6;


numG = [L1s*L2s*N^2 (L1s*K2*N^2+L2s*N^2*K1) K1*K2*N^2];
denG = [(L1s+L2s*N^2) (K1+K2*N^2) 0];

numG1 = [-295.43 2.5*10^5 -3.62*10^7 -2.9*10^8];
denG1 = [1 212.67 8.17*10^3 6.19*10^5];

numG2 = [-42.71 7.11*10^3 2.76*10^5 2.26*10^6];
denG2 = [1 212.08 4606 4.38*10^5];
```

APPENDIX D: POWER COEEFICIENT TABLE

Table 3 - Power Coefficients for the rotor at different pitch angles

β / λ	0°	2°	4°	6°	10°	14°	18°	22°	26°	30°
2	0.058	0.064	0.07	0.078	0.096	0.112	0.12	0.118	0.104	0.074
3	0.162	0.183	0.204	0.219	0.228	0.204	0.156	0.093	0.018	-0.048
4	0.34	0.356	0.356	0.34	0.272	0.184	0.076	-0.048	-0.148	-0.168
4.5	0.4185	0.4095	0.387	0.3555	0.2655	0.1485	0.009	-0.1485	-0.207	-0.2475
5	0.445	0.43	0.4	0.36	0.25	0.1	-0.08	-0.255	-0.28	-0.365
5.5	0.4565	0.44	0.407	0.3575	0.22	0.0385	-0.187	-0.3685	-0.374	-0.517
6	0.462	0.45	0.408	0.354	0.186	-0.036	-0.318	-0.438	-0.492	-0.714
6.25	0.4625	0.45	0.4125	0.35	0.1625	-0.08125	-0.39375	-0.48125	-0.5625	-0.83125
6.5	0.4615	0.4485	0.4095	0.3445	0.143	-0.13	-0.468	-0.5265	-0.6435	-0.962
7	0.455	0.448	0.406	0.329	0.084	-0.238	-0.616	-0.637	-0.826	-1.267
8	0.432	0.432	0.376	0.272	-0.048	-0.52	-0.952	-0.92	-1.336	-2.048
9	0.396	0.396	0.333	0.198	-0.225	-0.882	-1.323	-1.323	-2.043	-3.078
12	0.204	0.216	0.096	-0.18	-1.14	-2.472	-2.364	-3.492	-5.58	-8.196
15	-0.135	-0.12	-0.345	-0.855	-2.7	-4.635	-4.635	-9.675	-12.975	-16.74

APPENDIX E: SUPPORTED RESOURCES

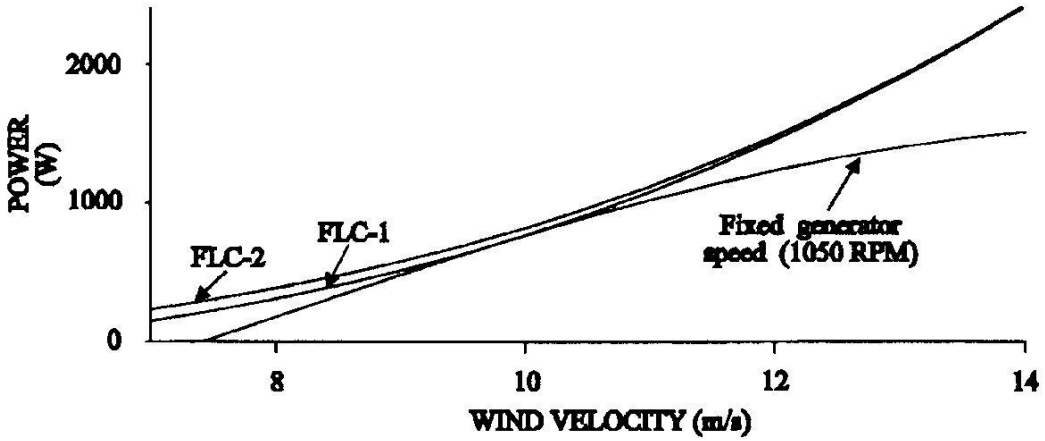

Figure E. 1 - Steady-state line side power boost with first and second fuzzy logic controllers

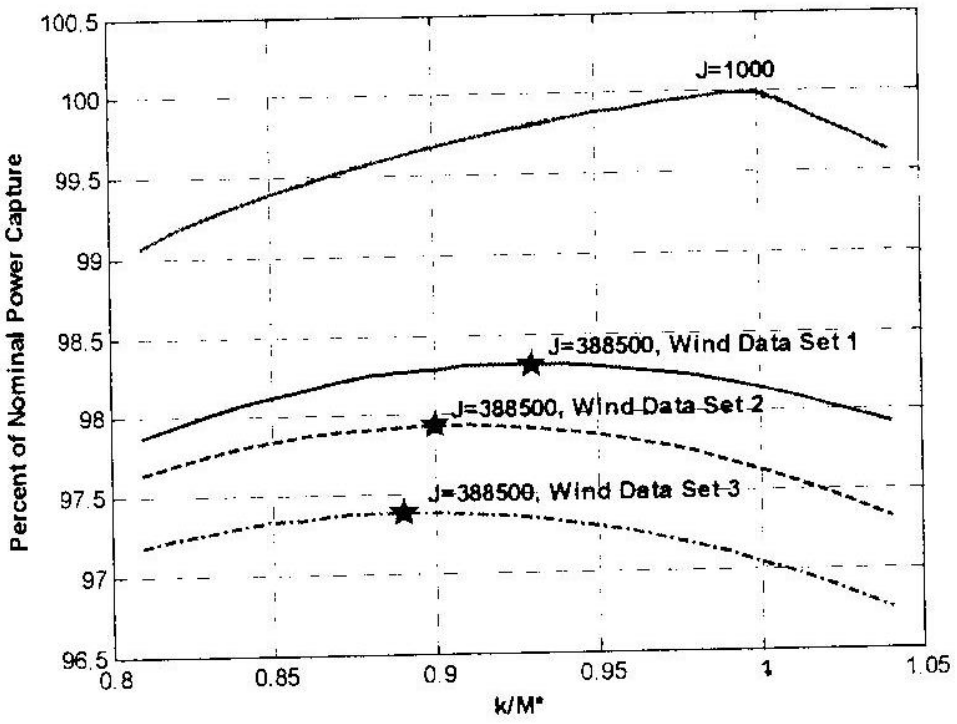

Figure E. 2 - Average Power Capture for Normal and Low Inertia

$k = Torque\ Control\ Gain$

$M^* = The\ Nominal\ Value$

$$M^* = \frac{1}{2} AR^3 \frac{C_{p\,max}}{\lambda_*^3}$$

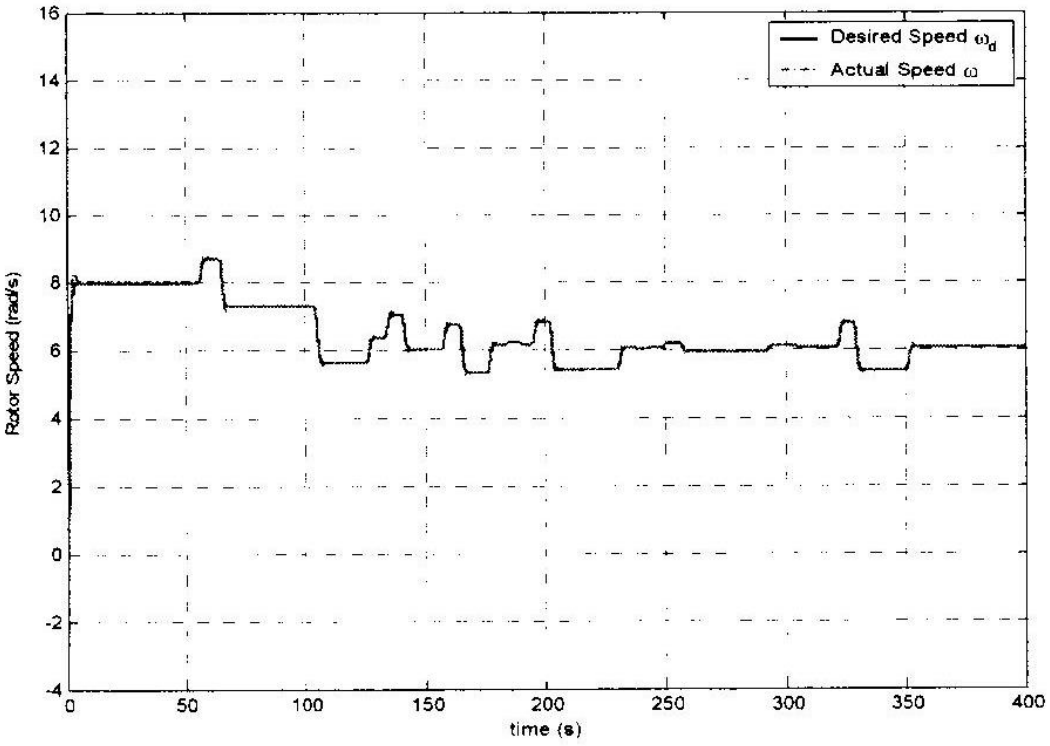

Figure E. 3 - Desired rotor speed and Actual rotor speed

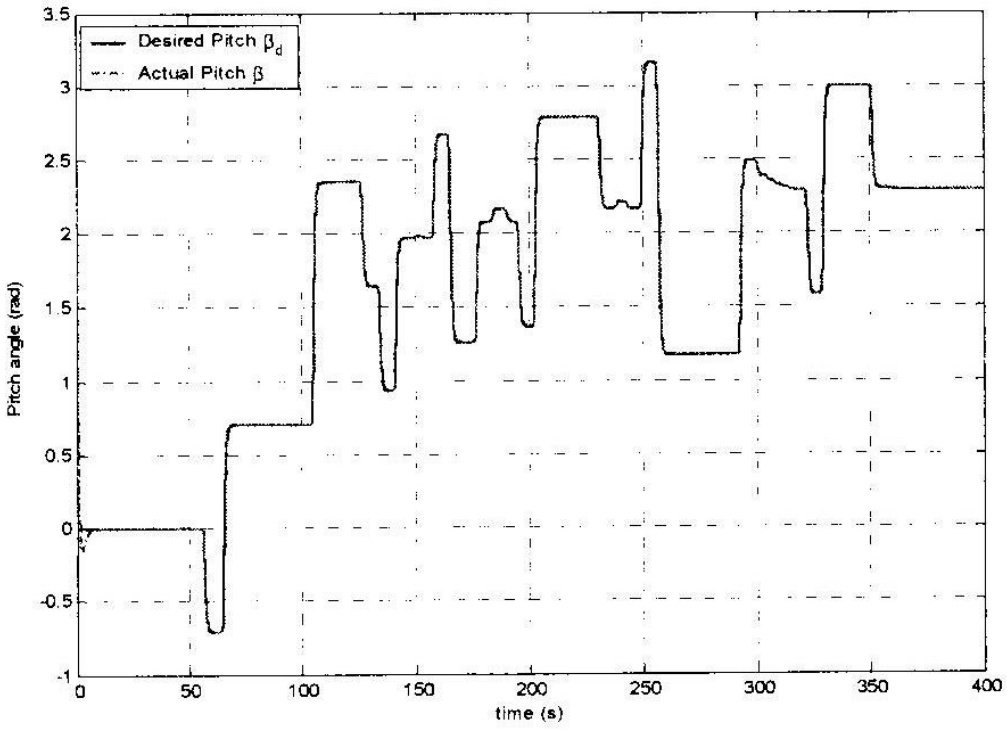

Figure E. 4 - Desired blade pitch and Actual blade pitch

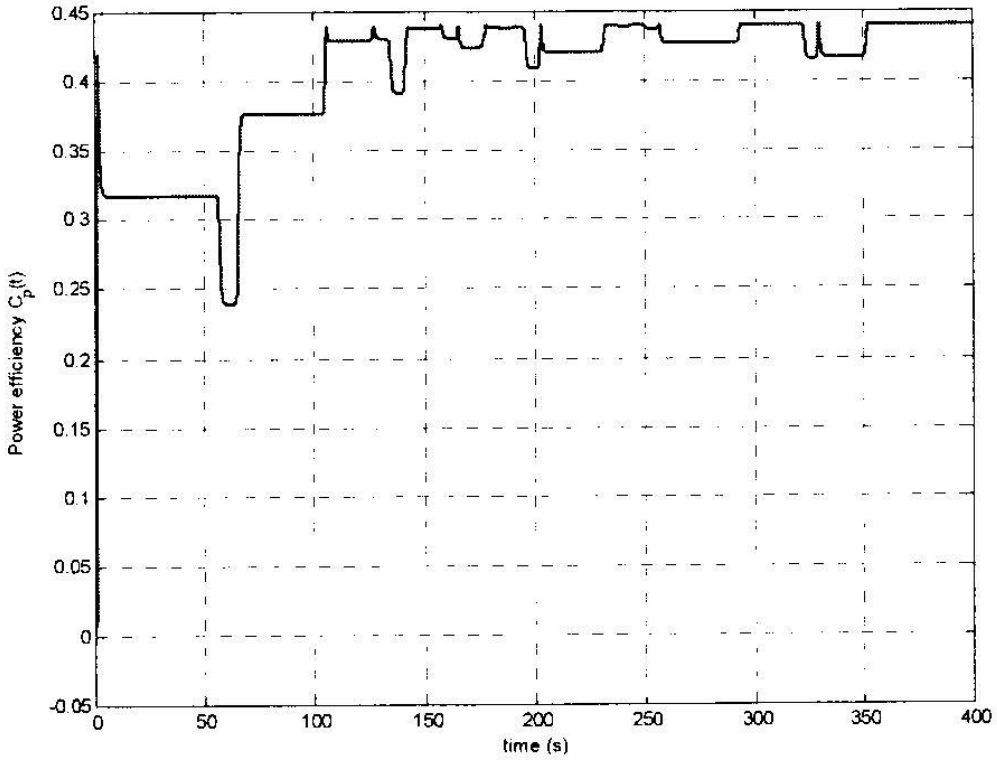

Figure E. 5 - Maximum rotor power coefficient from numerical optimization algorithm

Table 4 - Aerodynamic efficiency results for different turbulences and different controller gain for a mean wind speed of 7.5 m/s

Turbulence (%)	Controller Gain	Aerodynamic efficiency (%)
5 %	0.2	99.75 %
	0.1753	99.93 %
	0.15	99.79 %
	0.12	99.33 %
10 %	0.2	99.68 %
	0.1753	99.87 %
	0.15	99.74 %
	0.12	99.29 %
15 %	0.2	99.57 %
	0.1753	99.77 %
	0.15	99.66 %
	0.12	99.22 %

Table 5 - Aerodynamic efficiency results for different turbulences and different controller gain for a mean wind speed of 8.5 m/s

Turbulence (%)	Controller Gain	Aerodynamic efficiency (%)
5 %	0.2	99.79 %
	0.1753	99.93 %
	0.15	99.82 %
	0.12	99.46 %
10 %	0.2	99.70 %
	0.1753	99.88 %
	0.15	99.78 %
	0.12	99.42 %
15 %	0.2	99.62 %
	0.1753	99.79 %
	0.15	99.71 %
	0.12	99.30 %